Electronic Supporting Information

Cyclometalated Platinum(II) Complexes with Acyclic Diaminocarbene Ligands for OLED Application

Svetlana A. Katkova, Daria O. Kozina, Kristina S. Kisel, Dmitriy A. Tarvanen, Maria A. Sandzhieva, Sergey V. Makarov,* Vitaly V. Porsev, Sergey P. Tunik, and Mikhail A. Kinzhalov

Table of content:

S1. Materials and instrumentation, synthetic work and characterization

Reagents and materials used. Solvents, organic and inorganic reagents were obtained from commercial sources and used as received. Isocyanides (4-isocyano-*N*,*N*-dimethylaminaniline, 1-chloro-4-isocyanobenzene, 1-bromo-4-isocyanobenzene, 1-iodo-4-isocyanobenzene, and 1-isocyano-4-(trifluoromethyl)benzene) were synthesized by the modified version of the published method.[1] Complex [{Pt(ppy)(μ-Cl)}$_2$] was prepared by the known method[2], that includes heating of $K_2[PtCl_4]$ at 110 °C with 2.5 equivs of 2-phenylpyridine in a acetic acid. Complexes **S1e**[3] and **S2a**–**f**[4] were prepared as reported earlier.

Instrumentation and methods. C, H, and N elemental analyses were carried out on a Euro EA 3028 HT CHNSO analyzer. High resolution mass spectra were recorded in the positive ion mode on a Shimadzu LCMS-9030 Q-TOF liquid chromatograph mass spectrometer equipped with an ESI interface during direct probe injection in the range of 100–1000 m/z, and on Bruker micrOTOF spectrometer equipped with ESI source during direct probe injection in the range of 50–3000; a CH_2Cl_2/MeOH or MeCN/0,1%FA mixture was used as the solvent. The capillary voltage of the ion source was set at –4500 V (ESI^+) and the capillary exit at +(70–150) V. The nebulizer gas pressure was 0.4 bar and drying gas flow was 3.0–4.0 L/min. The most intensive peak in the isotopic pattern is reported. Infrared spectra were recorded on Shimadzu IRAffinity-1 FTIR instrument (4000–400 cm^{-1}, resolution 2 cm^{-1}) in KBr pellets. NMR spectra were recorded on Bruker AVANCE III 400 spectrometers in $CDCl_3$ at ambient temperature (at 400, 100, 162, and 86 MHz for ^1H, ^{13}C, ^{31}P, and ^{195}Pt NMR, respectively). Chemical shifts are given in δ-values [ppm] referenced to the residual signals of undertreated solvent ($CHCl_3$): δ 7.26 (^1H) and 77.2 (^{13}C). ^1H and ^{13}C NMR data assignment for **1**–**2** was achieved by using 2D (^1H,^1H-COSY, ^1H,^1H-NOESY, ^1H,^{13}C-HMQC/HSQC and ^1H,^{13}C-HMBC) NMR correlation experiments. UV/Vis spectra were recorded with a Shimadzu UV-2550 spectrophotometer. The CP/MAS NMR spectra were acquired using a double-resonance 4 mm MAS Bruker probe at a resonance frequency of 162 MHz under 14 kHz MAS. ^{195}Pt CP/MAS NMR spectra were acquired using a direct excitation technique (DE). The CP contact time in all experiments was 3.5 μs with a delay between acquisitions of 1 sec and number of scans was collected 20000. The 0.1 *M* $[K_2Pt(CN)_4]$ water solution is used as an external reference (δ –3822.71).

UV–vis absorption spectra were recorded on a Shimadzu UV-1800 spectrophotometer. The excitation and emission spectra in solution (DCE) and in the solid state were recorded with a HORIBA FluoroMax-4 spectrofluorimeter. Excited state lifetimes and absolute photoluminescence quantum yields in the solid phase were measured on a HORIBA Scientific FluoroLog-3 spectrofluorometer using a HORIBA Quanta-phi integration sphere. The uncertainty of the quantum yield determinations was in the range of ±5% (an average of three replications, each of which was done with different orientations of the sample). The emission quantum yield in solutions was determined by comparative method using coumarin 102 in ethanol (Φr = 0.764) as reference;[5] refraction indexes of DCE and EtOH equal to 1.4448 and 1.3614, respectively. The electroluminescence spectra were obtained with an Instrument Systems CAS 120 Array spectrometer sensitive within 200–1100 nm. Current-voltage characteristics were measured by using Keithley 2400 source-meter measurement unit.

X-ray Structure Determinations. Single crystals of **1a**–**f**·and **2b** suitable for single crystal X-ray analysis were obtained by slow evaporation of the reaction mixture. A SCXRD experiment was carried out using Xcalibur, Eos diffractometer. The crystal was kept 100(2) K during all data collection. Structures were solved by the direct methods and refined by means of the ShelXL[6] program, incorporated in the OLEX2 program package.[7] Empirical absorption correction was applied

in CrysAlisPro (Agilent Technologies, 2012) program complex using spherical harmonics, implemented in SCALE3 ABSPACK scaling algorithm. CCDC numbers 2232158–2232160, 2232167–2232169, 2232172 contains the supplementary crystallographic data for this paper. These data can be obtained free of charge from the Cambridge Crystallographic Data Centre via www.ccdc.cam.ac.uk/data_request/cif.

Computational details. The calculations were performed using Gaussian 16 computer code [8] in the DFT methodology. A hybrid exchange–correlation functional B3LYP [9] was chosen for the most accurate description of experimental trends. The Stuttgart-Dresden effective core pseudopotential (SDD) and the corresponding basis set were used for platinum.[10] The Pople's 6-31G* basis set was chosen for carbon and hydrogen atoms and 6-311G* for bromine and iodine atoms, for all other atoms 6-311+G* basis set was used.[11] The 2f was necessary to be calculated using SDD for all atoms. However, this modification of the basis set did not have a significant impact that was tested on other compounds. The non-specific solvation effect of dichloroethane was taken into account by the Polarizable Continuum Model (PCM).[12] Contribution of fragments to orbitals were calculated by Hirshfeld method[13] using the Multiwfn 3.6 program.[14]

The electronic absorption spectra were calculated within TD-DFT methodology with 250 excited states for all complexes. The convoluting of UV/Vis spectra from calculated oscillator strengths was obtained using method described in ref.[15] modified for Lorentzian broadening. Emission energies were obtained as the difference between energies of optimized triplet and singlet states.

Qualitative picture of the displacement of the electron density during absorption and emission transitions was established by the construction of NTO.[16] A number of electrons transferred between the parts of the molecules has been obtained by IFCT (Interfragment charge transfer) method.[14] The Multiwfn 3.6 program[14] was used for both methods. The changes in electronic density Δρ during the $S_0 \rightarrow S_i$ transitions were calculated as:

$$\Delta\rho(S_0 \rightarrow S_i) = \sum_k |\Psi_{ik}(virt)|^2 - \sum_k |\Psi_{ik}(occ)|^2 \quad (1),$$

where Ψ_{ik}(occ) and Ψ_{ik}(virt) are NTO pairs for $S_0 \rightarrow S_i$ transition. The electronic density's change during T1 →S0 transition was calculated in analogous manner.

Synthesis of ***S1a–f***. [{Pt(ppy)(μ-Cl)}$_2$] (100 mg, 0.13 mmol) was suspended in DCE (4 mL), whereupon a solution of an isocyanide (0.26 mmol) in DCE (2 mL) was added dropwise. The reaction mixture was refluxed in air for approximately 2 h. During this period, the reaction mixture gradually turned from yellow suspension to light yellow (in case for **S1a** – dark brown) solution. The sediment had been obtained by addition of *n*-hexane (5 mL) to evaporated mixture (about 2 ml), after centrifugated residue was washed with Et_2O (three 2 mL portions) and dried in air at RT. The complexes are air- and moisture-stable at 20–200 °C; they are soluble in common aprotic solvents (e.g. CH_2Cl_2, $CHCl_3$) and in MeOH. Yields 67–86%.

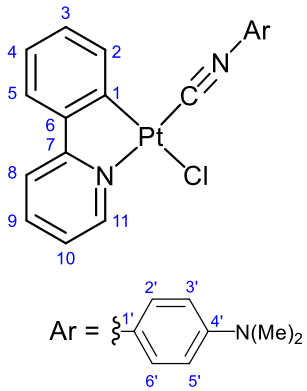

[Pt(ppy)Cl(CN-C_6H_4-4-N(Me)$_2$)] **S1a**. (23 mg, 67%). Light orange solid. Anal. Calcd. (%) for $C_{35}H_{34}N_5BF_{10}O_2Pt$: C 45.25, H 3.42, N 7.91; found: C 45.38, H 3.40, N 7.65. HR-MS ESI$^+$ *m/z*: calcd. for $C_{40}H_{36}N_6ClPt_2^+$ 1026.1979, found 1026.1972 [2M – Cl]$^+$. IR (KBr, selected bands, cm^{-1}): 2190 s (C≡N). ^{1}H NMR (400.13 MHz, $CDCl_3$, δ): 3.03 (s, 6H, Me, Ar), 6.63–6.67 (m, 2H, Ar), 7.11 (td, 1H, $J_{H,H}$ 7.4, 1.5 Hz, H^3), 7.16 (td, 1H, $J_{H,H}$ 7.5, 1.3 Hz, H^4), 7.29 (ddd, 1H, $J_{H,H}$ = 7.3, 5.8, 1.3 Hz, H^{10}), 7.39–7.43 (d, 2H, $J_{H,H}$ 8.3 Hz, Ar), 7.55 (dd, 1H, $J_{H,H}$ 7.6, 1.3 Hz, H^5), 7.59 (dd, 1H, $J_{H,H}$ 7.5, 1.0 Hz, $J_{H,Pt}$ 67.5 Hz, H^2), 7.73–7.75 (m, 1H, H^8), 7.88 (td, 1H, $J_{H,H}$ 8.0, 1.5 Hz, H^9), 9.59 (dd with Pt satellites, $J_{H,H}$ 5.8, 0.9 Hz, $J_{H,Pt}$ 28.8 Hz, 1H, H^{11}). ^{13}C{^{1}H} NMR (100.61 MHz, $CDCl_3$, δ): 40.18 (Me), 111.75 (CH from Ar), 115.13 (C-ipso from AR), 118.45 (s with Pt satellites, $J_{C,Pt}$ = 35.5 Hz, C^8), 122.14 (s with Pt satellites, $J_{C,Pt}$ = 25.8 Hz, C^{10}), 124.09 (s with Pt satellites, $J_{C,Pt}$ = 39.3 Hz, C^5), 124.43 (C^4), 127.50 (CH from Ar), 131.31 (s with Pt satellites, $J_{C,Pt}$ = 73.3 Hz, C^3), 136.25 (s with Pt satellites, $J_{C,Pt}$ = 106.3 Hz, C^2), 139.99 (C^9), 141.26 (C^1), 144.07 (C^6), 148.98 (s with Pt satellites, $J_{C,Pt}$ = 21.3 Hz, C^{11}), 150.75 (CN(Me)$_2$ from Ar), 166.39 (C^7); the $C_{isocyanide}$ resonances were not detected. ^{195}Pt{^{1}H} NMR (80.015 MHz, $CDCl_3$, δ): –3899.

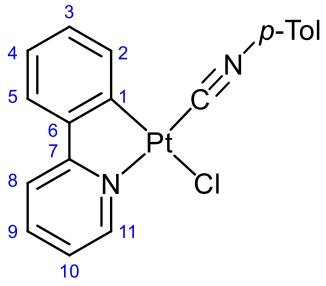

[Pt(ppy)Cl(CN*p*-Tol)] **S1b**. (24 mg, 73%). Light yellow solid. Anal. Calcd. (%) for $C_{19}H_{15}N_2ClPt$: C 45.17, H 3.01, N 5.58; found: C 45.61, H 2.94, N 5.44. HR-MS ESI$^+$ *m/z*: calcd. for $C_{19}H_{15}N_2Pt^+$ 466.0877, found 466.0883 [M – Cl]$^+$. IR (KBr, selected bands, cm^{-1}): 2187 s (C≡N). ^{1}H NMR (400.13 MHz, $CDCl_3$, δ): 2.42 (s, 3H, Me), 7.12 (td, 1H, $J_{H,H}$ 7.4, 1.5 Hz, H^3), 7.18 (td, 1H, $J_{H,H}$ 7.5, 1.2 Hz, H^4), 7.28 (d, 2H, $J_{H,H}$ 8.3 Hz, *p*-tol), 7.32 (ddd, 1H, $J_{H,H}$ = 7.3, 5.8, 1.4 Hz, H^{10}), 7.47 (d, 2H, $J_{H,H}$ 8.3 Hz, *p*-tol), 7.55–7.59 (m, 2H, H^2 and H^5), 7.75–7.77 (m, 1H, H^8), 7.90 (td, 1H, $J_{H,H}$ 7.9, 1.6 Hz, H^9), 9.59 (dd with Pt satellites, $J_{H,H}$ 5.8, 0.8 Hz, $J_{H,Pt}$ 29.4 Hz, 1H, H^{11}). ^{13}C{^{1}H} NMR (100.61 MHz, $CDCl_3$, δ): 21.52 (Me), 118.51 (C^8), 122.22 (C^{10}), 124.18 (C^5), 124.64 (C^4), 126.30 (CH from *p*-tol), 130.30 (CH from *p*-tol), 131.42 (C^3), 136.17 (C^2), 140.17 (C^9), 140.70 (CMe from *p*-tol), 141.32 (C^1), 144.05 (C^6), 149.00 (C^{11}), 166.41 (C^7); the $C_{isocyanide}$ resonances were not detected. ^{195}Pt{^{1}H} NMR (80.015 MHz, $CDCl_3$, δ): –3897.

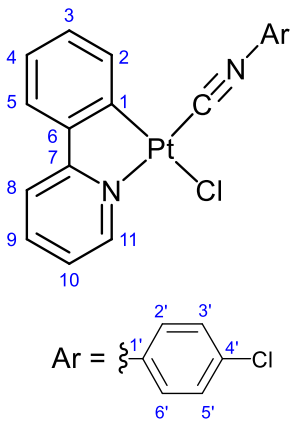

[Pt(ppy)Cl{CNC$_6$H$_4$Cl}] **S1c**. (26 mg, 75%). Light yellow solid. Anal. Calcd. (%) for $C_{18}H_{12}N_2ClPt$: C 41.39, H 2.32, N 5.36; found: C 40.91, H 2.21, N 5.30. HRESI-MS$^+$ *m/z*: calcd. for $C_{18}H_{12}ClN_2Pt^+$ 487.0333, found 487.0333 [M – Cl]$^+$. IR (KBr, selected bands, cm^{-1}): s 2195 ν(N≡C). ^{1}H NMR (400.13 MHz, $CDCl_3$, δ): 7.11 (td, 1H, $J_{H,H}$ = 7.4, 1.5 Hz, H^3), 7.16 (td, 1H, $J_{H,H}$ = 7.5, 1.2 Hz, H^4), 7.30 (ddd, 1H, $J_{H,H}$ = 7.5, 5.9, 1.2, H^{10}), 7.43–7.47 (m, 2H, 2H from C$_6$H$_4$Cl), 7.52–7.55 (m, 2H from H^2 and H^5, 2H from C$_6$H$_4$Cl), 7.73–7.75 (m, 1H, H^8), 7.89 (td, 1H, $J_{H,H}$ = 7.8, 1.5 Hz, H^9), 9.54 (dd with Pt satellites, $J_{H,H}$ = 5.8, 0.8 Hz, $J_{H,Pt}$ = 29.0 Hz, 1H, H^{11}). ^{13}C{^{1}H} NMR (100.61 MHz, $CDCl_3$, δ): 118.58 (s with Pt satellites, $J_{C,Pt}$ = 33.9 Hz, C^8), 122.24 (s with Pt satellites, $J_{C,Pt}$ = 27.7 Hz, C^{10}), 124.25 (s with Pt satellites, $J_{C,Pt}$ = 40 Hz, C^5), 124.78 (C^4), 125.90 (C–Cl from C$_6$H$_4$Cl), 127.74 (C–H from C$_6$H$_4$Cl), 130.12 (C–H from C$_6$H$_4$Cl), 131.48 (s with Pt satellites, $J_{C,Pt}$ = 70.1 Hz, C^3), 136.10 (s with Pt satellites, $J_{C,Pt}$ = 106.4 Hz, C^2), 136.23 (C-ipso from C$_6$H$_4$Cl), 140.33 (C^9), 141.37 (C^1), 144.99 (C^6), 148.94 (s with Pt satellites, $^3J_{C,Pt}$ = 23.1 Hz, C^{11}), 166.33 (C^{7}N). ^{195}Pt {^{1}H} NMR (80.015 MHz, $CDCl_3$, δ): –3883.

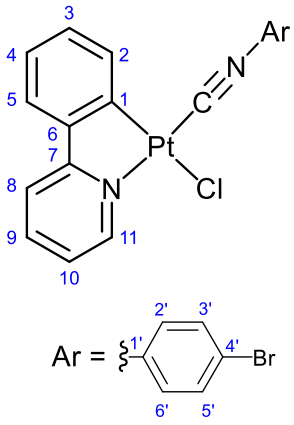

[Pt(ppy)Cl{CNC$_6$H$_4$Br}] **S1d**. (32 mg, 87%). Light green solid. Anal. Calcd. (%) for $C_{18}H_{12}N_2BrPt$: C 38.15, H 2.13, N 4.94; found: C 38.19, H 2.12, N 4.93. HRESI-MS$^+$ *m/z*: calcd. for $C_{18}H_{12}BrN_2Pt^+$ 530.9810, found 530.9814 [M – Cl]$^+$. IR (KBr, selected bands, cm^{-1}): s 2169 ν(N≡C). ^{1}H NMR (400.13 MHz, $CDCl_3$, δ): 7.09 (td, 1H, $J_{H,H}$ = 7.4, 1.4 Hz, H^3), 7.14 (td, 1H, $J_{H,H}$ = 7.4, 1.3 Hz, H^4), 7.25–7.28 (m, 1H, H^{10}), 7.42–7.44 (m, 2H, 2H from C$_6$H$_4$Br), 7.49–7.51 (m, 2H from H^2 and H^5), 7.57–7.60 (m, 2H, 2H from C$_6$H$_4$Br), 7.70–7.72 (m, 1H, H^8), 7.87 (td, 1H, $J_{H,H}$ = 8.0, 1.5 Hz, H^9), 9.49 (dd with Pt satellites, $J_{H,H}$ = 5.8, 0.8 Hz, $J_{H,Pt}$ = 28.4 Hz, 1H, H^{11}). ^{13}C{^{1}H} NMR (100.61 MHz, $CDCl_3$, δ): 118.60 (s with Pt satellites, $^3J_{C,Pt}$ = 35.6 Hz, C^8), 122.24 (s with Pt satellites, $J_{C,Pt}$ = 26.1 Hz, C^{10}), 124.23 (C$_{Ar}$Br from C$_6$H$_4$Br), 124.24 (s with Pt satellites, $J_{C,Pt}$ = 19.6 Hz, C^5), 124.75 (C^4), 126.39 (CN from CNC$_6$H$_4$Br), 127.92 (C$_{Ar}$H from C$_6$H$_4$Br), 131.47 (s with Pt satellites, $J_{C,Pt}$ = 72.1 Hz, C^3), 133.05 (C$_{Ar}$H from C$_6$H$_4$Br), 136.10 (s with Pt satellites, $J_{C,Pt}$ = 104.6 Hz, C^2), 140.33 (C^9), 141.38 (s with Pt satellites, $J_{C,Pt}$ = 1005.1 Hz, C^1), 143.93 (s with Pt satellites, $J_{C,Pt}$ = 34.8 Hz, C^6), 148.86 (s with Pt satellites, $J_{C,Pt}$ = 21.5 Hz, C^{11}), 166.25 (s with Pt satellites, $J_{C,Pt}$ = 95.1 Hz, C^{7}N). ^{195}Pt {^{1}H} NMR (80.015 MHz, $CDCl_3$, δ): –3879.

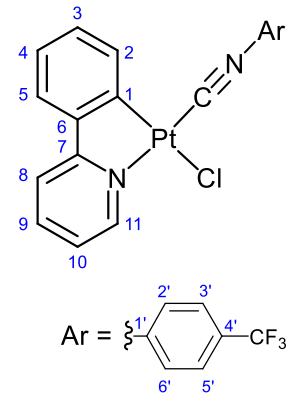

[Pt(ppy)Cl(CNC$_6$H$_4$-4-CF$_3$)] **S1f**. (26 mg, 73%). Light green solid. Anal. Calcd. (%) for $C_{19}H_{12}N_2ClF_3Pt$: C 41.06, H 2.18, N 5.04; found: C 41.19, H 2.11, N 4.92. HR-MS ESI$^+$ *m/z*: calcd. for $C_{19}H_{12}F_3N_2Pt^+$ 520.0597, found 520.0595 [M – Cl]$^+$. IR (KBr, selected bands, cm^{-1}): 2194 s (C≡N). ^{1}H NMR (400.13 MHz, $CDCl_3$, δ): 7.08 (td, 1H, $J_{H,H}$ 7.3, 1.7 Hz, H^3), 7.12 (td, 1H, $J_{H,H}$ 7.4, 1.5 Hz, H^4), 7.23–7.26 (m, 1H, H^{10}), 7.49 (ddd, $J_{H,H}$ 12.7, 7.3, 1.4 Hz, 2H, H^2 and H^5), 7.68–7.73 (m, 5H, H^8 and 4H from C$_6$H$_4$-4-CF$_3$), 7.85 (td, 1H, $J_{H,H}$ 7.9, 1.6 Hz, H^9), 9.46 (dd with Pt satellites, 1H, $J_{H,H}$ 5.8, 1.0 Hz, $J_{H,Pt}$ 28.4 Hz, H^{11}). ^{13}C{^{1}H} NMR (100.61 MHz, $CDCl_3$, δ): 118.61 (s with Pt satellites, $J_{C,Pt}$ 35.1 Hz, C^8), 122.26 (s with Pt satellites, $J_{C,Pt}$ 26.6 Hz, C^{10}),

123.21 (q, $J_{C,F}$ 272.8 Hz, CF_3), 123.55 ($C^{1'}$)124.25 (s with Pt satellites, $J_{C,Pt}$ 38.9 Hz, C^5), 124.80 (C^4), 127.03 (q, $J_{C,F}$ 3.8 Hz, $C^{3'}$ and $C^{5'}$), 127.08($C^{2'}$ and $C^{6'}$), 131.49 (s with Pt satellites, $J_{C,Pt}$ 71.6 Hz, C^3), 131.83 (q, $J_{C,F}$ 33.4 Hz, $C^{4'}$-CF_3), 133.01 ($C_{isocyanide}$), 136.11 (s with Pt satellites, $J_{C,Pt}$ 105.3 Hz, C^2), 140.37 (C^9), 141.51 (s with Pt satellites, $J_{C,Pt}$ 1004.0 Hz, C^1), 143.86 (s with Pt satellites, $J_{C,Pt}$ 35.4 Hz, C^6), 148.83 (s with Pt satellites, $J_{C,Pt}$ 21.0 Hz, C^{11}), 166.18 (C^7). $^{195}Pt\{^1H\}$ NMR (80.015 MHz, $CDCl_3$, δ): –3866. ^{19}F NMR (376.50 MHz, $CDCl_3$, δ): –63.0.

*General procedure for the synthesis of **1a–f** and **2a–f**.* The morpholine (44 mg, 0.40 mmol) was added to a solution of **S1a**–**f**) (0.04 mmol) or a suspension **S2a**–**f** (0.04 mmol) in CH_2Cl_2 (2 mL) at RT. The reaction mixture was ultrasound-treated for 1–2 min until formation a homogeneous colorless solution of reaction mixture. The solvent was evaporated to a volume of 2 mL and then *n*-heptane (5 mL) was added. The formed solid product was separated by centrifugation, washed with three 2 mL portions of Et_2O and then dried in air at RT.

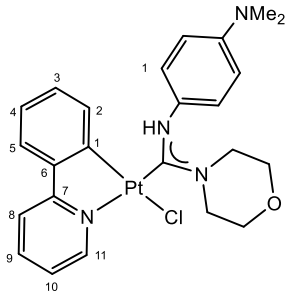

1a. Pale yellow solid (20 mg, yield 80%). Anal. Calcd. (%) for $C_{24}H_{27}N_4ClOPt$: C 46.64, H 4.40, N 9.07; found: C 46.18, H 4.47, N 8.90. HR-MS ESI$^+$ *m/z*: calcd. for $C_{24}H_{27}N_4OPt^+$ 582.1829, found 582.1816 [M–Cl]$^+$. IR (KBr, selected bands, cm^{-1}): 1481 (s) *ν*(C=N and C=C from Ar), 1520 (vs), 1541 (vs) ν(N–$C_{carbene}$), 1585 (s), 1609 (s), 2924 (m-w), 3250 (m), 3327 (m) *ν*(N−H). ^1H NMR (400.13 MHz, $CDCl_3$, δ): 2.82 (s, 6H, Me), 3.62–3.91 (m, 6H, CH_2), 4.64–4.79 (m, 2H, CH_2), 6.52 (d, $J_{H,H}$ = 8.9, 2H, H_{Ar} from $C_6H_4NMe_2$), 7.00–7.08 (m, 2H, H^3 and H^4), 7.13–7.17 (m, 1H, H^{10}), 7.22 (dd, 1H, $J_{H,H}$ = 7.0, 1.5, H^2), 7.42–7.47 (m, 3H, H^5 and H_{Ar} from $C_6H_4NMe_2$), 7.58–7.61 (m, 2H, H^8 and NH), 7.74 (td, $J_{H,H}$ = 8.0, 1.5, 1H, H^9), 9.41–9.43 (m, 1H, H^{11}). $^{13}C\{^1H\}$ NMR (100.61 MHz, $CDCl_3$, δ): 31.88 (Me), 40.52 (Me), 65.80 (CH_2), 67.23 (CH_2), 112.24 (C_{Ar}–H from $C_6H_4NMe_2$), 117.84 (C^8), 121.84 (C^{10}), 122.58 (C^5), 123.49 (C^4), 126.87 (C_{Ar}–H from $C_6H_4NMe_2$), 130.31 (C^3), 134.56 (C^2), 138.18 (C^9, C_{Ar}–NMe_2), 142.14 (C^1), 144.37 (C^6), 148.72 (C^1), 148.75 (C_{Ar}–ipso from $C_6H_4NMe_2$), 164.97 (C^7), 185.18 ($C_{carbene}$). ^{195}Pt $\{^1H\}$ NMR (86.015 MHz, $CDCl_3$, δ): –3619.

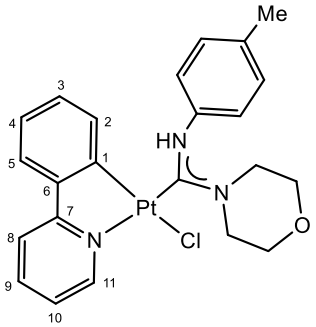

1b. Yield 21 mg, 88%. Light green solid. Calcd. (%) for $C_{23}H_{24}ClN_3OPt$: C 46.80, H 4.11, N 7.13; found: C 47.22, H 4.05, N 7.02. HRESI-MS+ m/z: calcd. for C23H25N3OPt+ 553.1619, found 553.1525 [M-Cl]+. IR (KBr, selected bands, cm–1): 763 (m), 816 (m) δ (C–H); 1027 (m), 1063 (m), 1524 (s) δ(N–H), 1540 (s) ν(N–Ccarbene), 1610 (s), 3347 (m) ν(N–H). 1H NMR (400.13 MHz, CDCl3, δ): 2.19 (s, 3H, Me), 3.70–3.94 (m, 6H, morpholine), 4.64–4.69 (m, 1H, morpholine), 4.81–4.86 (m, 1H, morpholine), 6.98 (d, 2H, JH,H = 8.2, 2H from p-tol), 7.02–7.08 (m, 2H, H3 and H4), 7.15–7.20 (m, 2H, H10 and H5), 7.45 (dd, 1H, JH,H = 7.5, 1.4, H2), 7.56–7.64 (m, 4H, H8, NH-carbene and 2H from p-tol), 7.76 (td, 1H, JH,H = 7.9, 1.6, H9), 9.43 (dd, 1H, JH,H = 5.6, 0.9, H11). 13C{1H} NMR (100.61 MHz, CDCl3, δ): 20.97 (Me from p-tol), 45.86, 55.98, 65.77, 67.38 (C from morpholine); 117.89 (C8), 121.92 (C10), 122.72 (C5), 123.53 (C4), 125.10 (C–H from p-tol), 129.23 (C–H from p-tol), 130.38 (C3), 134.43 (C2), 135.58 (C–Me from p-tol), 137.67 (C–ipso from p-tol), 138.28 (C9), 141.96 (C1), 144.36 (C6), 148.78 (C11), 164.97 (C7), 185.30 (C-carbene). 195Pt {1H} NMR (86.015 MHz, CDCl3, δ): –3608.

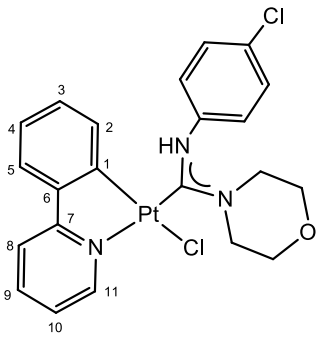

1c. Yield 20 mg, 83%. Light yellow solid. Anal. Calcd. (%) for $C_{22}H_{21}Cl_2N_3OPt$: C 46.36, H 3.47, N 6.90; found: C 45.88, H 3.55, N 6.78. HRESI-MS$^+$ *m/z*: calcd. for $C_{22}H_{21}ClN_3Pt^+$ 574.1011, found 574.1026 [M–Cl]$^+$**.** IR (KBr, selected bands, cm^{-1}): 1043 (m), 1104 (s), 1310 (m), 1432 (m), 1452 (m) *ν*(N–$C_{carbene}$ and C=C from Ar), 1549 (m) ν(N–$C_{carbene}$), 3287 (m), 3417 (m) ν(N–H). ^{1}H NMR (400.13 MHz, $CDCl_3$, δ): 3.75–3.91 (m, 6H, CH_2), 4.65–4.71 (m, 1H, CH_2, 4.80–4.85 (m, 1H, CH_2), 7.07 (td, 1H, $J_{H,H}$ = 7.4, 1.4 Hz, H^3), 7.07 (td, 1H, $J_{H,H}$ = 7.5, 1.4 Hz, H^4), 7.10–7.15 (m, 2H, H_{Ar} from C_6H_4Cl), 7.21 (ddd, 1H, $J_{H,H}$ = 7.5, 5.7, 1.3, H^{10}), 7.46 (dd, 1H, $J_{H,H}$ = 7.5, 1.4, H^5), 7.64–7.75 (m, 4H, H^2, H^8 and H_{Ar} from C_6H_4Cl), 7.78 (td, 1H, $J_{H,H}$ = 7.8, 1.6 Hz, H^9), 7.84 (br, 1H, $NH_{carbene}$), 9.37 (dd, 1H, $J_{H,H}$ = 5.7, 0.9 Hz, H^{11}). ^{13}C{^{1}H} NMR (100.61 MHz, $CDCl_3$, δ): 44.16 (CH_2), 46.16 (CH_2), 56.20 (CH_2), 67.31(CH_2), 118.58 (C^8), 122.05 (C^{10}), 122.97 (C^5), 123.67 (s with Pt satellites, $J_{C,Pt}$ = 48 Hz, C^4), 126.44 (C_{Ar}–H from C_6H_4Cl), 128.57 (C_{Ar}–H from C_6H_4Cl), 130.49 (C_{Ar}–Cl from C_6H_4Cl), 131.20 (C^3), 134.21 (C^2), 138.50 (C_{Ar}-ipso from C_6H_4Cl), 139.07 (C^9), 141.46 (C^1), 144.35 (C^6), 148.66 (C^{11}), 164.92 (C^7), 185.31 ($C_{carbene}$). ^{195}Pt {^{1}H} NMR (80.015 MHz, $CDCl_3$, δ): –3606.

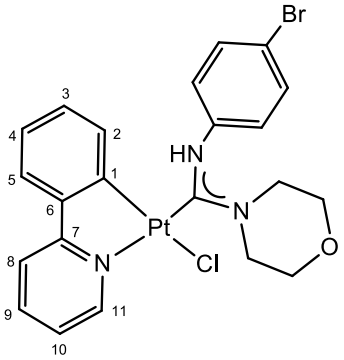

1d. Yield 24 mg, 92%. Light yellow solid. Anal. Calcd. (%) for $C_{22}H_{21}ClBrN_3OPt$: C 40.41, H 3.24, N 6.90; found: C 40.06, H 3.25, N 6.80. HRESI-MS$^+$ *m/z*: calcd. for $C_{22}H_{21}N_3OBrPt^+$ 618.0496, found 618.0512 [M–Cl]$^+$. IR (KBr, selected bands, cm^{-1}): 1227 (s), 1264 (s), 1307 (s), 1330 (s), 1424 (s), 1465 (s), 1486 (vs) *ν*(C=N and C=C from Ar); 1541 (vs), 1602 (s), 3258 (m) *ν*(N−H). ^{1}H NMR (400.13 MHz, $CDCl_3$, δ): 3.73–3.93 (m, 6H, CH_2), 4.66–4.84 (m, 6H, CH_2), 7.01 (td, 1H, $J_{H,H}$ 7.3, 1.3 Hz, H^3), 7.07 (td, 1H, $J_{H,H}$ 7.4, 1.0 Hz, H^4), 7.13 (dd, 1H, $J_{H,H}$ 7.4, 0.7 Hz, H^2), 7.18–7.21 (m, 1H, H^{10}), 7.27–7.30 (m, 2H, H_{Ar} from C_6H_4Br), 7.46 (dd, 1H, $J_{H,H}$ 7.7, 0.9, H^5), 7.54 (br, 0.3H, $NH_{carbene}$), 7.64–7.67 (m, 3H, H^8, H_{Ar} from C_6H_4Br), 7.79 (td, 1H, $J_{H,H}$ = 8.0, 1.5 Hz, H^9), 9.39 (dd, 1H, $J_{H,H}$ = 5.6, 0.7, 1H, H^{11}). ^{13}C{^{1}H} NMR (100.61 MHz, $CDCl_3$, δ): 46.03 (CH_2), 46.22 (CH_2), 56.22 (CH_2), 67.32 (CH_2), 118.02 (C^8), 119.23 (C_{Ar}–Br from C_6H_4Br), 122.04 (C^{10}), 122.96 (C^5), 123.68 (C^4), 126.80 (C_{Ar}–H from C_6H_4Br), 130.46 (C^3), 131.55 (C_{Ar}–H from C_6H_4Br), 134.16 (C^2), 138.49 (C^9), 139.49 (C_{Ar}–ipso from C_6H_4Br), 141.55 (C^1), 144.38 (C^6), 148.71 (C^{11}), 164.92 (C^{7}N), 185.46 ($C_{carbene}$). ^{195}Pt {^{1}H} NMR (80.015 MHz, $CDCl_3$, δ): –3606.

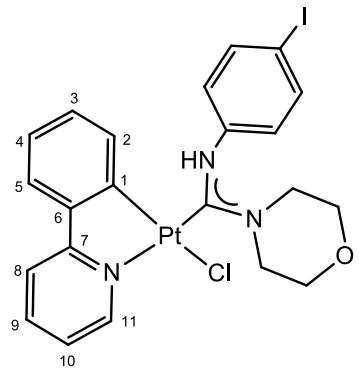

1e. Yield 23 mg, 82%. Light yellow solid. Anal. Calcd. (%) for $C_{22}H_{21}ClIN_3OPt$: C 37.70, H 3.02, N 6.00; found: C 36.85, H 2.97, N 6.15. HRESI-MS$^+$ *m/z*: calcd. for $C_{22}H_{22}ClIN_3Pt^+$ 700.0117, found 700.0126 [M+H]$^+$. IR (KBr, selected bands, cm^{-1}): 1268 (s), 1326 (vs), 1484 (s) *ν*(C=N and C=C from Ar); 1539 (s) *ν*(N–$C_{carbene}$); 1584 (s), 1605 (vs) *δ* (N–H); 3284 (m) ν(N−H). ^{1}H NMR (400.13 MHz, DMSO-d_6, δ): 4.42–4.46 (m, 1H, CH_2), 4.53–4.62 (m, 3H, CH_2), 3.90 (t, 2H, $J_{H,H}$ 4.3 Hz, CH_2), 4.42–4.46 (m, 1H, CH_2), 4.53–4.62 (m, 1H, CH_2), 6.96–7.03 (m, 2H, H^3 and H^4), 7.11 (dd, 1H, $J_{H,H}$ = 7.1, 1.4, H^2), 7.18 (br, 0.2H, $NH_{carbene}$), 7.41–7.45 (m, 1H, H^{10}), 7.15 (d, 2H, $J_{H,H}$ = 8.6 Hz, H_{Ar} from C_6H_4I), 7.61 (dd, 1H, $J_{H,H}$ = 7.6, 1.4, H^5), 7.64 (d, 2H, $J_{H,H}$ = 8.7 Hz, H_{Ar} from C_6H_4I), 7.96–8.04 (m, 2H, H^8 and H^9), 9.29 (d, 1H, $J_{H,H}$ = 5.3 Hz, H^{11}), 9.37 (br, 1H, $NH_{carbene}$). ^{13}C{^{1}H}

NMR (100.61 MHz, DMSO-d_6, δ): 47.43 (CH_2), 56.40 (CH_2), 66.30 (CH_2), 67.05 (CH_2), 89.96 (C_{Ar}–I from C_6H_4I), 119.21 (C^8), 122.93 (C^{10}), 123.01(C^5), 124.45 (C^4), 127.34 (C_{Ar}–H from C_6H_4I), 130.85 (C^3), 134.30 (C^2), 136.91 (C_{Ar}–H from C_6H_4I), 139.85 (C^9), 142.18 (C_{Ar}–ipso from C_6H_4I), 142.33 (C^1), 144.43 (C^6), 148.20 (C^{11}), 164.83 (C^7), 183.16 ($C_{carbene}$). ^{195}Pt {^{1}H} NMR (80.015 MHz, $CDCl_3$, δ): –3582.

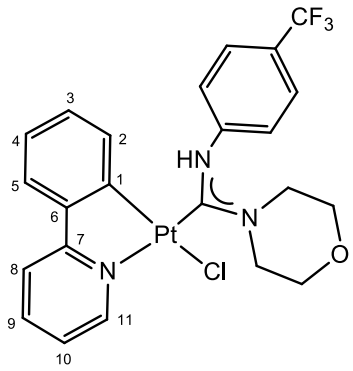

1f. Yield 24 mg, 92%. Light green solid. Anal. Calcd. (%) for $C_{23}H_{21}N_3ClF_3OPt$: C 42.97, H 3.29, N 6.54; found: C 43.05, H 3.37, N 6.45. HRESI-MS$^+$ *m/z*: calcd. for $C_{23}H_{21}F_3N_3Pt^+$ 607.1318, found 607.1318 $[M–Cl]^+$. IR (KBr, selected bands, cm^{-1}): 1112 (s), 1164 (s), 1322 (vs), 1482 (m) *ν*(C=N and C=C from Ar); 1548 (s) *ν*(N–$C_{carbene}$); 1608 (s) *δ* (N–H); 3446 (m) ν(N−H). ^{1}H NMR (400.13 MHz, $CDCl_3$, δ): 3.71–3.93 (m, 6H, CH_2), 4.74–4.82 (m, 2H, CH_2), 7.01 (td, $J_{H,H}$ = 7.3, 1.3, 1H, H^3), 7.09 (td, $J_{H,H}$ = 7.5, 1.2, 1H, H^4), 7.13 (dd, 1H, $J_{H,H}$ = 7.4, 1.0, H^2), 7.41 (ddd, $J_{H,H}$ = 7.3, 1.3, 1H, H^{10}), 7.43 (d, 2H, $J_{H,H}$ = 8.5 Hz, H from $C_6H_4CF_3$), 7.48 (dd, 1H, $J_{H,H}$ = 7.6, 1.1, H^5), 7.67 (d, 1H, $J_{H,H}$ = 8.1 Hz, H^8), 7.81 (td, $J_{H,H}$ = 8.0, 1.6, 1H, H^9), 7.85 (br, 0.7H, NH-carbene), 8.02 (d, 2H, $J_{H,H}$ = 8.4 Hz, H from $C_6H_4CF_3$), 9.41 (dd, 1H, $J_{H,H}$ = 5.7, 0.9 Hz, H^{11}). ^{13}C{^{1}H} NMR (100.61 MHz, $CDCl_3$, δ): 46.52 (CH_2), 56.67 (CH_2), 65.80 (CH_2), 67.23 (CH_2), 118.09 (C^8), 122.10 (C^{10}), 123.13(C^5), 123.75 (C^4), 124.16 (C–H from $C_6H_4CF_3$), 125.74 (q, $J_{C,F}$ = 3.7 Hz, C_{Ar}–H from $C_6H_4CF_3$), 127.04 (q, $J_{C,F}$ = 2.7 Hz, C_{Ar}–CF_3 from $C_6H_4CF_3$), 130.59 (C^3), 134.17 (C^2), 138.61 (C^9), 141.42 (C_{Ar}–ipso from $C_6H_4CF_3$), 143.54 (C^1), 144.39 (C^6), 148.72 (C^{11}), 164.95 (C^7), 186.40 ($C_{carbene}$). CF_3 wasn't detected. ^{19}F NMR (376.50 MHz, $CDCl_3$, δ): –62.2. ^{195}Pt {^{1}H} NMR (86.015 MHz, $CDCl_3$, δ): –3598.

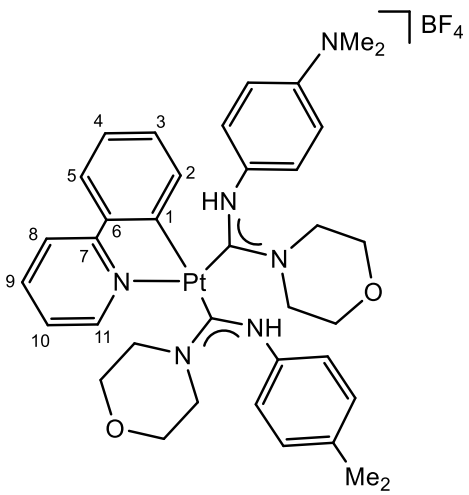

2a. Yield 29 mg, 76%. Light yellow solid. Anal. Calcd. (%) for $C_{37}H_{46}N_7BF_4O_2Pt$: C 49.23, H 5.14, N 10.86; found: C 50.05, H 5.21, N 10.77. HRESI-MS$^+$ *m/z*: calcd. for $C_{37}H_{46}N_7O_2Pt^+$ 815.3355, found 815.3340 $[M–BF_4]^+$. IR (KBr, selected bands, cm^{-1}): 1112 (s), 1334 (s), 1480 (m) *ν*(C=N and C=C from Ar); 1521 (vs), 1538 (vs) *ν*(N–$C_{carbene}$); 1607 (s) *δ* (N–H); 3236 (m), 3347 (m), 3419 (m) ν(N−H). ^{1}H NMR (400.13 MHz, $CDCl_3$, δ): 2.84 (d, 12H, $J_{H,H}$ = 2.6 Hz, Me), 3.05–3.29 (m, 7H, CH_2), 3.45–3.82 (m, 7H, CH_2), 4.27 (d, 1H, $J_{H,H}$ = 14.1 Hz, CH_2), 4.40 (d, 1H, $J_{H,H}$ = 13.9 Hz, CH_2), 6.59–6.62 (m, 4H, H_{Ar} from $C_6H_4N(CH_3)_2$), 7.19–7.30 (m, 5H, H^3, H^4, H^{10}, H_{Ar} from $C_6H_4N(CH_3)_2$), 7.43 (d, 2H, $J_{H,H}$ = 13.9 Hz, H_{Ar} from $C_6H_4N(CH_3)_2$), 7.49 (dd, 1H, $J_{H,H}$ = 7.1, 1.0 Hz, H^2), 7.68 (dd, 1H, $J_{H,H}$ = 7.1, 1.0 Hz, H^5), 7.89–7.91 (m, 1H, H^8), 7.97–8.07 (m, 2H, H^9, $NH_{carbene}$), 8.52 (br, 1H, $NH_{carbene}$), 8.65 (s, 1H, $J_{H,H}$ = 5.0, H^{11}). ^{13}C{^{1}H} NMR (100.61 MHz, $CDCl_3$, δ): 31.88, 40.88, 40.91 (Me), 44.49 (CH_2), 45.33 (CH_2), 51.68 (CH_2), 53.47 (CH_2), 65.32 (CH_2), 65.72 (CH_2), 66.47 (CH_2), 66.94 (CH_2), 113.18, 113.25, 119.74 (C^8), 123.39 (C^{10}), 123.99 (C_{Ar} from $C_6H_4N(Me)_2$), 124.05 (C^4), 124.96(C^5), 125.24, 131.05, 131.08 (C_{Ar} from $C_6H_4N(Me)_2$), 131.24 (C^3), 137.33 (C^2), 139.05 (C^9), 146.01 (C_{Ar}–$N(Me)_2$ from $C_6H_4N(Me)_2$), 148.82 (C–ipso from $C_6H_4N(CH_3)_2$), 148.84 (C^1), 151.00 (C^{11}), 158.19 (C^6), 167.94 (C^7N), 178.99 ($C_{carbene}$), 199.93 ($C_{carbene}$). ^{195}Pt {^{1}H} NMR (80.015 MHz, $CDCl_3$, δ): –3573.

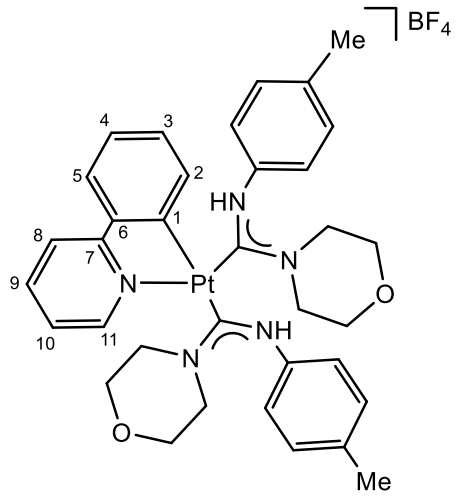

2b. Yield 30 mg, 83%. Light green solid. Anal. Calcd. (%) for $C_{35}H_{40}N_5BF_4O_2Pt$: C 49.77, H 4.77, N 8.29; found: C 50.11, H 4.81, N 8.34. HRESI-MS$^+$ *m/z*: calcd. for $C_{35}H_{40}N_5O_2Pt^+$ 757.2824, found 757.2780 $[M–BF_4]^+$. IR (KBr, selected bands, cm^{-1}): 1112 (s), 1334 (s), 1480 (m) *ν*(C=N and C=C from Ar); 1521 (vs), 1538 (vs) *ν*(N–$C_{carbene}$); 1607 (s) *δ* (N–H); 3236 (m), 3347 (m), 3419 (m) ν(N−H). ^{1}H NMR (400.13 MHz, $CDCl_3$, δ): 2.84 (d, 12H, $J_{H,H}$ = 2.6 Hz, Me), 3.04–4.10 (m, 14H, CH_2), 4.26 (d, 1H, $J_{H,H}$ = 13.2 Hz, CH_2), 4.39 (d, 1H, $J_{H,H}$ = 13.4 Hz, CH_2), 7.05 (t, 3H, $J_{H,H}$ = 4.9, H^3, H^4, H_{Ar} from *p*-tol), 7.22–7.28 (m, 3H, H^{10}, H_{Ar} from *p*-Tol), 7.34 (d, 2H, $J_{H,H}$ = 8.3 Hz, H_{Ar} from *p*-tol), 7.46–7.52 (m, 3H, H^2, H_{Ar} from *p*-tol), 7.70–7.72 (dd, 1H, $J_{H,H}$ = 7.6, 1.1 Hz, H^5), 7.90–7.92 (m, 1H, H^8), 7.98–8.02 (m, 1H, H^9), 8.11 (br, 1H, $NH_{carbene}$), 8.58 (br, 1H, $NH_{carbene}$), 8.63 (d, 1H, $J_{H,H}$ = 5.0, H^{11}). ^{13}C{^{1}H} NMR (100.61 MHz, $CDCl_3$, δ): 20.76 (Me), 20.80, (Me), 44.81 (CH_2), 45.68 (CH_2), 52.03 (CH_2), 53.69 (CH_2), 65.38 (CH_2), 65.75 (CH_2), 66.41(CH_2), 66.92 (CH_2), 119.86 (C^8), 123.29 (C^{10}), 123.45, 123.55 (C_{Ar} from *p*-tol), 124.11 (C^4), 124.25(C^5), 129.73, 129.86 (C_{Ar} from *p*-tol), 131.20 (C^3), 134.73, 134.90 (C_{Ar} from *p*-tol), 137.37 (C^2), 139.04 (C^9), 139.20, 139.23, 145.98 (C^1), 151.02 (C^{11}), 157.44 (C^6), 168.00 (C^7N), 179.06 ($C_{carbene}$), 200.95 ($C_{carbene}$). ^{195}Pt {^{1}H} NMR (80.015 MHz, $CDCl_3$, δ): –3552.

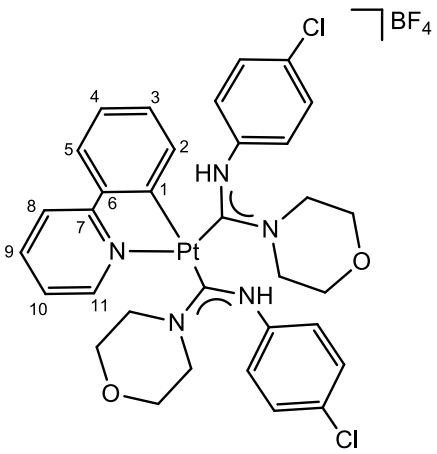

2c. Yield 28 mg, 88%. Light yellow solid. Anal. Calcd. (%) for $C_{33}H_{34}N_5BCl_2F_4O_2Pt$: C 44.76, H 3.87, N 7.91; found: C 44.94, H 3.80, N 7.79. Anal. HRESI-MS$^+$ *m/z*: calcd. for $C_{33}H_{34}N_5Cl_2O_2Pt^+$ 797.1723, found 797.1727 $[M–BF_4]^+$. IR (KBr, selected bands, cm^{-1}): 1108 (s), 1330 (s), 1489 (vs) *ν*(C=N and C=C from Ar); 1544 (vs), 1590 (s) *ν*(N–$C_{carbene}$); 1608 (s) *δ* (N–H); 3264 (m), 3423 (m) ν(N−H). ^{1}H NMR (400.13 MHz, $CDCl_3$, δ): 3.15–4.08 (m, 14H, CH_2), 4.33 (d, 1H, $J_{H,H}$ = 13.8 Hz, CH_2), 4.46 (d, 1H, $J_{H,H}$ = 13.4 Hz, CH_2), 7.20–7.29 (m, 5H, H^3, H^4, H^{10}, H_{Ar} from C_6H_5Cl), 7.45–7.51 (m, 3H, H^2, H_{Ar} from C_6H_5Cl), 7.66–7.69 (m, 3H, H^5, H_{Ar} from C_6H_5Cl), 7.92–7.96 (m, 1H, H^8), 7.98–8.03 (m, 1H, H^9), 7.92 (d, 1H, $J_{H,H}$ = 5.1 Hz, H^{11}), 9.14 (br, 1H, $NH_{carbene}$), 9.60 (br, 1H, $NH_{carbene}$). ^{13}C{^{1}H} NMR (100.61 MHz, $CDCl_3$, δ): 43.19 (CH_2), 46.47 (CH_2), 47.20 (CH_2), 52.29 (CH_2), 54.02 (CH_2), 65.57 (CH_2), 65.97 (CH_2), 66.25 (CH_2), 66.86 (CH_2), 120.07 (C^8), 123.50 (C^{10}), 124.30 (C^4), 124.50 (C_{Ar} from C_6H_4Cl), 124.58 (C_{Ar} from C_6H_4Cl), 124.74 (C^5), 129.08 (C_{Ar}–H from C_6H_4Cl), 129.21 (C_{Ar}–H from C_6H_4Cl), 130.22 (C_{Ar}-ipso from C_6H_4Cl), 130.48 (C_{Ar}-ipso from C_6H_4Cl), 131.37 (C^3), 137.33 (C^2), 139.45 (C^9), 140.62 (C_{Ar}–Cl from Ar), 140.70 (C_{Ar}–Cl from Ar), 146.01 (C^1), 150.83 (C^{11}), 156.89 (C^6), 168.05 (C^7N), 179.47 ($C_{carbene}$), 201.76 ($C_{carbene}$). ^{195}Pt {^{1}H} NMR (80.015 MHz, $CDCl_3$, δ): –3527.

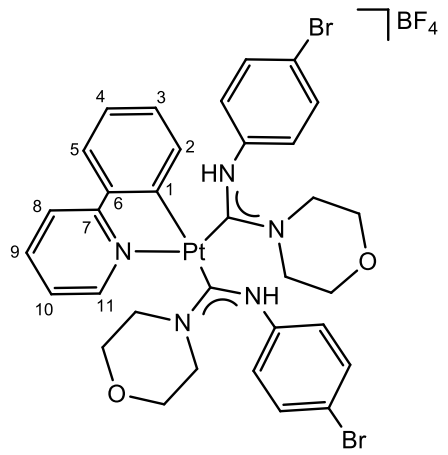

2d. Yield 38 mg, 93%. Light yellow solid. Anal. Calcd. (%) for $C_{33}H_{34}N_5BCl_2F_4O_2Pt$: C 44.76, H 3.87, N 7.91; found: C 44.94, H 3.80, N 7.79. HRESI-MS$^+$ *m/z*: calcd. for $C_{33}H_{34}N_5O_2Br_2Pt^+$ 888.0704, found 888.0717 $[M–BF_4]^+$. IR (KBr, selected bands, cm^{-1}): 1116 (s), 1316 (s), 1486 (s) ν(C=N and C=C from Ar); 1538 (vs), 1586 (s) ν(N–$C_{carbene}$); 1603 (m) δ (N–H); 3224 (m), 3419 (m) ν(N−H). ^{1}H NMR (400.13 MHz, $CDCl_3$, δ): 3.15–3.36 (m, 6H, CH_2), 3.49 (t, 1H, $J_{H,H}$ = 9.7 Hz, CH_2), 3.55 (t, 1H, $J_{H,H}$ = 9.7 Hz, CH_2), 3.78 (d, 1H, $J_{H,H}$ = 11.9 Hz, CH_2), 3.85 (d, 1H, $J_{H,H}$ = 11.9 Hz, CH_2), 4.05–4.11 (m, 2H, $J_{H,H}$ = 9.7 Hz, CH_2), 4.33 (d, 1H, $J_{H,H}$ = 13.8 Hz, CH_2), 4.46 (d, 1H, $J_{H,H}$ = 13.4 Hz, CH_2), 7.20–7.29 (m, 5H, H^3, H^4, H^{10}, H_{Ar} from C_6H_4Br), 7.45–7.51 (m, 3H, H^2, H_{Ar} from C_6H_4Br), 7.66–7.69 (m, 3H, H^5, H_{Ar} from C_6H_4Br), 7.92–7.96 (m, 1H, H^8), 7.98–8.03 (m, 1H, H^9), 7.92 (d, 1H, $J_{H,H}$ = 5.1 Hz, H^{11}), 9.14 (br, 1H, $NH_{carbene}$), 9.60 (br, 1H, $NH_{carbene}$). $^{13}C\{^1H\}$ NMR (100.61 MHz, $CDCl_3$, δ): 45.95 (CH_2), 46.74 (CH_2), 52.45 (CH_2), 54.09 (CH_2), 65.46 (CH_2), 65.84 (CH_2), 66.28 (CH_2), 66.87 (CH_2), 120.10 (C^8), 123.57 (C^{10}), 124.34 (C^4), 124.91 (C_{Ar} from C_6H_4Br), 124.65 (C_{Ar} from C_6H_4Br), 124.74 (C^5), 131.42 (C_{Ar} from C_6H_4Br), 131.65 (C_{Ar} from C_6H_4Br), 132.08 (C_{Ar}-ipso from C_6H_4Br), 132.22 (C_{Ar}-ipso from C_6H_4Br), 131.37 (C^3), 137.26 (C^2), 133.48 (C^9), 140.90 (C_{Ar}-Br from C_6H_4Br), 140.99 (C_{Ar}-Br from C_6H_4Br), 145.98 (C^1), 150.83 (C^{11}), 156.61 (C^6), 168.05 (C^7N), 179.57 ($C_{carbene}$), 201.71 ($C_{carbene}$). ^{195}Pt $\{^1H\}$ NMR (80.015 MHz, $CDCl_3$, δ): –3527.

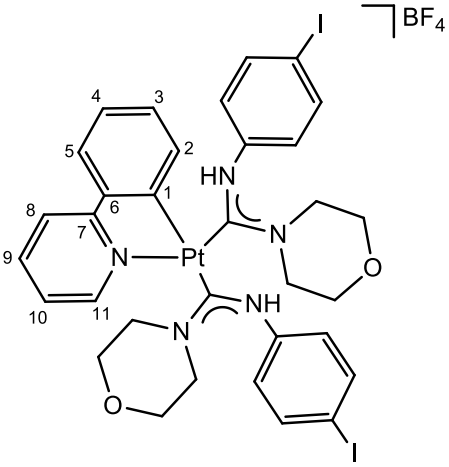

2e. Yield 41 mg, 91%. Light yellow solid. Anal. Calcd. (%) for $C_{33}H_{34}N_5BBr_2F_4O_2Pt$: C 40.68, H 3.52, N 7.19; found: C 45.02, H 3.63, N 7.10. HRESI-MS$^+$ *m/z*: calcd. for $C_{33}H_{34}N_5I_2O_2Pt^+$ 981.0441, found 981.0452 $[M–BF_4]^+$. IR (KBr, selected bands, cm^{-1}): 1108 (s), 1311 (s), 1481 (vs) ν(C=N and C=C from Ar); 1537 (s), 1583 (m) ν(N–$C_{carbene}$); 1604 (m) δ (N–H); 3346 (m), 3610 (m) ν(N−H). ^{1}H NMR (400.13 MHz, $CDCl_3$, δ): 3.14–3.93 (m, 14H, morpholine), 4.30 (d, 1H, $J_{H,H}$ = 13.9 Hz, CH_2O-morpholine), 4.41 (d, 1H, $J_{H,H}$ = 13.8 Hz, CH_2O-morpholine), 7.21–7.29 (m, 5H, H^3, H^4, H^{10}, C_6H_4I), 7.42–7.45 (m, 2H, C_6H_4I), 7.53–7.59 (m, 3H, C_6H_4I, H^2), 7.67–7.69 (m, 1H, H^5), 7.92–7.94 (m, 1H, H^8), 8.00–8.07 (m, 1H, H^9), 8.50 (br, 1H, NH-carbene), 8.58 (d, 1H, $J_{H,H}$ = 4.8 Hz, H^{11}), 8.93 (br, 1H, NH-carbene). $^{13}C\{^1H\}$ NMR (100.61 MHz, $CDCl_3$, δ): 43.63, 46.61, 52.51, 54.12, 65.41, 65.78, 66.28, 66.87 (C-morpholine); 120.11 (C^8), 123.57 (C^{10}), 124.36 (C^4), 124.66(C^5), 124.95 (C from C_6H_4I), 125.21(C from C_6H_4I), 131.45 (C^3), 137.19 (C^2), 138.07 (C from C_6H_4I), 138.21 (C from C_6H_4I), 139.52 (C^9), 141.45 (C–I from C_6H_4I), 141.53 (C–I from C_6H_4I), 145.94 (C^1), 150.79 (C^{11}), 156.47 (C^6), 168.07 (C^7N), 179.52 (C-carbene), 201.71 (C-carbene). ^{195}Pt $\{^1H\}$ NMR (80.015 MHz, $CDCl_3$, δ): –3535.

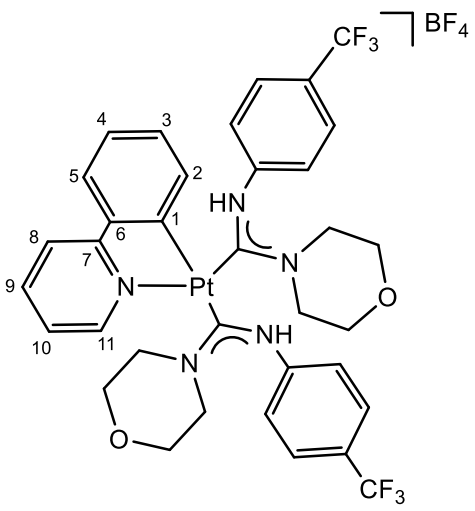

2f. Yield 36 mg, 90%. Anal. Calcd. (%) for $C_{35}H_{34}N_5BF_{10}O_2Pt$: C 44.13, H 3.60, N 7.35; found: C 45.00, H 3.61, N 7.43. Light green solid. HRESI-MS$^+$ *m/z*: calcd. for $C_{35}H_{34}N_5F_6O_2Pt^+$ 865.2262, found 865.2269 $[M–BF_4]^+$. IR (KBr, selected bands, cm^{-1}): IR (KBr, selected bands, cm^{-1}): 1118 (s), 1321 (vs), 1436 (m), 1481 (m) *ν*(C=N and C=C from Ar); 1544 (s) *ν*(N–$C_{carbene}$); 1607 (s) *δ* (N–H); 3325 (m) *ν*(N−H). ^{1}H NMR (400.13 MHz, $CDCl_3$, δ): 3.05–4.10 (m, 14H, morpholine), 4.29 (d, 1H, $J_{H,H}$ = 14.1 Hz, CH_2O-morpholine), 4.40 (d, 1H, $J_{H,H}$ = 14.3 Hz, CH_2O-morpholine), 7.23–7.31 (m, 3H, H^3, H^4, H^{10}), 7.43–7.55 (m, 5H, H^2, $C_6H_4CF_3$), 7.64–7.66 (m, 2H, $C_6H_4CF_3$), 7.70–7.72 (m, 1H, H^5), 7.83–7.85 (m, 2H, $C_6H_4CF_3$), 7.96–7.98 (m, 1H, H^8), 8.03–8.07 (m, 1H, H^9), 8.60 (d, 1H, $J_{H,H}$ = 4.9, H^{11}), 8.67 (br, 1H, NH-carbene), 9.11 (br, 1H, NH-carbene). ^{13}C{^{1}H} NMR (100.61 MHz, $CDCl_3$, δ): 45.90, 46.81, 52.81, 54.35, 65.32, 65.68, 66.05, 66.66 (C-morpholine); 120.28 (C^8), 122.31 (C^{10}), 122.49 (C^5), 123.69 (C^4), 124.51, 124.89 (C–H from $C_6H_4CF_3$), 125.29 (d, $J_{C,F}$ = 11.4 Hz, C–H from $C_6H_4CF_3$), 126.30–126.49 (m, C–H from $C_6H_4CF_3$), 127.04 (q, $J_{C,F}$ = 2.7 Hz, C–CF_3 from $C_6H_4CF_3$), 128.83, 131.59 (C^3), 137.10 (C^2), 139.73 (C^9), 144.82 (C–ipso from $C_6H_4CF_3$), 145.96 , 150.72 (C^1), 155.85 (C^{11}), 155.85 (C^6), 168.11 (C^7N), 180.45 (C-carbene), 202.83 (C-carbene), CF_3 wasn't detected. ^{19}F NMR (376.50 MHz, $CDCl_3$, δ): –62.18, –62.23. ^{195}Pt {^{1}H} NMR (86.015 MHz, $CDCl_3$, δ): –3526.

Table S1.1. Peak positions of *ν*(CN) in FTIR spectra of complexes **1a–f**.

Isocyanide	*ν*(CN) in CNAr, cm^{-1}	*ν*(CN) in [Pt(ppy)Cl(CNR)] , cm^{-1}	Δ *ν*(CN)
4-isocyano-*N*,*N*-dimethylaniline	2115	2190	75
1-isocyano-4-methylbenzene	2128[17]	2187	59
1-chloro-4-isocyanobenzene	2126	2195	69
1-bromo-4-isocyanobenzene	2125	2169	44
1-iodo-4-isocyanobenzene	2128[3]	2187	69
1-isocyano-4-(trifluoromethyl)benzene	2128	2194	68

S2. X-ray Structure Determination

Table S2.1. Crystallographic data for complexes **1a–d**

Identification code	**1a**	**1b**	**1c**	**1d**
Empirical formula	$C_{25}H_{29}Cl_3N_4OPt$	$C_{23.5}H_{25}Cl_2N_3OPt$	$C_{22}H_{21}Cl_2N_3OPt$	$C_{22}H_{21}BrClN_3OPt$
Formula weight	702.96	631.45	609.41	653.87
Crystal system	100.01(11)	100.01(13)	100.01(10)	100(2)
Temperature/K	monoclinic	monoclinic	triclinic	monoclinic
Space group	$P2_1/n$	$P2_1/n$	P-1	$P2_1/n$
a/Å	20.05120(15)	19.2185(2)	9.5239(2)	14.5762(5)
b/Å	11.10207(8)	10.5181(2)	9.9437(2)	11.5198(3)
c/Å	24.15392(17)	26.3711(4)	12.3820(4)	14.8132(5)
α/°	90	90	108.371(2)	90
β/°	97.6964(6)	93.2060(10)	90.650(2)	105.883(4)
γ/°	90	90	111.780(2)	90
Volume/Å^3	5328.47(7)	5322.37(14)	1022.40(5)	2392.40(14)
Z	8	8	2	4
ρ_{calc}g/cm^3	1.753	1.576	1.980	1.815
μ/mm^{-1}	12.819	11.849	7.143	7.664
F(000)	2752.0	2456.0	588.0	1248.0
Crystal size/mm^3	0.22 × 0.12 × 0.08	0.05 × 0.05 × 0.05	0.3 × 0.25 × 0.25	0.2 × 0.13 × 0.11
Radiation	CuKα (λ = 1.54184)	CuKα (λ = 1.54184)	MoKα (λ = 0.71073)	MoKα (λ = 0.71073)
2Θ range for data collection/°	5.386 to 134.982	5.546 to 134.97	5.146 to 61.016	4.958 to 54.996
Index ranges	$-24 \le h \le 24$, $-13 \le k \le 13$, $-28 \le l \le 28$	$-21 \le h \le 23$, $-12 \le k \le 11$, $-30 \le l \le 31$	$-13 \le h \le 12$, $-13 \le k \le 13$, $-17 \le l \le 17$	$-18 \le h \le 15$, $-13 \le k \le 14$, $-19 \le l \le 18$
Reflections collected	35754	48124	18795	12073
Independent reflections	9599 [R_{int} = 0.0423, R_{sigma} = 0.0349]	9582 [R_{int} = 0.0594, R_{sigma} = 0.0400]	5598 [R_{int} = 0.0387, R_{sigma} = 0.0440]	5498 [R_{int} = 0.0355, R_{sigma} = 0.0550]
Data/restraints/parameters	9599/0/642	9582/1/560	5598/1/266	5498/0/262
Goodness-of-fit on F^2	1.064	1.045	1.030	0.991
Final R indexes [I>=2σ (I)]	R_1 = 0.0329, wR_2 = 0.0815	R_1 = 0.0447, wR_2 = 0.1194	R_1 = 0.0240, wR_2 = 0.0460	R_1 = 0.0281, wR_2 = 0.0503
Final R indexes [all data]	R_1 = 0.0329, wR_2 = 0.0824	R_1 = 0.0501, wR_2 = 0.1228	R_1 = 0.0293, wR_2 = 0.0479	R_1 = 0.0352, wR_2 = 0.0528
Largest diff. peak/hole / e Å^{-3}	3.66/-1.70	2.22/-1.40	1.42/-0.94	1.47/-1.35
Flack parameter				
CCDC number	2232169	2232168	2232158	2232159

Table S2.2. Crystallographic data for complexes **1e,f** and **2b**

Identification code	**1e**	**1f**	**2b**
Empirical formula	$C_{22}H_{21}ClIN_3OPt$	$C_{23}H_{21}ClF_3N_3OPt$	$C_{35}H_{40}BF_4N_5O_2Pt$
Formula weight	700.86	642.97	844.62
Crystal system	100(2)	296.00(10)	99.99(18)
Temperature/K	triclinic	triclinic	triclinic
Space group	P-1	P-1	P-1
a/Å	9.7955(6)	9.9036(5)	11.6565(7)
b/Å	9.9523(6)	9.9576(5)	11.9574(7)
c/Å	12.1746(9)	12.3123(5)	15.1337(7)
α/°	91.527(5)	89.573(3)	80.977(4)
β/°	106.491(6)	72.113(4)	83.061(4)
γ/°	111.705(5)	69.091(4)	68.144(5)
Volume/Å^3	1045.75(12)	1072.26(9)	1929.0(2)
Z	2	2	2
ρ_{calc}g/cm^3	2.226	1.991	1.454
μ/mm^{-1}	8.332	6.715	7.266
F(000)	660.0	620.0	840.0
Crystal size/mm^3	0.34 × 0.3 × 0.2	0.35 × 0.24 × 0.21	0.24 × 0.2 × 0.1
Radiation	MoKα (λ = 0.71073)	MoKα (λ = 0.71073)	CuKα (λ = 1.54184)
2Θ range for data collection/°	5.258 to 54.998	5.304 to 64.552	8.026 to 134.984
Index ranges	$-12 \le h \le 12$, $-12 \le k \le 12$, $-15 \le l \le 15$	$-14 \le h \le 14$, $-14 \le k \le 14$, $-17 \le l \le 17$	$-13 \le h \le 13$, $-14 \le k \le 14$, $-18 \le l \le 18$
Reflections collected	11047	22956	12973
Independent reflections	4801 [R_{int} = 0.0292, R_{sigma} = 0.0421]	6998 [R_{int} = 0.0394, R_{sigma} = 0.0426]	6932 [R_{int} = 0.0627, R_{sigma} = 0.0595]
Data/restraints/parameters	4801/0/266	6998/0/293	6932/1/443
Goodness-of-fit on F^2	1.060	1.039	1.023
Final R indexes [I>=2σ (I)]	R_1 = 0.0227, wR_2 = 0.0418	R_1 = 0.0265, wR_2 = 0.0581	R_1 = 0.0355, wR_2 = 0.0873
Final R indexes [all data]	R_1 = 0.0254, wR_2 = 0.0431	R_1 = 0.0303, wR_2 = 0.0604	R_1 = 0.0380, wR_2 = 0.0893
Largest diff. peak/hole / e Å^{-3}	1.19/-0.88	2.25/-1.66	1.84/-1.84
CCDC number	2232160	2232167	2232172

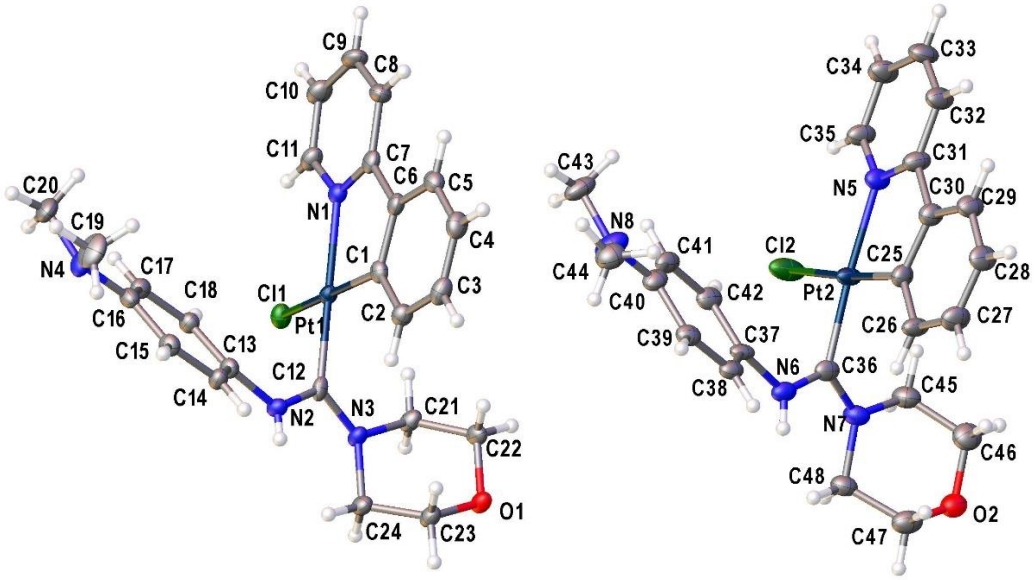

Figure S2.1. Molecular view of molecule A (left) and B (right) of complex **1a**. Thermal ellipsoids for are drawn at the 50% probability level.

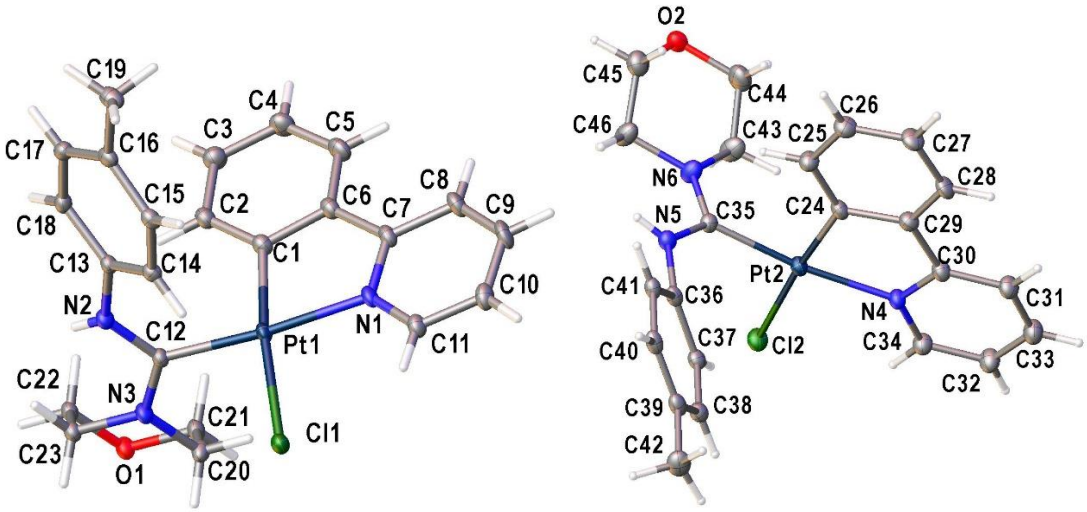

Figure S2.2. Molecular view of molecule A (left) and B (right) of complex **1b**. Thermal ellipsoids for are drawn at the 50% probability level.

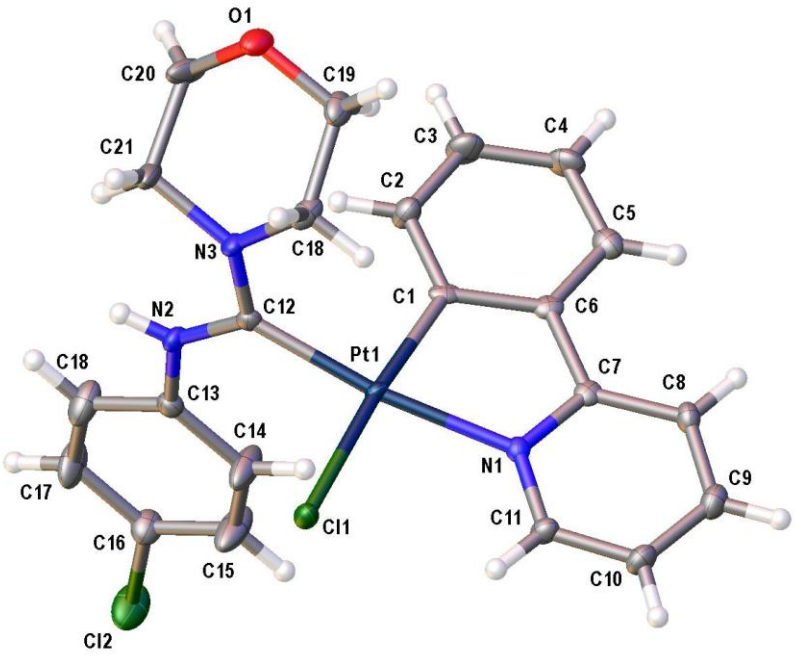

Figure S2.3. Molecular view of complex **1c**. Thermal ellipsoids for are drawn at the 50% probability level.

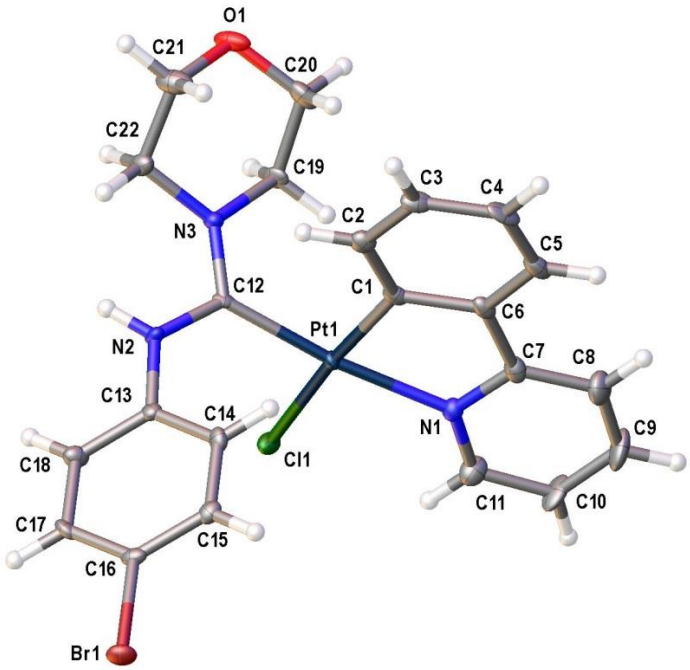

Figure S2.4. Molecular view of complex **1d**. Thermal ellipsoids for are drawn at the 50% probability level.

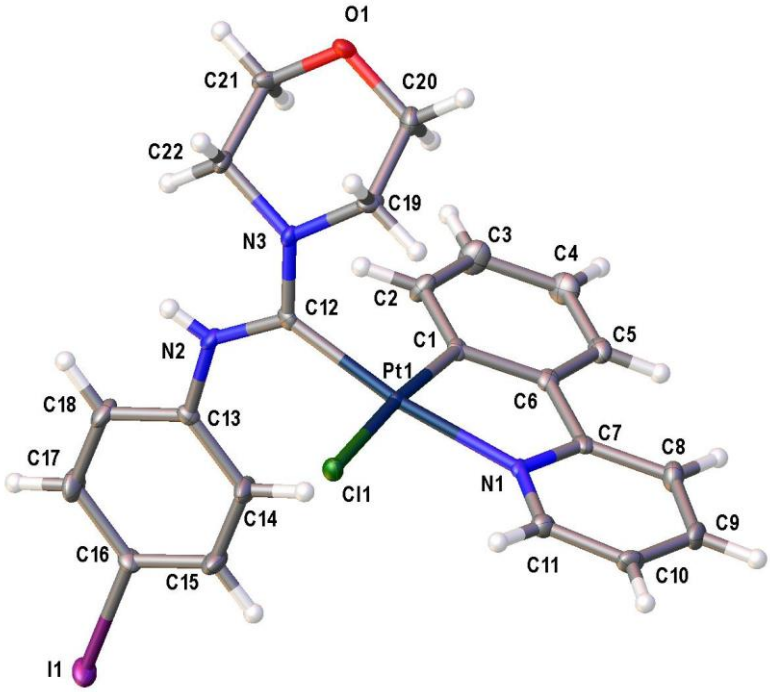

Figure S2.5. Molecular view of complex **1e**. Thermal ellipsoids for are drawn at the 50% probability level.

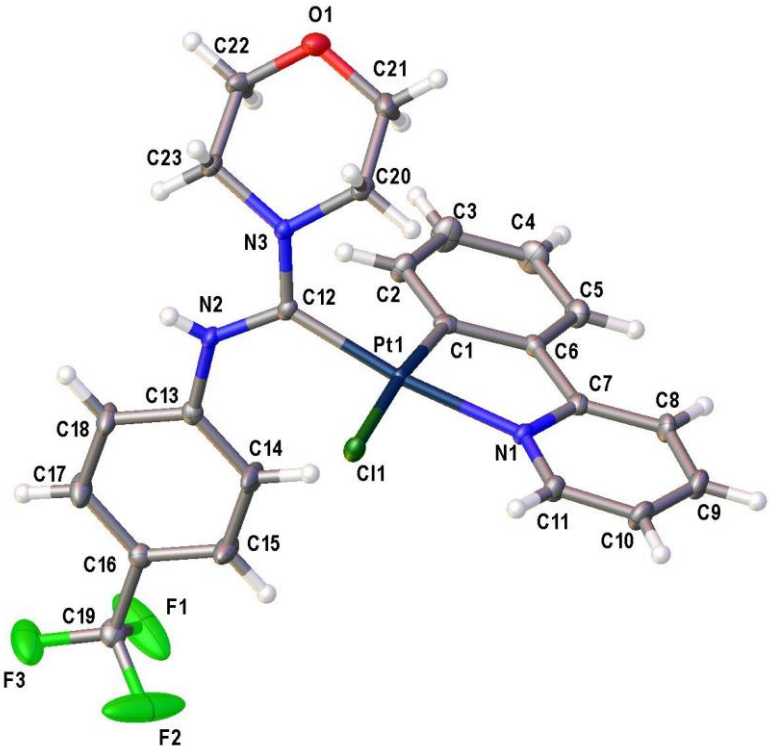

Figure S2.6. Molecular view of complex **1f**. Thermal ellipsoids for are drawn at the 50% probability level.

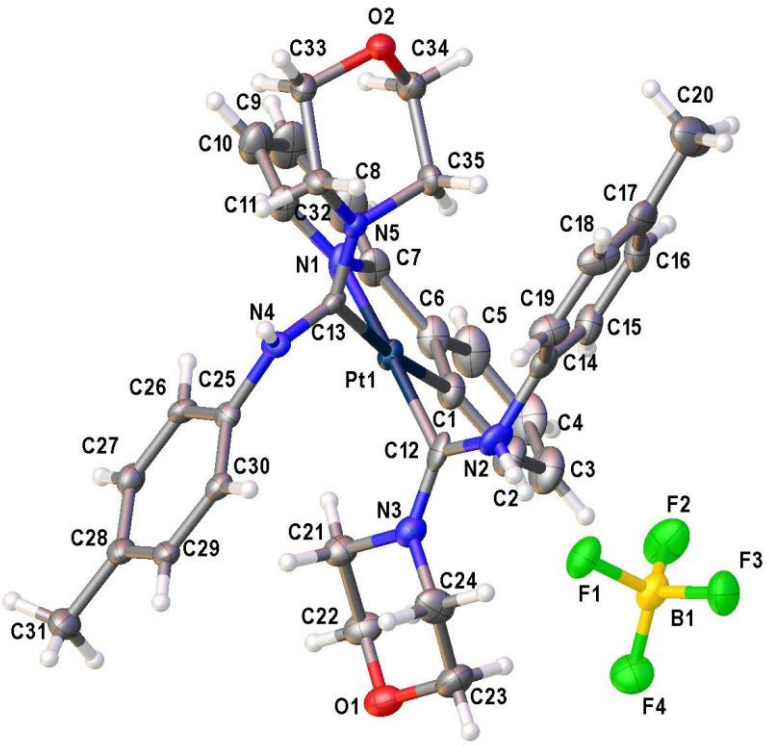

Figure S2.7. Molecular view of complex **2b**. Thermal ellipsoids for are drawn at the 50% probability level.

Table S2.3. Selected bond lengths (Å) and angles (°) for **1a–b**.

	1a		**1b**	
	A	**B**	**A**	**B**
Pt1–N1	2.078(4)	2.082(4)	2.080(5)	2.059(5)
Pt1–C1	1.992(5)	1.997(5)	1.990(6)	1.998(6)
Pt1-Cl1	2.4201(11)	2.4061(11)	2.4171(15)	2.4191(15)
Pt1–C12	1.978(5)	1.990(5)	1.998(6)	1.998(6)
N2–C12	1.344(6)	1.331(7)	1.339(8)	1.329(8)
N3–C12	1.343(6)	1.338(6)	1.340(8)	1.338(8)
∠(C1–Pt1–N1)	81.16(16)	81.37(18)	81.3(2)	81.10(2)
∠(N1–Pt1–Cl1)	94.51(11)	94.60(11)	94.02(16)	94.65(15)
∠(N2–C12–Pt1)	121.1(3)	121.7(4)	122.0(4)	122.3(5)
∠(N3–C12–Pt1)	122.3(3)	121.0(4)	120.6(5)	119.002)
∠(N3–C12–N2)	116.6(4)	117.3(4)	117.3(5)	118.5(3)

Table S2.4. Selected bond lengths (Å) and angles (°) for **1c–f**.

	1c	**1d**	**1e**	**1f**
Pt1–N1	2.078(4)	2.082(3)	2.070(3)	2.073(2)
Pt1–C1	1.991(4)	1.994(4)	1.970(3)	1.984(3)
Pt1-Cl1	2.4203(10)	2.4010(9)	2.4052(8)	2.4008(7)
Pt1–C12	1.985(3)	1.982(4)	1.987(3)	1.988(3)
N2–C12	1.356(4)	1.350(5)	1.347(4)	1.356(4)
N3–C12	1.334(4)	1.346(5)	1.339(4)	1.341(4)
∠(C1–Pt1–N1)	81.10(11)	81.06(14)	81.09(12)	80.98(11)
∠(N1–Pt1–Cl1)	94.07(7)	93.83(9)	94.00(8)	93.86(7)
∠(N2–C12–Pt1)	125.3(2)	124.5(3)	125.7(2)	125.5(2)
∠(N3–C12–Pt1)	119.2(2)	120.2(3)	118.0(2)	119.2(2)
∠(N3–C12–N2)	115.3(3)	115.2(3)	116.3(3)	115.3(3)

Table S2.5. Selected bond lengths (Å) and angles (°) for **2b**.

Bond lengths	**2b**	Angles (minimal value)	**2b**
Pt1–N1	2.077(4)	**∠(C1–Pt1–N1)**	80.62(18)
Pt1–C1	2.054(4)	**∠(N1–Pt1–C12)**	173.99(16)
Pt1–C12	2.025(5)	**∠(N1–Pt1–C13)**	94.54(17)
Pt1–C13	2.078(4)	**∠(N3–C12–N2)**	117.9(4)
N2–C12	1.323(6)	**∠(N4–C13–N5)**	116.0(17)
N3–C12	1.339(6)	**∠(C12–Pt1–C13)**	90.83(16)
N4–C13	1.347(5)	**∠(C1–Pt1–C13)**	172.84(17)
N5–C13	1.330(5)		

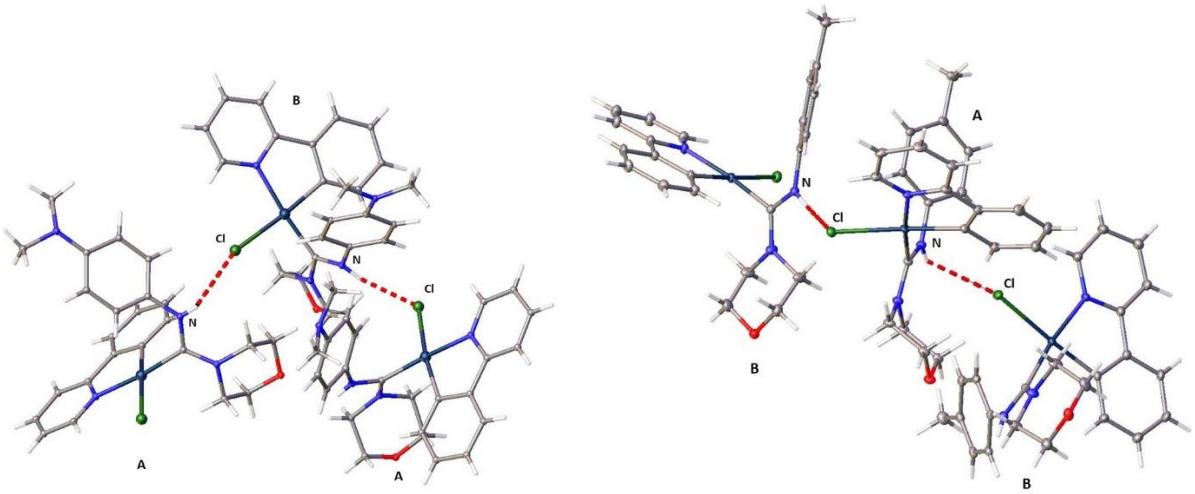

Figure S2.8. N–$H_{carbene}$•••Cl interactions in **1a** (left) and **1b** (right) in the solid state.

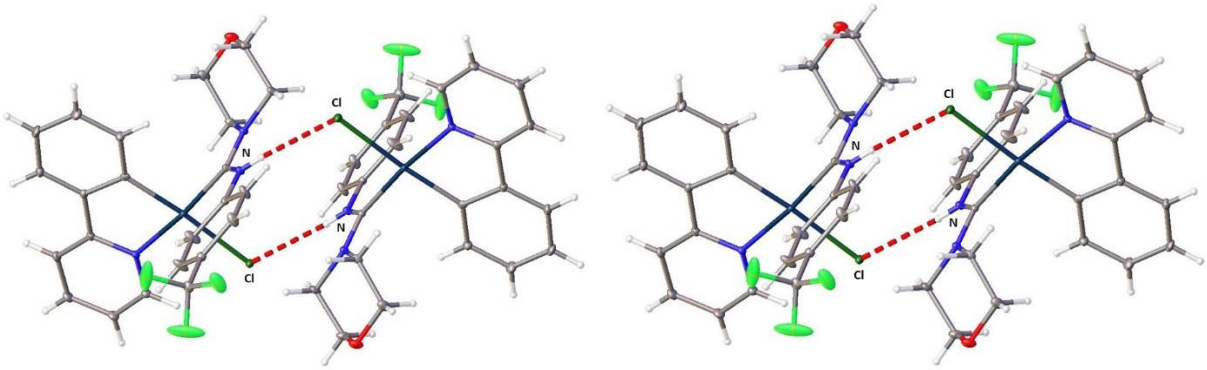

Figure S2.9. N–$H_{carbene}$•••Cl interactions in **1c** (left) and **1f** (right) in the solid state.

Table S2.6. Distances and angles for N2$H_{carbene}$•••Cl interactions in **1a–f**.

Compound	Distance N•••Cl, Å	Distance H•••Cl, Å	∠(N–H•••Cl), °	**Figure**
1a	3.286(6)	2.50(5)	168(5)	S2.8
1b	3.512(6) 3.340(6)	2.96(5) 2.70(4)	141(8) 157(5)	S2.8
1c	3.414(2)	2.608(16)	167(2)	
1d	3.354(3)	2.5584(10)	150.7(2)	
1e	3.486(3)	2.75(3)	168(4)	S2.9
1f	3.422(3)	2.70(3)	170(4)	S2.9

Comparison, Å	
Bondi VdW radii	3.30
Alvarez VdW radii	3.48

S3. Photophysical data

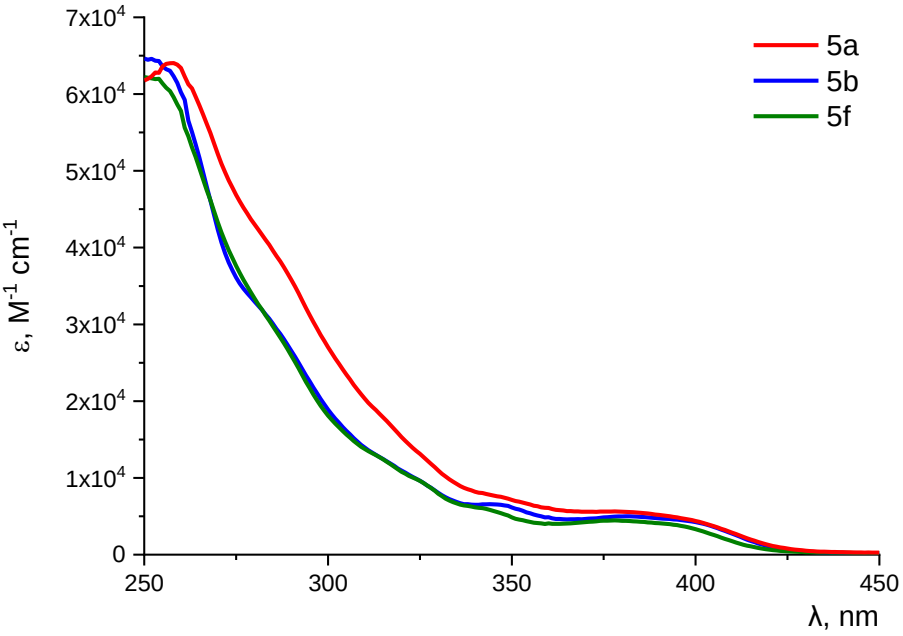

Figure S3.1. Absorption spectra of **1a**,**b**,**f** in DCE, 298K (aerated).

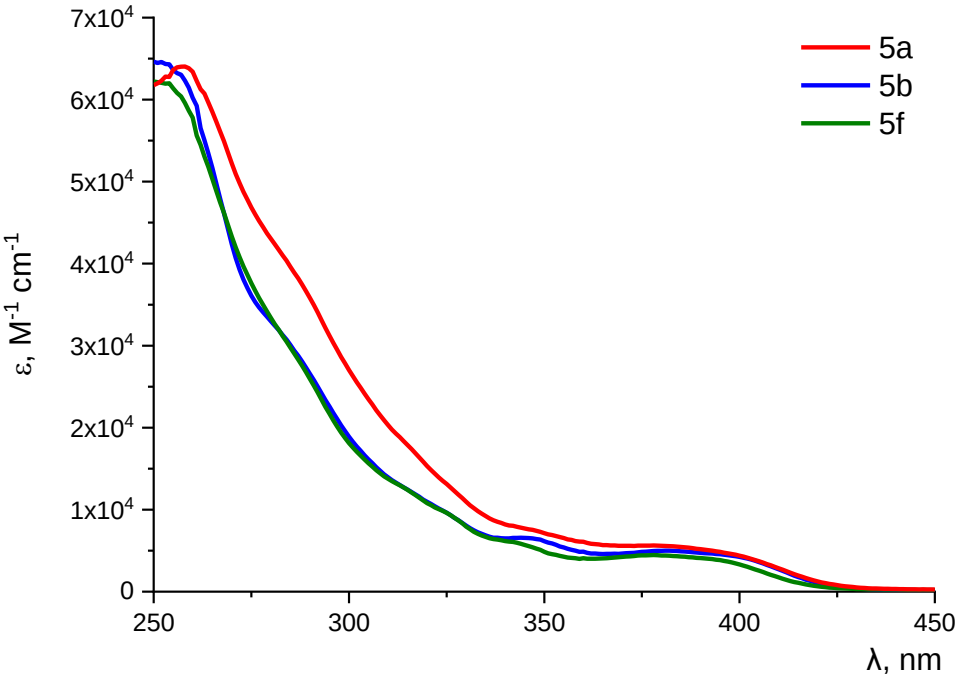

Figure S3.2. Absorption spectra of **1a**,**b**,**f** in DCE, 298K (aerated).

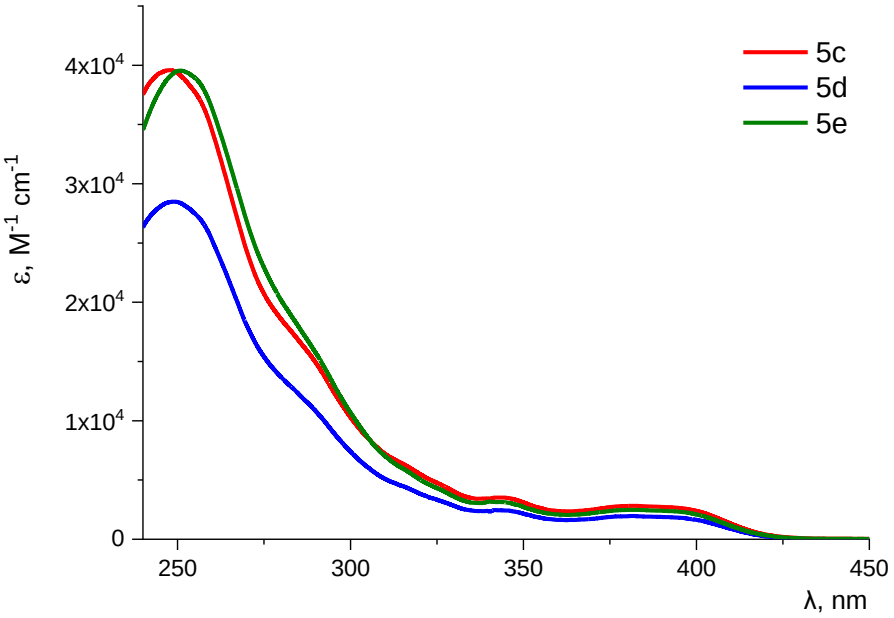

Figure S3.3. Absorption spectra of **1c–e** in DCE, 298K (aerated).

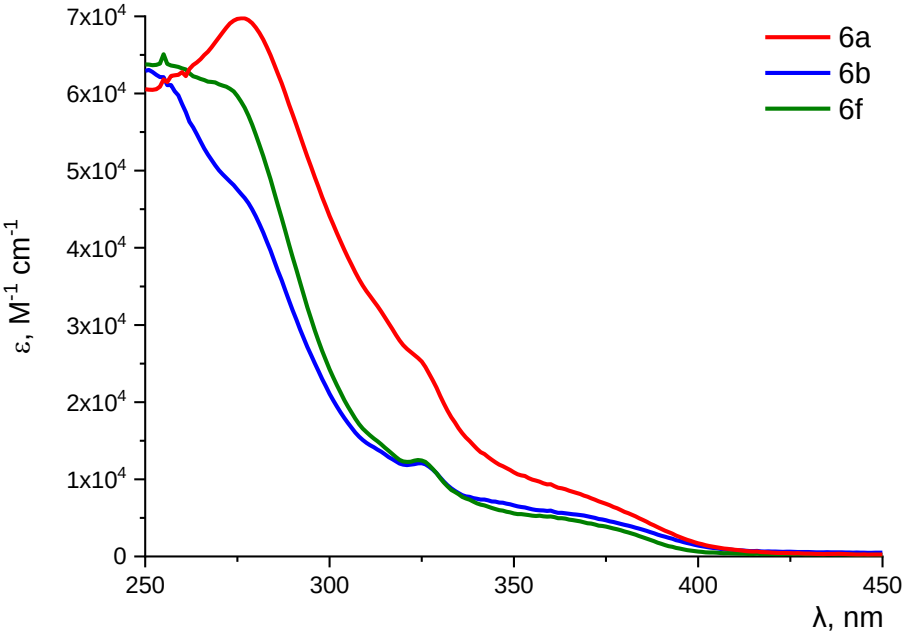

Figure S3.4. Absorption spectra of **2a**,**b**,**f** in DCE, 298K (aerated).

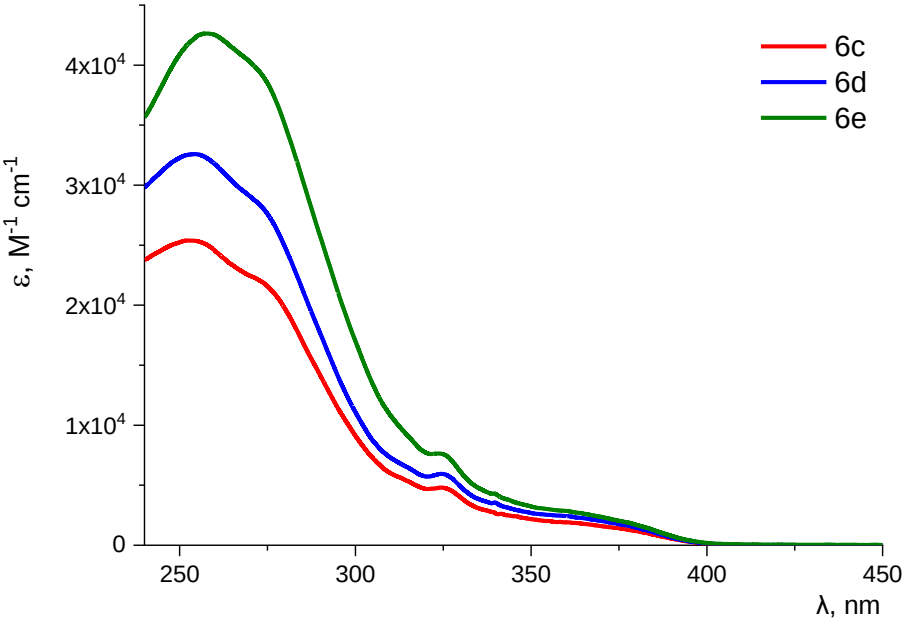

Figure S3.5. Absorption spectra of **2c**–**e** in DCE, 298K (aerated).

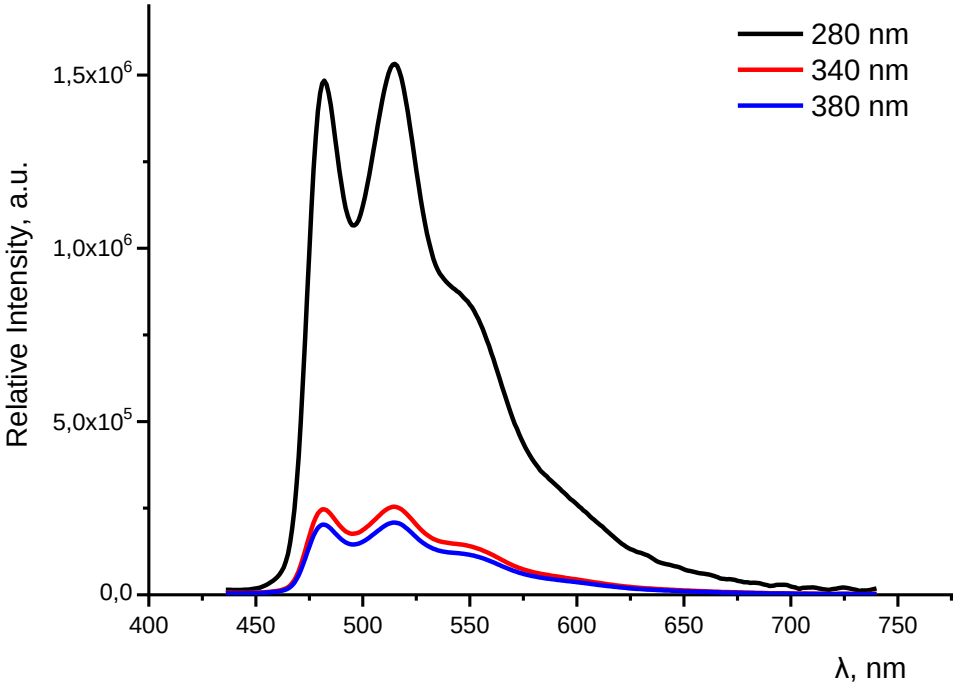

Figure S3.6. Emission spectra of **1c** in DCE at different λ_{ex}, 298K (aerated).

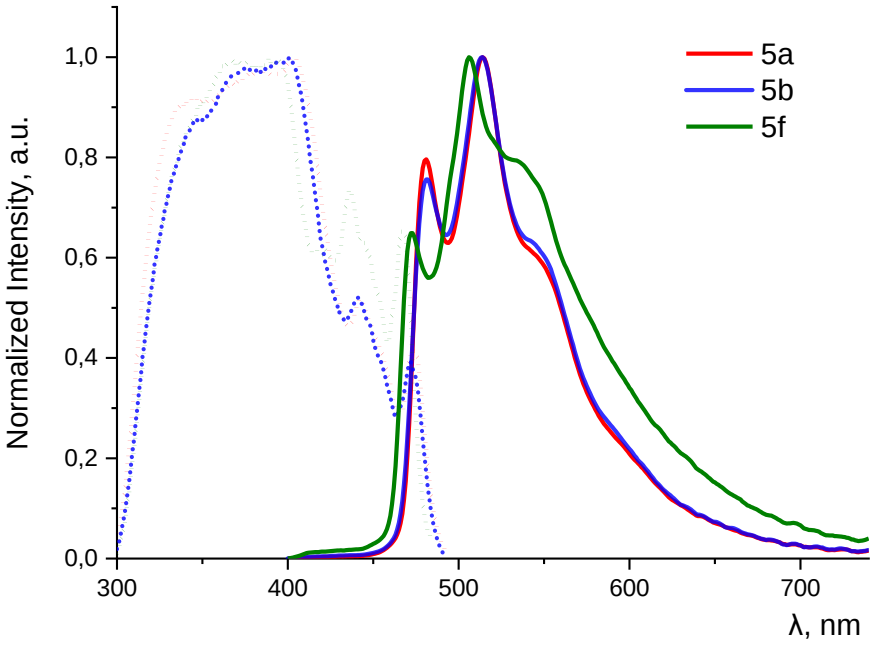

Figure S3.7. Excitation (dotted line) and emission (solid line) spectra of **1a**,**b**,**f**, 298K, in solid state.

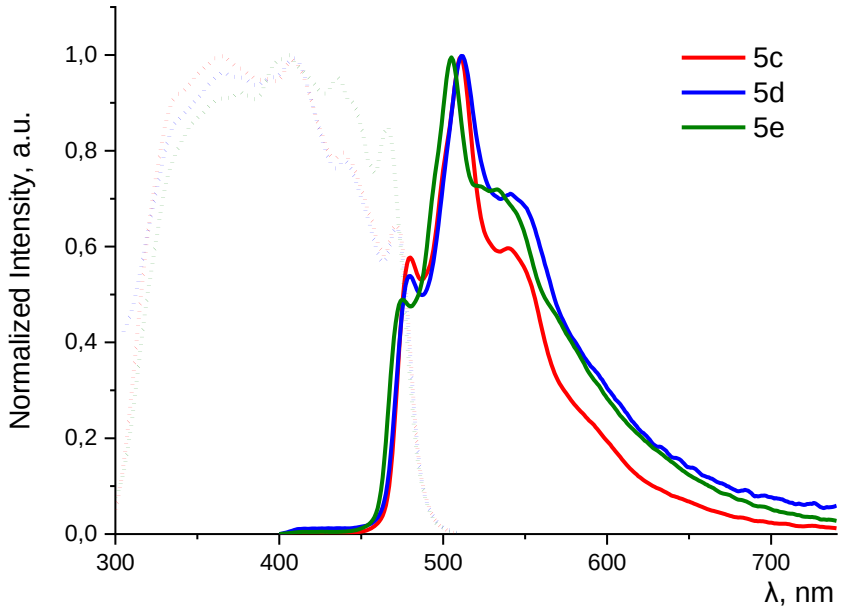

Figure S3.8. Excitation (dotted line) and emission (solid line) spectra of **1c–e**, 298K, in solid state.

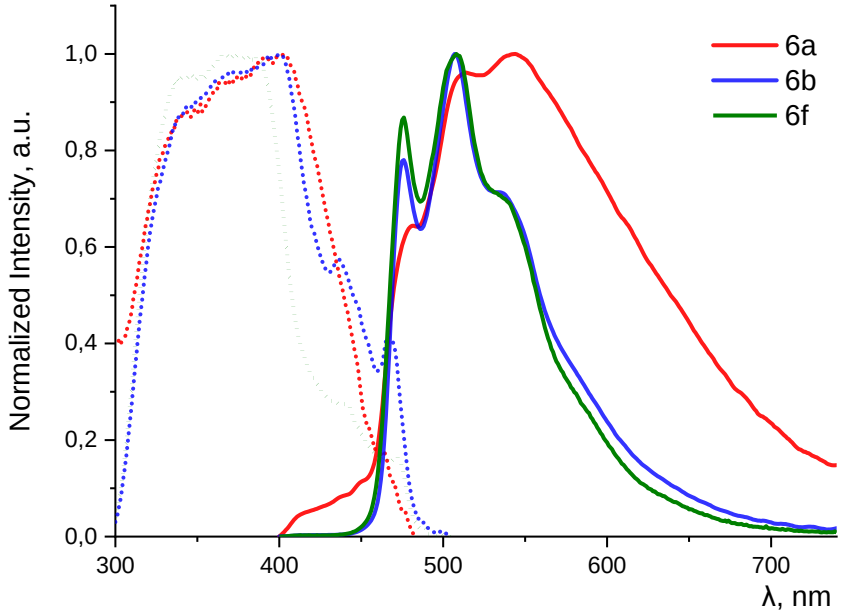

Figure S3.9. Excitation (dotted line) and emission (solid line) spectra of **2a**,**b**,**f** 298K, in solid state.

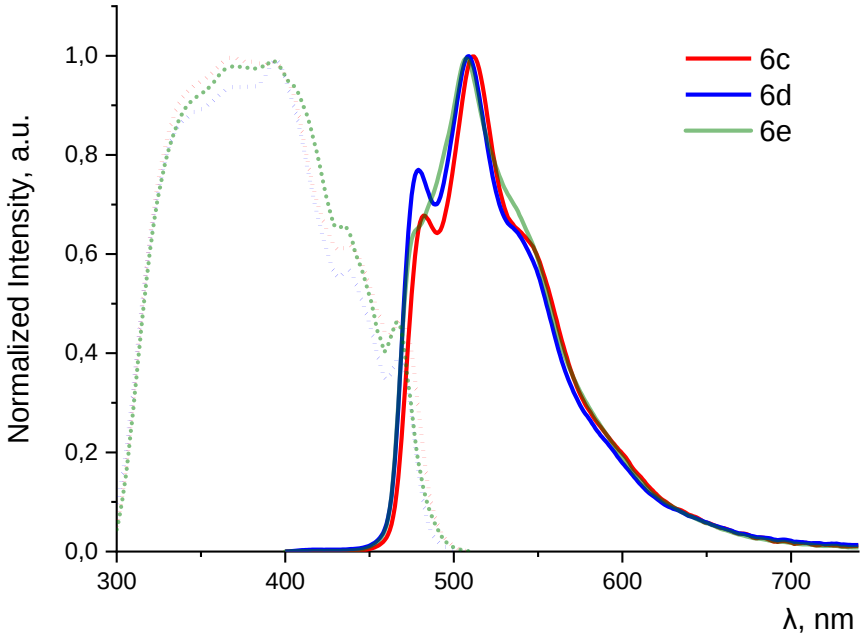

Figure S3.10. Excitation (dotted line) and emission (solid line) spectra of **2c**–**e**, 298K, in solid state.

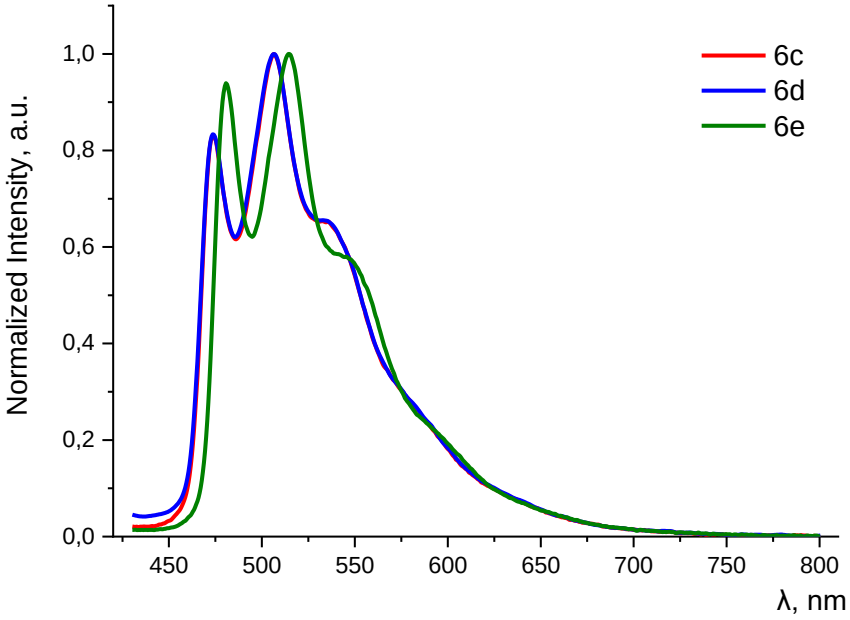

Figure S3.11. Emission spectra of **2c–e** in the solid state (λ_{ex}=365 nm, RT).

S4. Computational results

Table S4.1. Selected bond lengths (Å) and angles (°) for **1a–c** of DFT optimized geometries for ground state in DCE.

	1a		**1b**		**1c**	
	X-ray (mol. A)	**S_0**	**X-ray (mol. A)**	**S_0**	**X-ray**	**S_0**
Pt1–N1	2.078(4)	2.129380	2.080(5)	2.124383	2.074(3)	2.12732
Pt1–C1	1.992(5)	2.008950	1.990(6)	2.00742	1.976(3)	2.009221
Pt1-Cl1	2.4201(11)	2.522786	2.4171(15)	2.528533	2.4056(8)	2.518508
Pt1–C12	1.980(5)	2.013763	1.998(6)	2.01568	1.984(3)	2.011494
N2–C12	1.344(6)	1.347539	1.339(8)	1.350477	1.357(4)	1.354797
N3–C12	1.342(6)	1.350011	1.340(8)	1.345793	1.333(4)	1.345576
∠(C1–Pt1–N1)	81.12(18)	80.201518	81.3(2)	80.244634	81.09(12)	80.226375
∠(N1–Pt1–Cl1)	94.53(11)	94.984879	94.02(16)	95.335725	94.09(8)	95.047361
∠(N2–C12–Pt1)	121.0(3)	120.606775	122.0(4)	121.021399	125.3(2)	120.850703
∠(N3–C12–Pt1)	122.3(3)	122.617592	120.6(5)	121.85226	119.3(2)	122.849833
∠(N3–C12–N2)	116.7(4)	116.761802	117.3(5)	117.126331	115.3(3)	116.237237

Table S4.2. Selected bond lengths (Å) and angles (°) for **1d–f** of DFT optimized geometries for ground state in DCE

	1d		**1e**		**1f**	
	X-ray	**S_0**	**X-ray**	**S_0**	**X-ray**	**S_0**
Pt1–N1	2.082(3)	2.127812	2.070(3)	2.126723	2.073(2)	2.127342
Pt1–C1	1.994(4)	2.009116	1.970(3)	2.009171	1.984(3)	2.009515
Pt1-Cl1	2.4010(9)	2.518807	2.4052(8)	2.517664	2.4008(7)	2.516396
Pt1–C12	1.982(4)	2.010638	1.987(3)	2.010701	1.988(3)	2.009222
N2–C12	1.350(5)	1.345497	1.347(4)	1.355395	1.356(4)	1.359178
N3–C12	1.346(5)	1.354942	1.339(4)	1.345671	1.341(4)	1.343979
∠(C1–Pt1–N1)	81.06(14)	80.193715	81.09(12)	80.187060	80.98(11)	80.202382
∠(N1–Pt1–Cl1)	93.83(9)	95.259735	94.00(8)	95.188018	93.86(7)	95.134179
∠(N2–C12–Pt1)	124.5(3)	121.006739	125.7(2)	121.330772	125.5(2)	121.344493
∠(N3–C12–Pt1)	120.2(3)	122.790031	118.0(2)	122.603632	119.2(2)	122.813114

∠(N3–C12–N2)	115.2(3)	116.143017	116.3(3)	116.000018	115.3(3)	115.751804

Table S4.3. Selected bond lengths (Å) and angles (°) for **2b**,**d** of DFT optimized geometries for ground state in DCE.

	2b		**2d**	
	X-ray	**S_0**	**X-ray**	**S_0**
Pt1–N1	2.077(4)	2.137849	2.071(4)	2.138301
Pt1–C1	2.054(4)	2.060517	2.042(5)	2.060443
Pt1–C12	2.025(5)	2.027271	2.009(5)	2.026620
Pt1–C13	2.078(4)	2.144223	2.065(4)	2.148776
N2–C12	1.323(6)	1.354535	1.351(7)	1.345722
N3–C12	1.339(6)	1.348723	1.341(7)	1.358710
N4–C13	1.347(5)	1.351661	1.370(6)	1.355310
N5–C13	1.330(5)	1.348710	1.316(6)	1.345811
∠(C1–Pt1–N1)	80.62(18)	79.561166	81.04(19)	79.579703
∠(N1–Pt1–C12)	173.99(16)	172.667804	174.74(18)	172.641711
∠(N1–Pt1–C13)	94.54(17)	95.43307	94.40(16)	95.482342
∠(N3–C12–N2)	117.9(4)	115.600294	116.0(3)	115.404965
∠(N4–C13–N5)	116.0(17)	115.466153	115.3(4)	115.340235
∠(C12–Pt1–C13)	90.83(16)	91.192501	90.48(19)	91.376408
∠(C1–Pt1–C13)	172.84(17)	173.560005	172.8(2)	173.585815

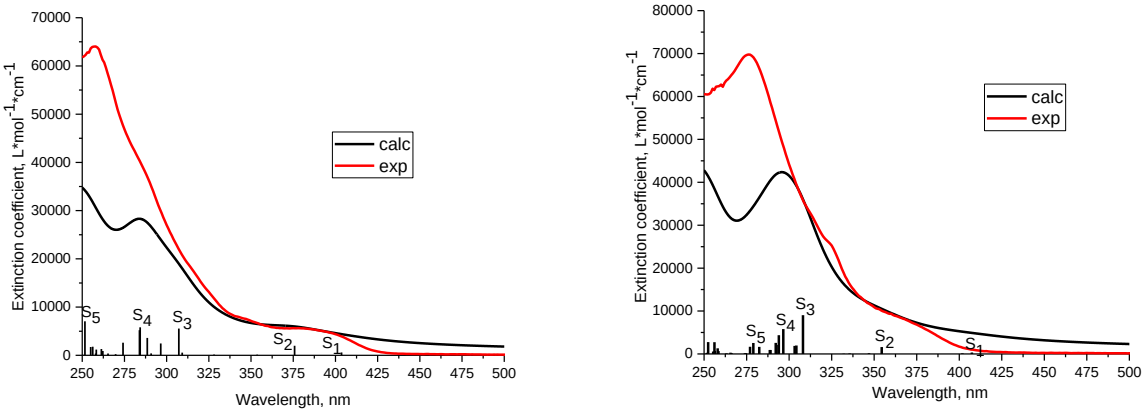

Figure S4.1. Absorption spectra of **1a** (left) and **2a** (right) in DCE solution: experimental (red) and calculated (black) lines with oscillator strengths of electronic transitions (bars).

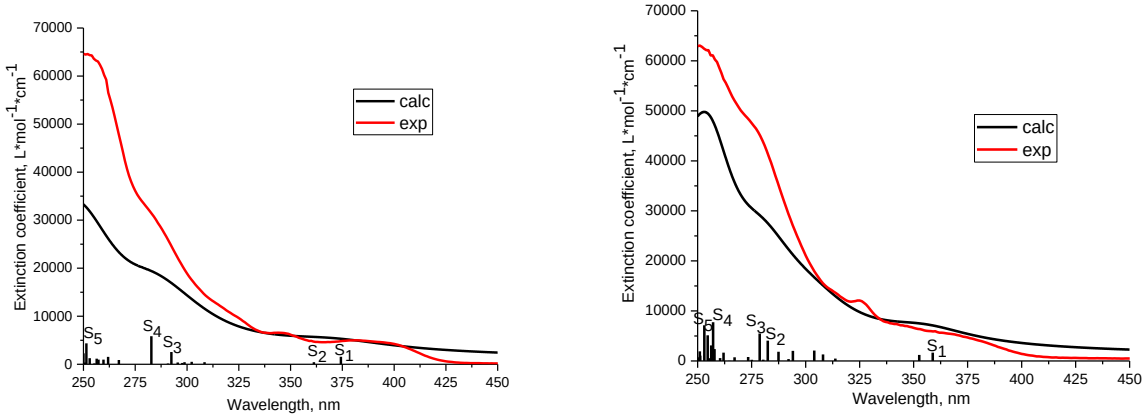

Figure S4.2. Absorption spectra of **1b** (left) and **2b** (right) in DCE solution: experimental (red) and calculated (black) lines with oscillator strengths of electronic transitions (bars).

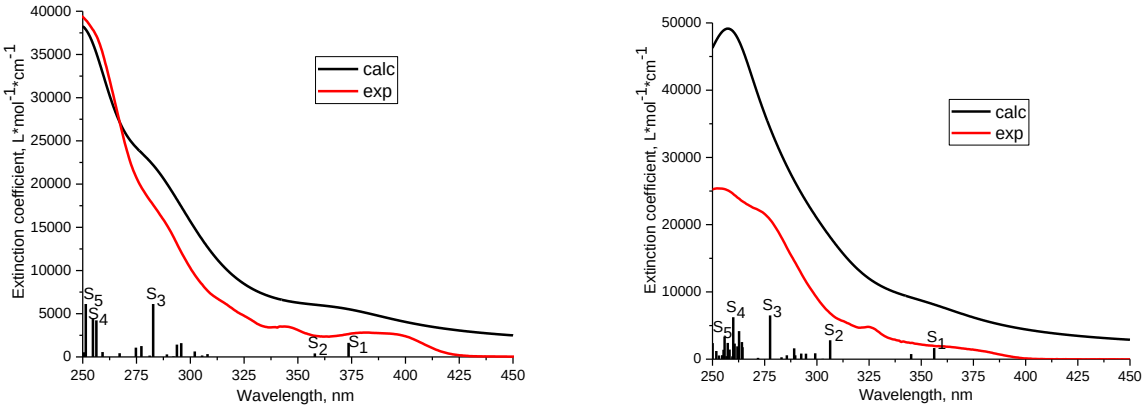

Figure S4.3. Absorption spectra of **1c** (left) and **2c** (right) in DCE solution: experimental (red) and calculated (black) lines with oscillator strengths of electronic transitions (bars).

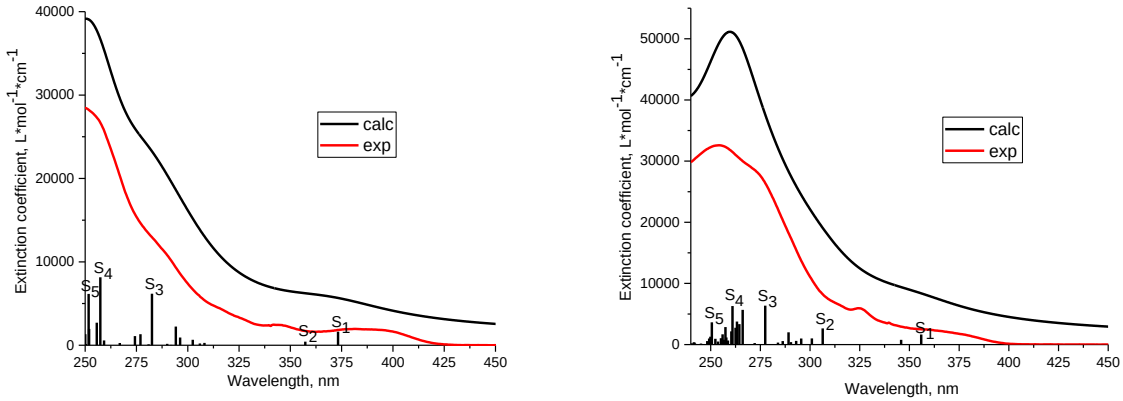

Figure S4.4. Absorption spectra of **1d** (left) and **2d** (right) in DCE solution: experimental (red) and calculated (black) lines with oscillator strengths of electronic transitions (bars).

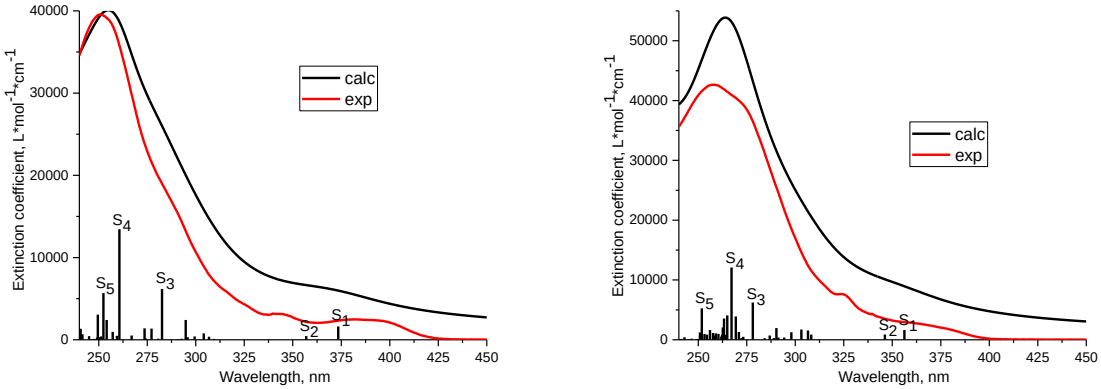

Figure S4.5. Absorption spectra of **1e** (left) and **2e** (right) in DCE solution: experimental (red) and calculated (black) lines with oscillator strengths of electronic transitions (bars).

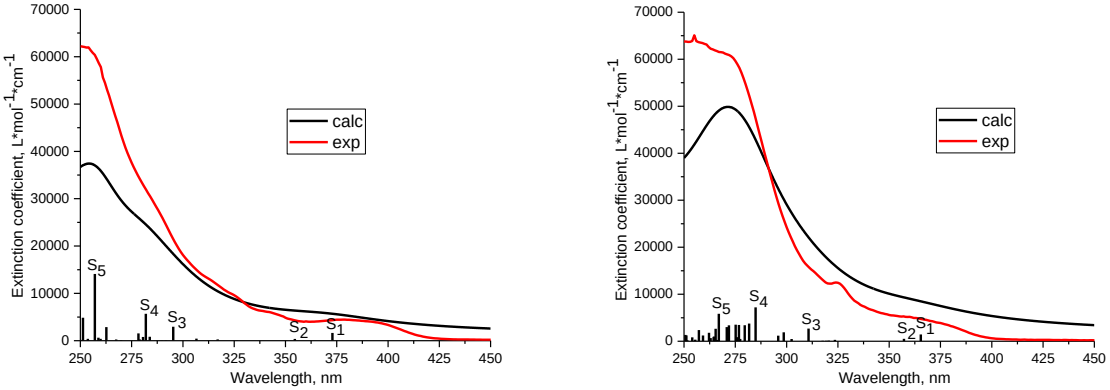

Figure S4.6. Absorption spectra of **1f** (left) and **2f** (right) in DCE solution: experimental (red) and calculated (black) lines with oscillator strengths of electronic transitions (bars).

Table S4.4. Experimental and calculated absorption maxima (λ), extinction coefficients (ε), oscillator strengths (f) of **1a**–**f** .

Complex	λ_{abs}, nm (exp)	$\varepsilon\times10^{-4}$, $L\times mol^{-1}\times cm^{-1}$ (exp)	Transitions	λ_{abs}, nm (calc)	*f* (calc)	Contribution of main NTO pair in transition (%)
1a	257	6.4	$S_0\rightarrow S_5$	252	0.19	52
	281sh	4.2	$S_0\rightarrow S_4$	284	0.16	60
			$S_0\rightarrow S_3$	307	0.15	87
	344	0.8	$S_0\rightarrow S_2$	376	0.05	97
	377	0.6	$S_0\rightarrow S_1$	404	0.02	99
1b	250	6.5	$S_0\rightarrow S_5$	251	0.15	52
	282sh	3.2	$S_0\rightarrow S_4$	283	0.20	81
			$S_0\rightarrow S_3$	292	0.09	54
	347	0.7	$S_0\rightarrow S_2$	361	0.01	99
	382	0.5	$S_0\rightarrow S_1$	374	0.05	97
1c	274	4.0	$S_0\rightarrow S_5$	251	0.21	62
			$S_0\rightarrow S_4$	255	0.15	86
	282sh	1.8	$S_0\rightarrow S_3$	283	0.21	79
	343	0.3	$S_0\rightarrow S_2$	358	0.01	97
	383	0.3	$S_0\rightarrow S_1$	374	0.06	97
1d	250	2.9	$S_0\rightarrow S_5$	252	0.21	72
			$S_0\rightarrow S_4$	257	0.28	83
	279sh	1.4	$S_0\rightarrow S_3$	283	0.21	77
	344	0.2	$S_0\rightarrow S_2$	357	0.01	99
	385	0.2	$S_0\rightarrow S_1$	373	0.06	97
1e	251	4.0	$S_0\rightarrow S_5$	252	0.19	45
			$S_0\rightarrow S_4$	261	0.46	71
	280sh	2.0	$S_0\rightarrow S_3$	283	0.21	78
	344	0.3	$S_0\rightarrow S_2$	357	0.02	99
	385	0.3	$S_0\rightarrow S_1$	373	0.06	97
1f	250	6.2	$S_0\rightarrow S_5$	257	0.48	87
	283sh	3.1	$S_0\rightarrow S_4$	282	0.19	77
			$S_0\rightarrow S_3$	295	0.10	80
	341	0.6	$S_0\rightarrow S_2$	355	0.01	99

	377	0.4	$S_0 \rightarrow S_1$	373	0.06	97

Table S4.5. Experimental and calculated absorption maxima (λ), extinction coefficients (ε), oscillator strengths (f) of **2a**–**f**.

Complex	λ_{abs}, nm (exp)	$\varepsilon\times10^{-4}$, $L\times mol^{-1}\times cm^{-1}$ (exp)	Transitions	λ_{abs}, nm (calc)	*f* (calc)	Contribution of main NTO pair in transition (%)
2a	276	7.0	$S_0\rightarrow S_5$	279	0.09	51
			$S_0\rightarrow S_4$	297	0.20	79
	323	2.6	$S_0\rightarrow S_3$	308	0.31	93
	361sh	0.9	$S_0\rightarrow S_2$	354	0.05	96
			$S_0\rightarrow S_1$	407	0.01	98
2b	250	6.3	$S_0\rightarrow S_5$	253	0.19	49
			$S_0\rightarrow S_4$	257	0.21	66
	273sh	4.9	$S_0\rightarrow S_3$	279	0.15	52
			$S_0\rightarrow S_2$	282	0.11	39
	325	1.2				
	358sh	0.6	$S_0\rightarrow S_1$	359	0.04	96
2c	253	2.5	$S_0\rightarrow S_5$	256	0.11	48
			$S_0\rightarrow S_4$	260	0.21	63
	272sh	2.2	$S_0\rightarrow S_3$	278	0.22	67
	325	0.5	$S_0\rightarrow S_2$	306	0.10	78
	359sh	0.2	$S_0\rightarrow S_1$	356	0.06	96
2d	254	3.3	$S_0\rightarrow S_5$	251	0.12	68
			$S_0\rightarrow S_4$	261	0.21	41
	272sh	2.9	$S_0\rightarrow S_3$	277	0.22	64
	325	0.6	$S_0\rightarrow S_2$	306	0.09	80
	357sh	0.2	$S_0\rightarrow S_1$	356	0.06	96
2e	258	4.3	$S_0\rightarrow S_5$	252	0.18	49
			$S_0\rightarrow S_4$	267	0.41	77
	373sh	2.2	$S_0\rightarrow S_3$	278	0.21	68
	324	0.8	$S_0\rightarrow S_2$	346	0.03	97
	356sh	0.3	$S_0\rightarrow S_1$	356	0.06	96
2f	255	6.5	$S_0\rightarrow S_5$	267	0.20	48
	268	6.2	$S_0\rightarrow S_4$	285	0.24	61
	324	1.2	$S_0\rightarrow S_3$	310	0.09	73

	357sh	0.5	$S_0 \rightarrow S_2$ $S_0 \rightarrow S_1$	357 365	0.02 0.05	97 96

Table S4.6. The decrease (violet) and increase (terracota) of electron density for most intensive electronic absorption transitions of **1a**. The data for the corresponding interfragment charge transfer (IFCT) are given below the figures. Diagonal values represent intraligand transitions, off-diagonal values represent a charge transfer from "Donor" to "Acceptor".

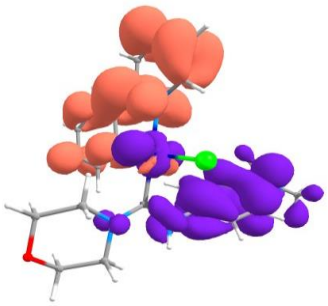

$S_0 \rightarrow S_1$

Donor	Acceptor			
	Pt	**ppy**	**ADC**	**Cl**
Pt	0.006	0.121	0.004	0.000
ppy	0.001	0.017	0.000	0.000
ADC	0.040	0.788	0.023	0.001
Cl	0.000	0.000	0.000	0.000

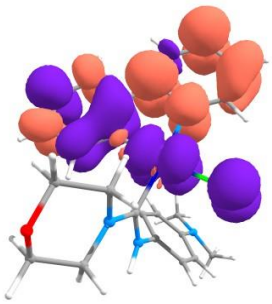

$S_0 \rightarrow S_2$

Donor	Acceptor			
	Pt	**ppy**	**ADC**	**Cl**
Pt	0.019	0.369	0.011	0.001
ppy	0.023	0.461	0.013	0.001
ADC	0.000	0.002	0.000	0.000
Cl	0.005	0.092	0.003	0.000

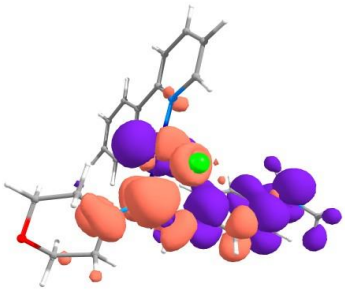

$S_0 \rightarrow S_3$

Donor	Acceptor			
	Pt	**ppy**	**ADC**	**Cl**
Pt	0.090	0.017	0.128	0.000
ppy	0.021	0.004	0.029	0.000
ADC	0.297	0.057	0.419	0.000
Cl	0.000	0.000	0.000	0.000

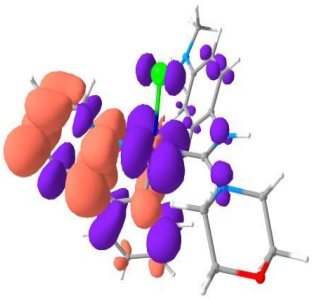

$S_0 \rightarrow S_4$

Donor	Acceptor			
	Pt	**ppy**	**ADC**	**Cl**
Pt	0.032	0.287	0.062	0.000
ppy	0.029	0.262	0.057	0.000
ADC	0.021	0.183	0.040	0.000
Cl	0.003	0.024	0.005	0.000

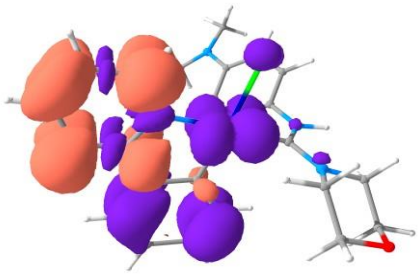

$S_0 \rightarrow S_5$

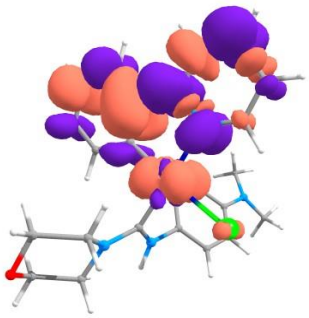

$T_1 \rightarrow S_0$

Donor	Acceptor				Donor	Acceptor			
	Pt	ppy	ADC	Cl		Pt	ppy	ADC	Cl
Pt	0.009	0.204	0.087	0.002	Pt	0.010	0.042	0.000	0.001
ppy	0.017	0.397	0.170	0.004	ppy	0.167	0.736	0.002	0.016
ADC	0.001	0.015	0.006	0.000	ADC	0.004	0.019	0.000	0.000
Cl	0.003	0.059	0.025	0.006	Cl	0.000	0.002	0.000	0.000

Table S4.7. The decrease (violet) and increase (terracota) of electron density for most intensive electronic absorption transitions of **1b**. The data for the corresponding interfragment charge transfer (IFCT) are given below the figures. Diagonal values represent intraligand transitions, off-diagonal values represent a charge transfer from "Donor" to "Acceptor".

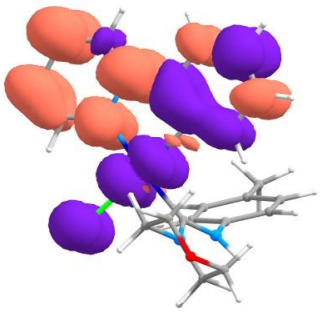

$S_0 \rightarrow S_1$

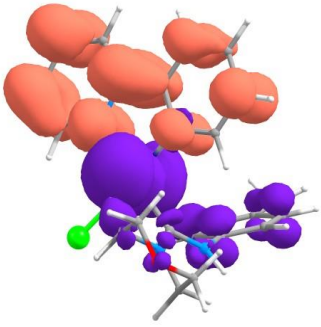

$S_0 \rightarrow S_2$

Donor	Acceptor				Donor	Acceptor			
	Pt	ppy	ADC	Cl		Pt	ppy	ADC	Cl
Pt	0.020	0.358	0.009	0.000	Pt	0.038	0.699	0.018	0.001
ppy	0.026	0.481	0.013	0.001	ppy	0.003	0.064	0.002	0.000
ADC	0.000	0.004	0.000	0.000	ADC	0.009	0.165	0.004	0.000
Cl	0.004	0.082	0.002	0.000	Cl	0.000	0.000	0.000	0.000

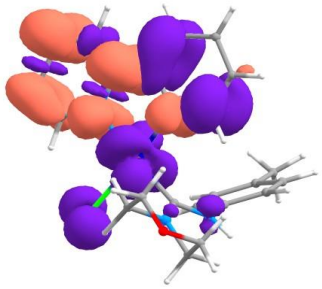

$S_0 \rightarrow S_3$

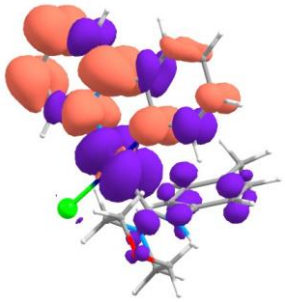

$S_0 \rightarrow S_4$

Donor	Acceptor			
	Pt	**ppy**	**ADC**	**Cl**
Pt	0.074	0.288	0.051	0.000
ppy	0.074	0.288	0.051	0.000
ADC	0.025	0.097	0.017	0.000
Cl	0.009	0.036	0.006	0.000

Donor	Acceptor			
	Pt	**ppy**	**ADC**	**Cl**
Pt	0.024	0.455	0.012	0.006
ppy	0.018	0.333	0.009	0.000
ADC	0.006	0.114	0.003	0.000
Cl	0.001	0.023	0.001	0.000

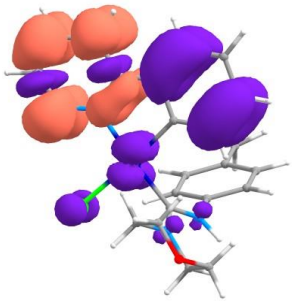

$S_0 \rightarrow S_5$

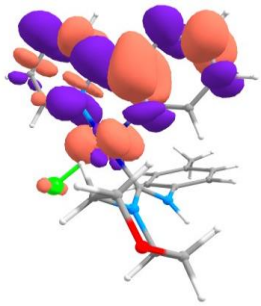

$T_1 \rightarrow S_0$

Donor	Acceptor			
	Pt	**ppy**	**ADC**	**Cl**
Pt	0.015	0.156	0.024	0.000
ppy	0.047	0.482	0.075	0.000
ADC	0.009	0.089	0.014	0.000
Cl	0.008	0.079	0.012	0.000

Donor	Acceptor			
	Pt	**ppy**	**ADC**	**Cl**
Pt	0.010	0.046	0.000	0.001
ppy	0.160	0.743	0.002	0.015
ADC	0.004	0.017	0.000	0.000
Cl	0.000	0.002	0.000	0.000

Table S4.8. The decrease (violet) and increase (terracota) of electron density for most intensive electronic absorption transitions of **1c**. The data for the corresponding interfragment charge transfer (IFCT) are given below the figures. Diagonal values represent intraligand transitions, off-diagonal values represent a charge transfer from “Donor” to “Acceptor”.

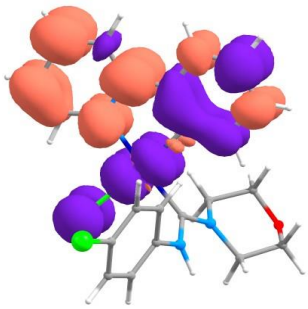

$S_0 \rightarrow S_1$

Donor	Acceptor			
	Pt	**ppy**	**ADC**	**Cl**
Pt	0.018	0.355	0.015	0.000
ppy	0.024	0.464	0.019	0.001
ADC	0.000	0.003	0.000	0.000
Cl	0.005	0.092	0.004	0.000

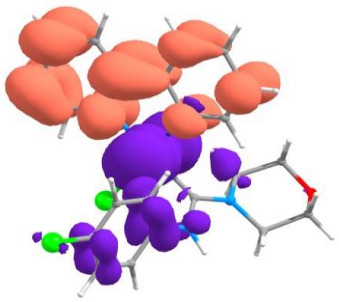

$S_0 \rightarrow S_2$

Donor	Acceptor			
	Pt	**ppy**	**ADC**	**Cl**
Pt	0.036	0.702	0.029	0.001
ppy	0.003	0.059	0.002	0.000
ADC	0.008	0.156	0.007	0.000
Cl	0.000	0.000	0.000	0.000

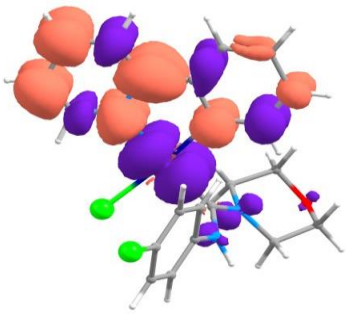

$S_0 \rightarrow S_3$

Donor	Acceptor			
	Pt	**ppy**	**ADC**	**Cl**
Pt	0.033	0.446	0.030	0.000
ppy	0.026	0.350	0.024	0.000
ADC	0.005	0.063	0.004	0.000
Cl	0.001	0.019	0.001	0.000

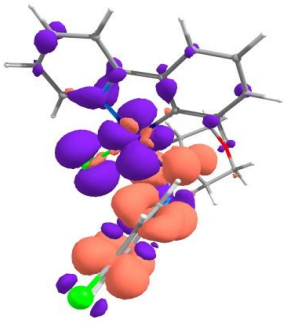

$S_0 \rightarrow S_4$

Donor	Acceptor			
	Pt	**ppy**	**ADC**	**Cl**
Pt	0.095	0.027	0.273	0.000
ppy	0.033	0.009	0.094	0.000
ADC	0.071	0.020	0.205	0.000
Cl	0.052	0.015	0.149	0.000

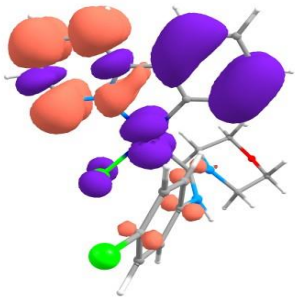

$S_0 \rightarrow S_5$

Donor	Acceptor

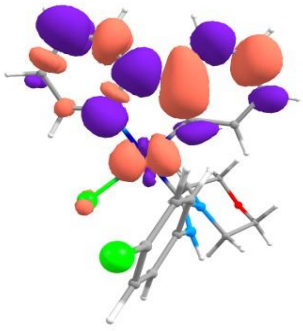

$T_1 \rightarrow S_0$

Donor	Acceptor

	Pt	ppy	ADC	Cl		Pt	ppy	ADC	Cl
Pt	0.009	0.168	0.040	0.000	**Pt**	0.009	0.043	0.000	0.001
ppy	0.026	0.492	0.117	0.000	**ppy**	0.155	0.741	0.002	0.016
ADC	0.005	0.092	0.022	0.000	**ADC**	0.005	0.025	0.000	0.001
Cl	0.001	0.027	0.006	0.000	**Cl**	0.000	0.002	0.000	0.000

Table S4.9. The decrease (violet) and increase (terracota) of electron density for most intensive electronic absorption transitions of **1d**. The data for the corresponding interfragment charge transfer (IFCT) are given below the figures. Diagonal values represent intraligand transitions, off-diagonal values represent a charge transfer from "Donor" to "Acceptor".

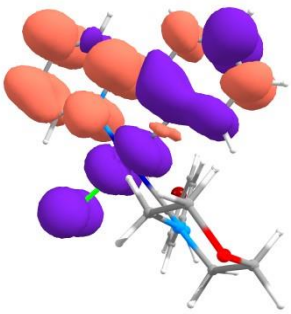

$S_0 \rightarrow S_1$

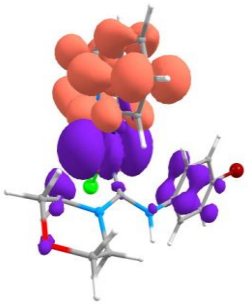

$S_0 \rightarrow S_2$

Donor	**Acceptor**				**Donor**	**Acceptor**			
	Pt	**ppy**	**ADC**	**Cl**		**Pt**	**ppy**	**ADC**	**Cl**
Pt	0.019	0.354	0.014	0.000	**Pt**	0.034	0.743	0.030	0.001
ppy	0.024	0.465	0.019	0.001	**ppy**	0.003	0.064	0.003	0.000
ADC	0.000	0.003	0.000	0.000	**ADC**	0.006	0.111	0.005	0.000
Cl	0.005	0.092	0.004	0.000	**Cl**	0.000	0.000	0.000	0.000

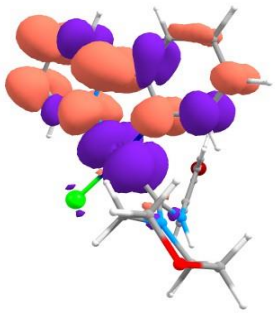

$S_0 \rightarrow S_3$

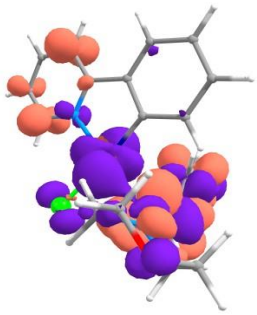

$S_0 \rightarrow S_4$

Donor	**Acceptor**				**Donor**	**Acceptor**			
	Pt	**ppy**	**ADC**	**Cl**		**Pt**	**ppy**	**ADC**	**Cl**
Pt	0.026	0.480	0.029	0.001	**Pt**	0.022	0.050	0.172	0.000
ppy	0.019	0.350	0.021	0.001	**ppy**	0.011	0.024	0.083	0.000
ADC	0.002	0.039	0.002	0.000	**ADC**	0.054	0.124	0.426	0.000

Cl	0.001	0.027	0.002	0.000	**Cl**	0.004	0.009	0.031	0.000

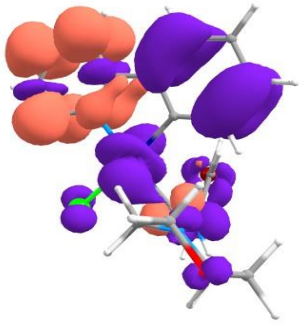

$S_0 \rightarrow S_5$

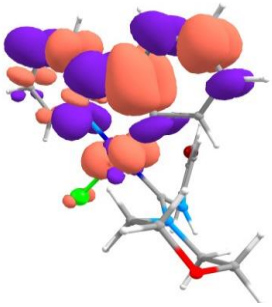

$T_1 \rightarrow S_0$

Donor	**Acceptor**				**Donor**	**Acceptor**			
	Pt	**ppy**	**ADC**	**Cl**		**Pt**	**ppy**	**ADC**	**Cl**
Pt	0.010	0.167	0.044	0.000	**Pt**	0.009	0.043	0.000	0.001
ppy	0.021	0.370	0.098	0.000	**ppy**	0.154	0.741	0.002	0.016
ADC	0.011	0.194	0.051	0.000	**ADC**	0.005	0.025	0.000	0.001
Cl	0.002	0.033	0.009	0.000	**Cl**	0.000	0.002	0.000	0.000

Table S4.10. The decrease (violet) and increase (terracota) of electron density for most intensive electronic absorption transitions of **1e**. The data for the corresponding interfragment charge transfer (IFCT) are given below the figures. Diagonal values represent intraligand transitions, off-diagonal values represent a charge transfer from "Donor" to "Acceptor".

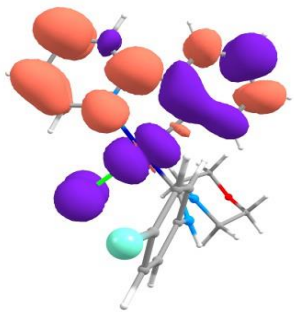

$S_0 \rightarrow S_1$

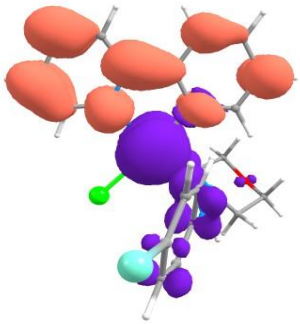

$S_0 \rightarrow S_2$

Donor	**Acceptor**				**Donor**	**Acceptor**			
	Pt	**ppy**	**ADC**	**Cl**		**Pt**	**ppy**	**ADC**	**Cl**
Pt	0.019	0.353	0.016	0.000	**Pt**	0.039	0.743	0.033	0.001
ppy	0.025	0.464	0.021	0.001	**ppy**	0.003	0.063	0.003	0.000
ADC	0.000	0.003	0.000	0.000	**ADC**	0.006	0.109	0.005	0.000
Cl	0.005	0.092	0.004	0.000	**Cl**	0.000	0.000	0.000	0.000

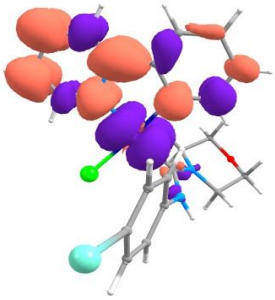

$S_0 \rightarrow S_3$

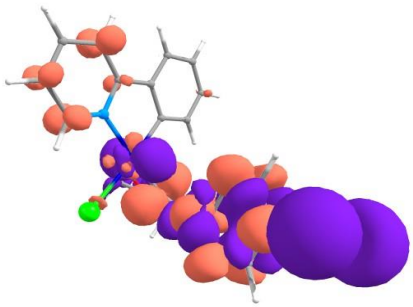

$S_0 \rightarrow S_4$

Donor	Acceptor			
	Pt	**ppy**	**ADC**	**Cl**
Pt	0.032	0.449	0.044	0.000
ppy	0.024	0.344	0.034	0.000
ADC	0.003	0.039	0.004	0.000
Cl	0.002	0.023	0.002	0.000

Donor	Acceptor			
	Pt	**ppy**	**ADC**	**Cl**
Pt	0.019	0.022	0.159	0.000
ppy	0.002	0.003	0.021	0.000
ADC	0.073	0.087	0.624	0.000
Cl	0.000	0.001	0.004	0.000

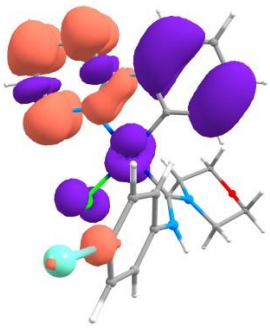

$S_0 \rightarrow S_5$

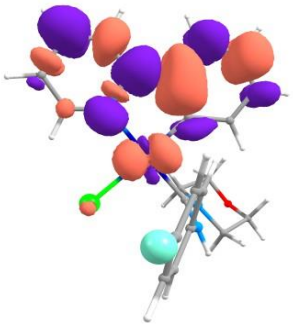

$T_1 \rightarrow S_0$

Donor	Acceptor			
	Pt	**ppy**	**ADC**	**Cl**
Pt	0.023	0.115	0.060	0.000
ppy	0.059	0.290	0.151	0.000
ADC	0.017	0.086	0.045	0.000
Cl	0.020	0.098	0.051	0.000

Donor	Acceptor			
	Pt	**ppy**	**ADC**	**Cl**
Pt	0.009	0.043	0.000	0.001
ppy	0.152	0.744	0.001	0.015
ADC	0.005	0.026	0.000	0.001
Cl	0.000	0.002	0.000	0.000

Table S4.11. The decrease (violet) and increase (terracota) of electron density for most intensive electronic absorption transitions of **1f**. The data for the corresponding interfragment charge transfer (IFCT) are given below the figures. Diagonal values represent intraligand transitions, off-diagonal values represent a charge transfer from “Donor” to “Acceptor”.

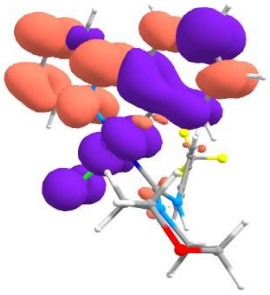

$S_0 \rightarrow S_1$

Donor	Acceptor			
	Pt	ppy	ADC	Cl
Pt	0.019	0.344	0.020	0.000
ppy	0.025	0.461	0.027	0.001
ADC	0.000	0.002	0.000	0.000
Cl	0.005	0.090	0.005	0.000

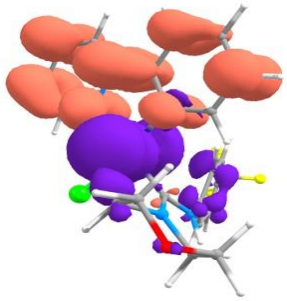

$S_0 \rightarrow S_2$

Donor	Acceptor			
	Pt	ppy	ADC	Cl
Pt	0.040	0.743	0.044	0.001
ppy	0.003	0.060	0.004	0.000
ADC	0.005	0.098	0.006	0.000
Cl	0.000	0.000	0.000	0.000

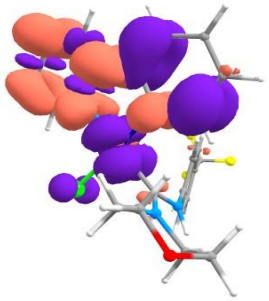

$S_0 \rightarrow S_3$

Donor	Acceptor			
	Pt	ppy	ADC	Cl
Pt	0.016	0.301	0.017	0.000
ppy	0.029	0.543	0.030	0.001
ADC	0.001	0.016	0.001	0.000
Cl	0.002	0.041	0.002	0.000

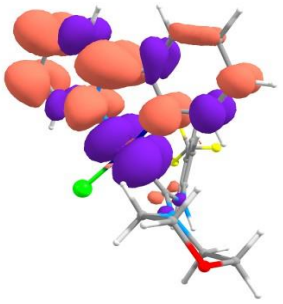

$S_0 \rightarrow S_4$

Donor	Acceptor			
	Pt	ppy	ADC	Cl
Pt	0.038	0.475	0.040	0.000
ppy	0.026	0.331	0.028	0.000
ADC	0.002	0.031	0.003	0.000
Cl	0.002	0.023	0.002	0.000

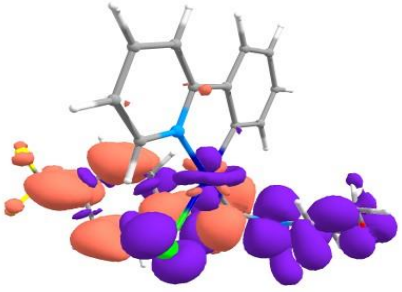

$S_0 \rightarrow S_5$

Donor	Acceptor

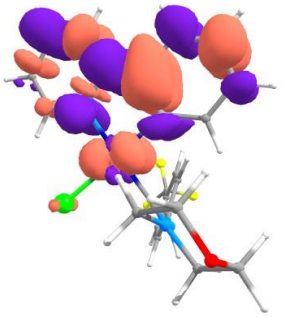

$T_1 \rightarrow S_0$

Donor	Acceptor

	Pt	ppy	ADC	Cl		Pt	ppy	ADC	Cl
Pt	0.006	0.004	0.092	0.000	**Pt**	0.009	0.043	0.000	0.001
ppy	0.002	0.001	0.024	0.000	**ppy**	0.148	0.745	0.001	0.015
ADC	0.047	0.030	0.732	0.000	**ADC**	0.006	0.029	0.000	0.001
Cl	0.004	0.003	0.064	0.000	**Cl**	0.000	0.002	0.000	0.000

Table S4.12. The decrease (violet) and increase (terracota) of electron density for most intensive electronic absorption transitions of **2a**. The data for the corresponding interfragment charge transfer (IFCT) are given below the figures. Diagonal values represent intraligand transitions, off-diagonal values represent a charge transfer from "Donor" to "Acceptor".

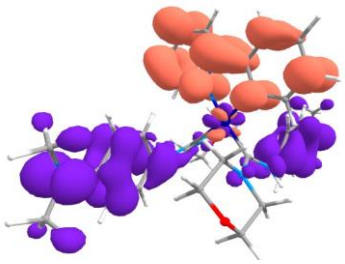

$S_0 \rightarrow S_1$

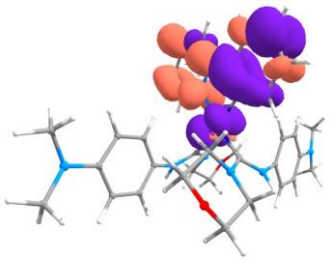

$S_0 \rightarrow S_2$

Donor	Acceptor			
	Pt	**ppy**	**ADC^{tC}**	**ADC^{tN}**
Pt	0.001	0.022	0.001	0.000
ppy	0.000	0.005	0.000	0.000
ADC^{tC}	0.018	0.415	0.009	0.009
ADC^{tN}	0.021	0.477	0.011	0.011

Donor	Acceptor			
	Pt	**ppy**	**ADC^{tC}**	**ADC^{tN}**
Pt	0.011	0.247	0.006	0.005
ppy	0.028	0.645	0.014	0.014
ADC^{tC}	0.001	0.018	0.000	0.000
ADC^{tN}	0.000	0.008	0.000	0.000

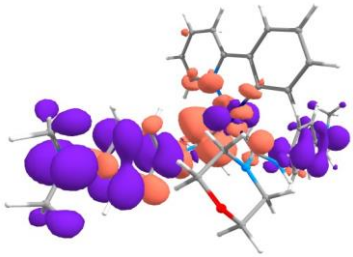

$S_0 \rightarrow S_3$

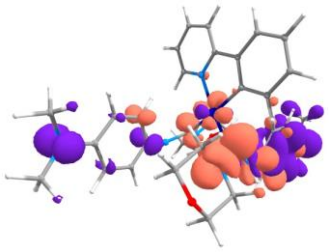

$S_0 \rightarrow S_4$

Donor	Acceptor			
	Pt	**ppy**	**ADC^{tC}**	**ADC^{tN}**
Pt	0.017	0.009	0.053	0.004
ppy	0.008	0.004	0.026	0.002
ADC^{tC}	0.120	0.061	0.376	0.029
ADC^{tN}	0.059	0.030	0.186	0.014

Donor	Acceptor			
	Pt	**ppy**	**ADC^{tC}**	**ADC^{tN}**
Pt	0.003	0.001	0.004	0.020
ppy	0.003	0.001	0.004	0.019
ADC^{tC}	0.025	0.011	0.031	0.147
ADC^{tN}	0.086	0.037	0.105	0.503

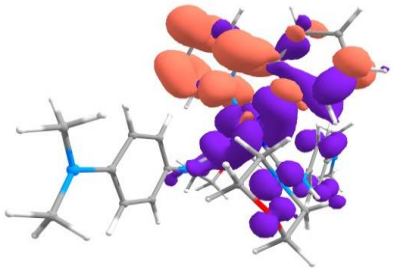

$S_0 \rightarrow S_5$

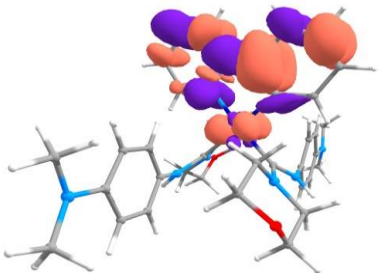

$T_1 \rightarrow S_0$

Donor	Acceptor			
	Pt	**ppy**	**ADC^{tC}**	**ADC^{tN}**
Pt	0.037	0.299	0.084	0.011
ppy	0.026	0.212	0.060	0.008
ADC^{tC}	0.010	0.080	0.023	0.003
ADC^{tN}	0.013	0.101	0.028	0.004

Donor	Acceptor			
	Pt	**ppy**	**ADC^{tC}**	**ADC^{tN}**
Pt	0.005	0.038	0.000	0.000
ppy	0.105	0.806	0.007	0.002
ADC^{tC}	0.002	0.016	0.000	0.000
ADC^{tN}	0.002	0.017	0.000	0.000

Table S4.13. The decrease (violet) and increase (terracota) of electron density for most intensive electronic absorption transitions of **2b**. The data for the corresponding interfragment charge transfer (IFCT) are given below the figures. Diagonal values represent intraligand transitions, off-diagonal values represent a charge transfer from "Donor" to "Acceptor".

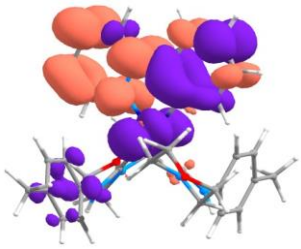

$S_0 \rightarrow S_1$

Donor	Acceptor			
	Pt	**ppy**	**ADC^{tC}**	**ADC^{tN}**
Pt	0.016	0.302	0.010	0.013
ppy	0.026	0.489	0.016	0.021
ADC^{tC}	0.004	0.077	0.002	0.003
ADC^{tN}	0.001	0.018	0.001	0.001

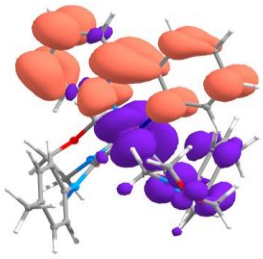

$S_0 \rightarrow S_2$

Donor	Acceptor			
	Pt	**ppy**	**ADC^{tC}**	**ADC^{tN}**
Pt	0.029	0.236	0.109	0.103
ppy	0.018	0.149	0.069	0.065
ADC^{tC}	0.003	0.024	0.011	0.011
ADC^{tN}	0.010	0.085	0.040	0.037

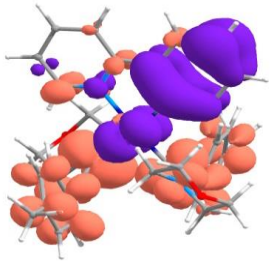

$S_0 \rightarrow S_3$

Donor	Acceptor			
	Pt	**ppy**	**ADC^{tC}**	**ADC^{tN}**
Pt	0.020	0.164	0.092	0.085
ppy	0.028	0.230	0.130	0.119
ADC^{tC}	0.002	0.015	0.009	0.008
ADC^{tN}	0.005	0.045	0.025	0.023

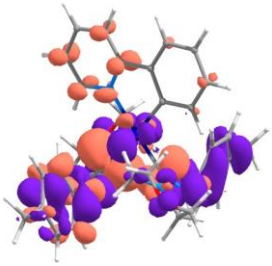

$S_0 \rightarrow S_4$

Donor	Acceptor			
	Pt	**ppy**	**ADC^{tC}**	**ADC^{tN}**
Pt	0.008	0.039	0.060	0.026
ppy	0.004	0.018	0.027	0.012
ADC^{tC}	0.025	0.119	0.184	0.079
ADC^{tN}	0.026	0.117	0.181	0.078

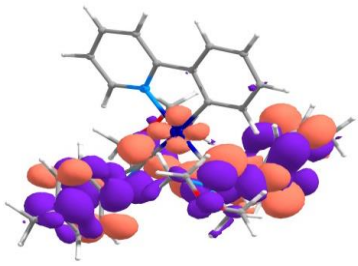

$S_0 \rightarrow S_5$

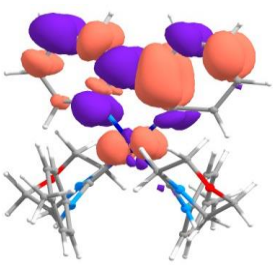

$T_1 \rightarrow S_0$

Donor	Acceptor			
	Pt	**ppy**	**ADC^{tC}**	**ADC^{tN}**
Pt	0.018	0.016	0.074	0.109
ppy	0.004	0.004	0.018	0.026
ADC^{tC}	0.028	0.024	0.112	0.164
ADC^{tN}	0.034	0.029	0.137	0.202

Donor	Acceptor			
	Pt	**ppy**	**ADC^{tC}**	**ADC^{tN}**
Pt	0.006	0.042	0.000	0.000
ppy	0.108	0.776	0.008	0.005
ADC^{tC}	0.003	0.021	0.000	0.000
ADC^{tN}	0.004	0.027	0.000	0.000

Table S4.14. The decrease (violet) and increase (terracota) of electron density for most intensive electronic absorption transitions of **2c**. The data for the corresponding interfragment charge transfer (IFCT) are given below the figures. Diagonal values represent intraligand transitions, off-diagonal values represent a charge transfer from "Donor" to "Acceptor".

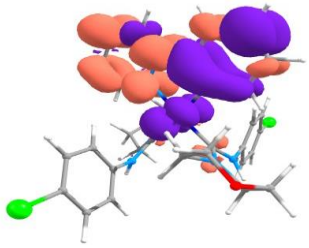

$S_0 \rightarrow S_1$

Donor	Acceptor			
	Pt	**ppy**	**ADC^{tC}**	**ADC^{tN}**
Pt	0.012	0.217	0.010	0.014
ppy	0.035	0.616	0.028	0.039
ADC^{tC}	0.001	0.022	0.001	0.001
ADC^{tN}	0.000	0.003	0.000	0.000

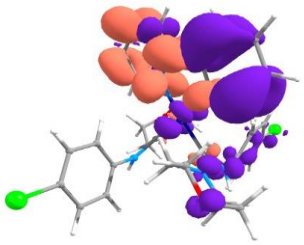

$S_0 \rightarrow S_2$

Donor	Acceptor			
	Pt	**ppy**	**ADC^{tC}**	**ADC^{tN}**
Pt	0.005	0.096	0.004	0.006
ppy	0.033	0.648	0.028	0.043
ADC^{tC}	0.001	0.013	0.001	0.001
ADC^{tN}	0.005	0.105	0.005	0.007

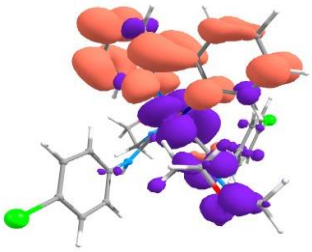

$0.S_0 \rightarrow S_3$

Donor	Acceptor			
	Pt	**ppy**	**ADC^{tC}**	**ADC^{tN}**
Pt	0.021	0.411	0.038	0.021
ppy	0.014	0.261	0.024	0.013
ADC^{tC}	0.002	0.036	0.003	0.002
ADC^{tN}	0.007	0.128	0.012	0.007

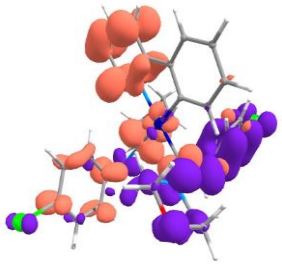

$S_0 \rightarrow S_4$

Donor	Acceptor			
	Pt	**ppy**	**ADC^{tC}**	**ADC^{tN}**
Pt	0.003	0.024	0.020	0.013
ppy	0.007	0.060	0.051	0.032
ADC^{tC}	0.009	0.086	0.073	0.046
ADC^{tN}	0.025	0.230	0.196	0.123

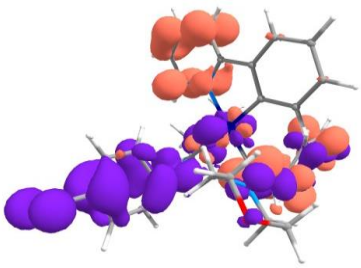

$S_0 \rightarrow S_5$

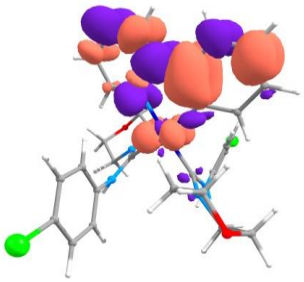

$T_1 \rightarrow S_0$

Donor	Acceptor			
	Pt	**ppy**	**ADC^{tC}**	**ADC^{tN}**
Pt	0.008	0.053	0.049	0.086
ppy	0.005	0.035	0.032	0.057
ADC^{tC}	0.015	0.104	0.097	0.170
ADC^{tN}	0.011	0.078	0.073	0.128

Donor	Acceptor			
	Pt	**ppy**	**ADC^{tC}**	**ADC^{tN}**
Pt	0.006	0.042	0.000	0.000
ppy	0.110	0.761	0.007	0.007
ADC^{tC}	0.004	0.025	0.000	0.000
ADC^{tN}	0.005	0.032	0.000	0.000

Table S4.15. The decrease (violet) and increase (terracota) of electron density for most intensive electronic absorption transitions of **2d**. The data for the corresponding interfragment charge transfer (IFCT) are given below the figures. Diagonal values represent intraligand transitions, off-diagonal values represent a charge transfer from "Donor" to "Acceptor".

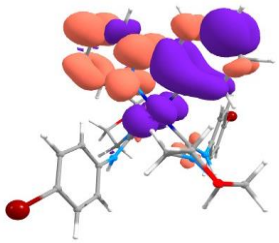

$S_0 \rightarrow S_1$

Donor	Acceptor			
	Pt	**ppy**	**ADC^{tC}**	**ADC^{tN}**
Pt	0.013	0.219	0.009	0.013
ppy	0.036	0.617	0.026	0.036
ADC^{tC}	0.001	0.024	0.001	0.001
ADC^{tN}	0.000	0.003	0.000	0.000

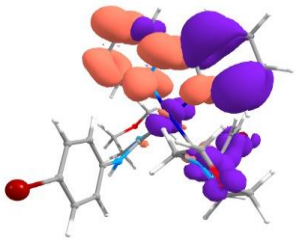

$S_0 \rightarrow S_2$

Donor	Acceptor			
	Pt	**ppy**	**ADC^{tC}**	**ADC^{tN}**
Pt	0.005	0.093	0.004	0.006
ppy	0.030	0.586	0.024	0.036
ADC^{tC}	0.001	0.019	0.001	0.001
ADC^{tN}	0.009	0.169	0.007	0.010

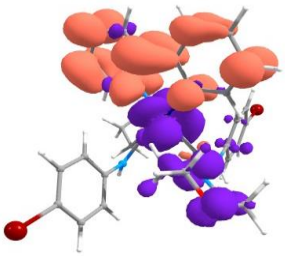

$S_0 \rightarrow S_3$

Donor	Acceptor			
	Pt	**ppy**	**ADC^{tC}**	**ADC^{tN}**
Pt	0.022	0.431	0.043	0.021
ppy	0.012	0.241	0.024	0.012
ADC^{tC}	0.001	0.026	0.003	0.001
ADC^{tN}	0.007	0.136	0.014	0.007

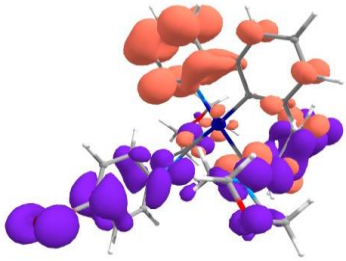

$S_0 \rightarrow S_4$

Donor	Acceptor			
	Pt	**ppy**	**ADC^{tC}**	**ADC^{tN}**
Pt	0.008	0.109	0.031	0.053
ppy	0.005	0.067	0.019	0.032
ADC^{tC}	0.012	0.169	0.047	0.082
ADC^{tN}	0.014	0.200	0.056	0.097

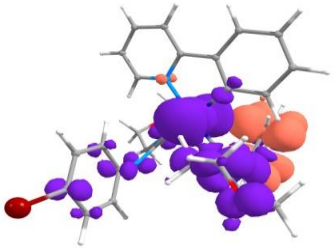

$S_0 \rightarrow S_5$

Donor	Acceptor

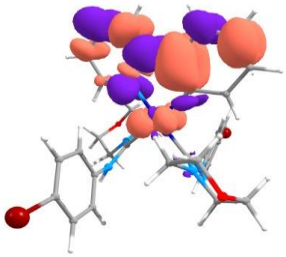

$T_1 \rightarrow S_0$

Donor	Acceptor

	Pt	**ppy**	**ADC^{tC}**	**ADC^{tN}**		**Pt**	**ppy**	**ADC^{tC}**	**ADC^{tN}**
Pt	0.016	0.025	0.018	0.297	**Pt**	0.006	0.043	0.000	0.000
ppy	0.003	0.005	0.003	0.053	**ppy**	0.104	0.770	0.006	0.006
ADC^{tC}	0.006	0.009	0.007	0.111	**ADC^{tC}**	0.003	0.024	0.000	0.000
ADC^{tN}	0.020	0.032	0.023	0.372	**ADC^{tN}**	0.004	0.031	0.000	0.000

Table S4.16. The decrease (violet) and increase (terracota) of electron density for most intensive electronic absorption transitions of **2e**. The data for the corresponding interfragment charge transfer (IFCT) are given below the figures. Diagonal values represent intraligand transitions, off-diagonal values represent a charge transfer from "Donor" to "Acceptor".

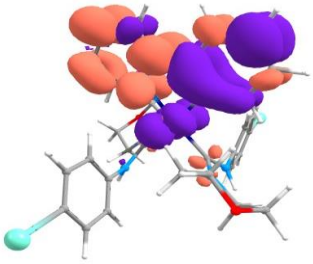

$S_0 \rightarrow S_1$

Donor	Acceptor			
	Pt	**ppy**	**ADC^{tC}**	**ADC^{tN}**
Pt	0.013	0.220	0.010	0.013
ppy	0.035	0.606	0.029	0.037
ADC^{tC}	0.002	0.029	0.001	0.002
ADC^{tN}	0.000	0.003	0.000	0.000

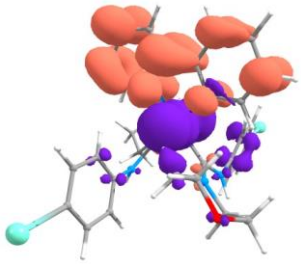

$S_0 \rightarrow S_2$

Donor	Acceptor			
	Pt	**ppy**	**ADC^{tC}**	**ADC^{tN}**
Pt	0.038	0.656	0.031	0.040
ppy	0.003	0.058	0.003	0.004
ADC^{tC}	0.003	0.046	0.002	0.003
ADC^{tN}	0.006	0.098	0.005	0.006

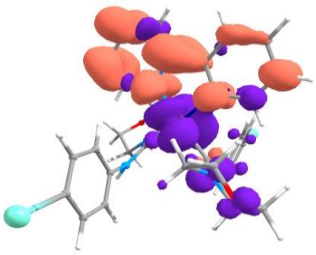

$S_0 \rightarrow S_3$

Donor	Acceptor			
	Pt	**ppy**	**ADC^{tC}**	**ADC^{tN}**
Pt	0.024	0.424	0.032	0.045
ppy	0.014	0.255	0.019	0.027
ADC^{tC}	0.001	0.026	0.002	0.003
ADC^{tN}	0.006	0.103	0.008	0.011

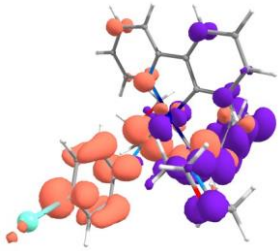

$S_0 \rightarrow S_4$

Donor	Acceptor			
	Pt	**ppy**	**ADC^{tC}**	**ADC^{tN}**
Pt	0.006	0.011	0.049	0.046
ppy	0.004	0.006	0.030	0.028
ADC^{tC}	0.004	0.007	0.035	0.033
ADC^{tN}	0.041	0.070	0.325	0.305

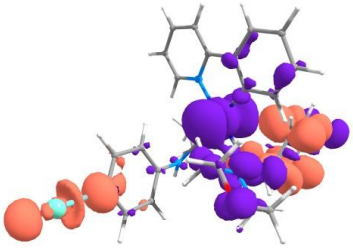

$S_0 \rightarrow S_5$

Donor	Acceptor

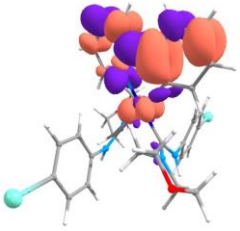

$T_1 \rightarrow S_0$

Donor	Acceptor

	Pt	**ppy**	**ADC^{tC}**	**ADC^{tN}**		**Pt**	**ppy**	**ADC^{tC}**	**ADC^{tN}**
Pt	0.014	0.017	0.115	0.223	**Pt**	0.005	0.044	0.000	0.000
ppy	0.003	0.003	0.021	0.041	**ppy**	0.097	0.776	0.007	0.004
ADC^{tC}	0.008	0.010	0.066	0.127	**ADC^{tC}**	0.003	0.026	0.000	0.000
ADC^{tN}	0.014	0.017	0.109	0.211	**ADC^{tN}**	0.004	0.033	0.000	0.000

Table S4.17. The decrease (violet) and increase (terracota) of electron density for most intensive electronic absorption transitions of **2f**. The data for the corresponding interfragment charge transfer (IFCT) are given below the figures. Diagonal values represent intraligand transitions, off-diagonal values represent a charge transfer from "Donor" to "Acceptor".

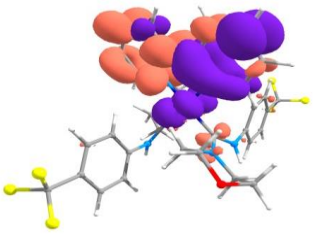

$S_0 \rightarrow S_1$

Donor	Acceptor			
	Pt	**ppy**	**ADC^{tC}**	**ADC^{tN}**
Pt	0.009	0.226	0.011	0.019
ppy	0.025	0.611	0.029	0.052
ADC^{tC}	0.001	0.014	0.001	0.001
ADC^{tN}	0.000	0.002	0.000	0.000

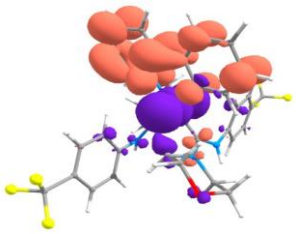

$S_0 \rightarrow S_2$

Donor	Acceptor			
	Pt	**ppy**	**ADC^{tC}**	**ADC^{tN}**
Pt	0.027	0.665	0.032	0.056
ppy	0.002	0.060	0.003	0.005
ADC^{tC}	0.002	0.054	0.003	0.005
ADC^{tN}	0.003	0.073	0.004	0.006

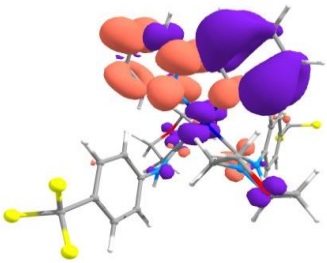

$S_0 \rightarrow S_3$

Donor	Acceptor			
	Pt	**ppy**	**ADC^{tC}**	**ADC^{tN}**
Pt	0.004	0.114	0.005	0.008
ppy	0.023	0.696	0.032	0.047
ADC^{tC}	0.001	0.037	0.002	0.003
ADC^{tN}	0.001	0.025	0.001	0.002

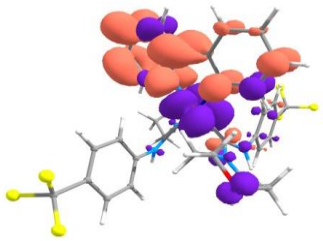

$S_0 \rightarrow S_4$

Donor	Acceptor			
	Pt	**ppy**	**ADC^{tC}**	**ADC^{tN}**
Pt	0.015	0.398	0.056	0.026
ppy	0.011	0.288	0.041	0.019
ADC^{tC}	0.001	0.037	0.005	0.002
ADC^{tN}	0.003	0.082	0.011	0.005

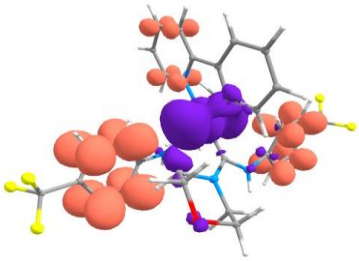

$S_0 \rightarrow S_5$

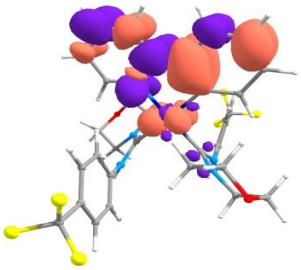

$T_1 \rightarrow S_0$

Donor	Acceptor			
	Pt	**ppy**	**ADC^{tC}**	**ADC^{tN}**
Pt	0.012	0.067	0.266	0.215
ppy	0.006	0.031	0.126	0.102
ADC^{tC}	0.002	0.011	0.043	0.035
ADC^{tN}	0.002	0.010	0.040	0.033

Donor	Acceptor			
	Pt	**ppy**	**ADC^{tC}**	**ADC^{tN}**
Pt	0.005	0.033	0.000	0.000
ppy	0.117	0.761	0.011	0.004
ADC^{tC}	0.003	0.021	0.000	0.000
ADC^{tN}	0.006	0.037	0.001	0.000

Table S4.18. Energies (eV) of selected frontier molecular orbitals for complexes **1a**,**c** and **2a**,**c** in DCE.

Orbital	E, эV	E, sm^{-1}
1a		
LUMO+2	-0.55	-4426.80
LUMO+1	-0.99	-7949.37
LUMO	-1.66	-13385.76
HOMO	-5.21	-42007.44
HOMO-1	-5.71	-46036.99
HOMO-2	-5.98	-48262.47
2a		
LUMO+2	-0.92	-7416.05
LUMO+1	-1.36	-10932.03
LUMO	-1.99	-16032.62
HOMO	-5.48	-44175.85
HOMO-1	-5.50	-44382.16
HOMO-2	-6.22	-50145.56
1c		
LUMO+2	-0.95	-7668.44
LUMO+1	-1.04	-8353.20
LUMO	-1.71	-13815.93
HOMO	-5.78	-46603.24
HOMO-1	-6.01	-48484.14
HOMO-2	-6.48	-52232.76
2c		
LUMO+2	-1.40	-11291.97
LUMO+1	-1.43	-11542.17
LUMO	-2.10	-16952.22
HOMO	-6.31	-50913.72
HOMO-1	-6.49	-52357.86
HOMO-2	-6.70	-53999.53

Table S4.19. Composition (%) of Frontier MOs in terms of ligands and metals for **1a**,**c** and **2a**,**c** in DCE

	HOMO	**LUMO**
1a		
Pt	4.16	5.31
ppy	0.50	91.46
ADC^{tN}	95.14	2.72
1c		
Pt	37.59	5.34
ppy	51.15	90.25
ADC^{tN}	0.88	3.86
2a		
Pt	2.41	4.87
ppy	0.29	90.74
ADC^{tC}	78.64	2.21
ADC^{tN}	18.66	2.18
2c		
Pt	24.38	5.11
ppy	71.52	84.96
ADC^{tC}	3.31	4.16
ADC^{tN}	0.79	5.77

In order to explain the differences nature of the transition in complexes with NMe_2 substituted, analysis of frontier molecular orbitals (FMO) for **1a** and **2a** and their representative counterpart **1c** and **2c** have been performed. Figure 6 shows the shape and energy of these for **1a**, **1c**, **2a** and **2c**, on top of that FMO's compositions are given in Table S5.19 and figs. S4.7-4.9. In all cases, the lowest unoccupied molecular orbitals (LUMOs) are mostly dominated by the π^* molecular orbitals on the ppy ligands, explaining the observation of the minor impact of the nature of the auxiliary ligands on the computed LUMO energies. The change of the substituent in the aryl ring of ACD ligands induces minor effects on the electron densities of the LUMOs of complexes, in addition, it significantly reshapes the electron density in the high occupied molecular orbitals (HOMOs). For **1c** and **2c** the HOMOs are mainly located on the aryl ring of the cyclometalated ligand (51%– **1c** and 72% – **2c**) and the platinum center (38% and 24%

respectively), opposite for NMe_2-substituted complexes **1a** and **2a** the HOMOs are mainly delocalized by the π molecular orbitals on the aryl ring connected with the nitrogen atom of diaminocarbene species (contribution of aryls > 95%), whereas the contribution of the metal d orbitals is insignificant (<5%). In accordance with this, the electron-donor group NMe_2 produces a larger destabilization of HOMO over LUMO, which leads to less HOMO-LUMO energy gaps. There is a correlation between the HOMO–LUMO energy difference and the red-shifted absorption bands determined experimentally for **2a** with electron-donating NMe_2 group relative to its counterpart **2c.**

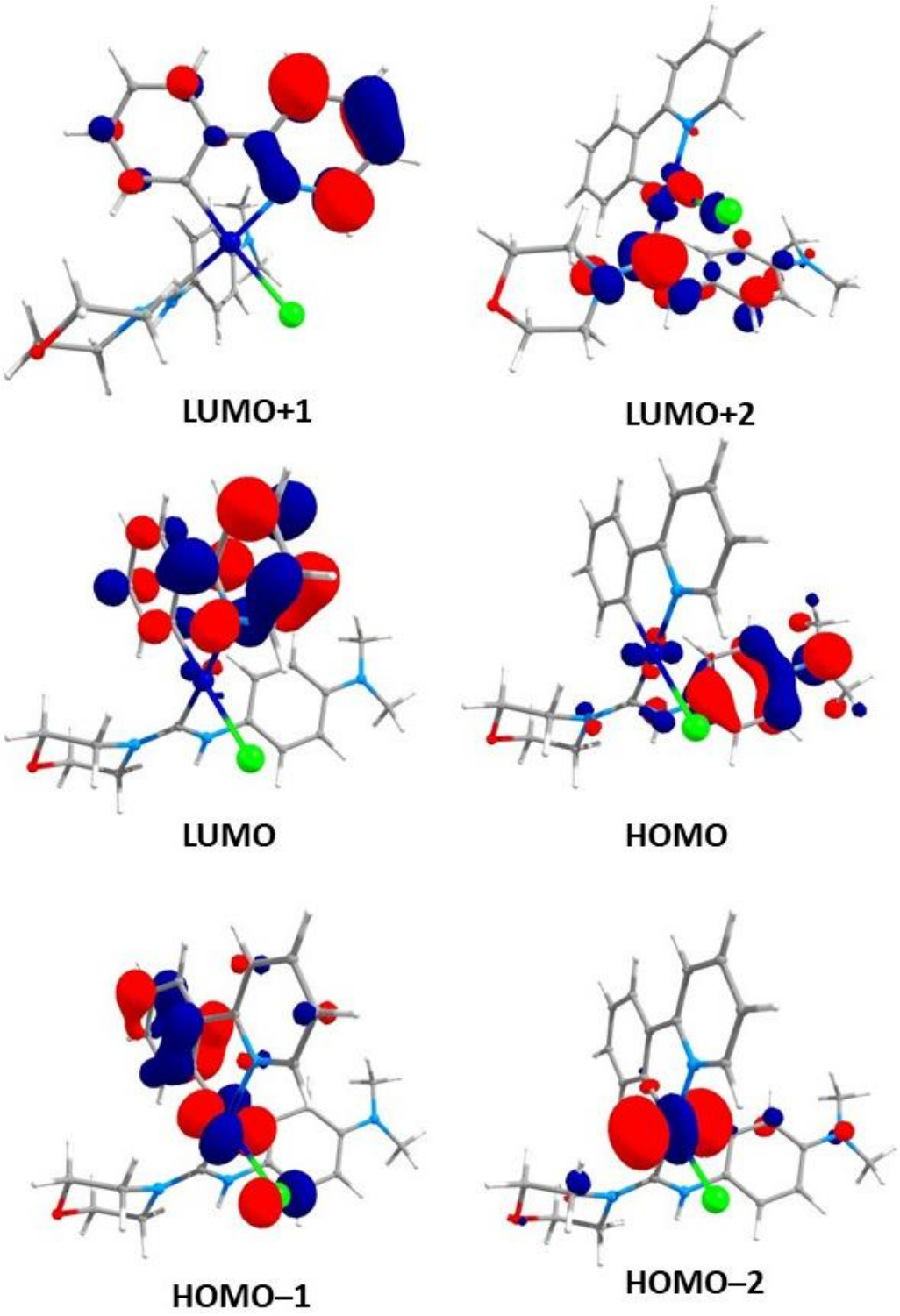

Figure S4.7. Selected frontier Molecular Orbitals for **1a** in the DCE.

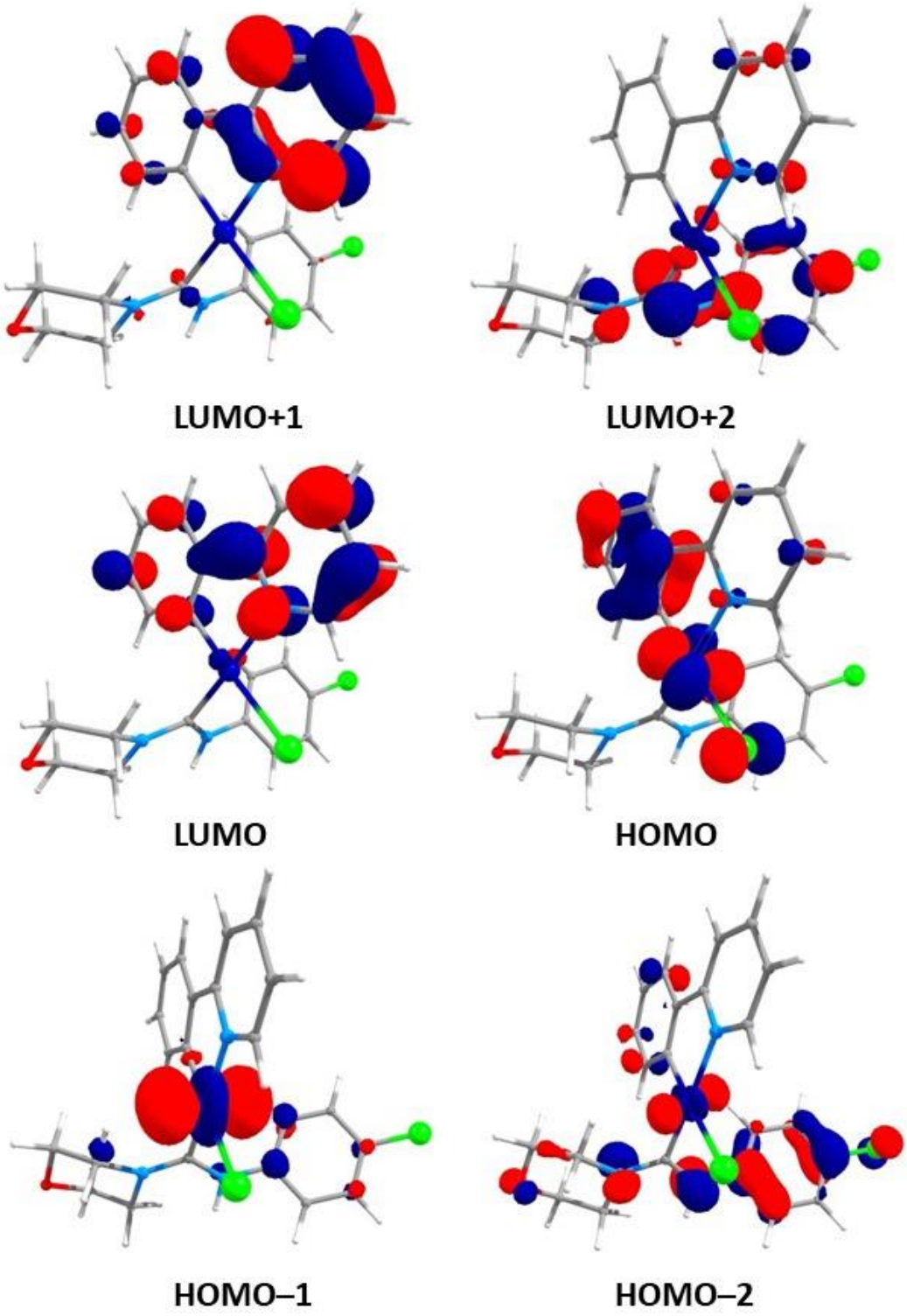

Figure S4.8. Selected frontier Molecular Orbitals for **1c** in the DCE.

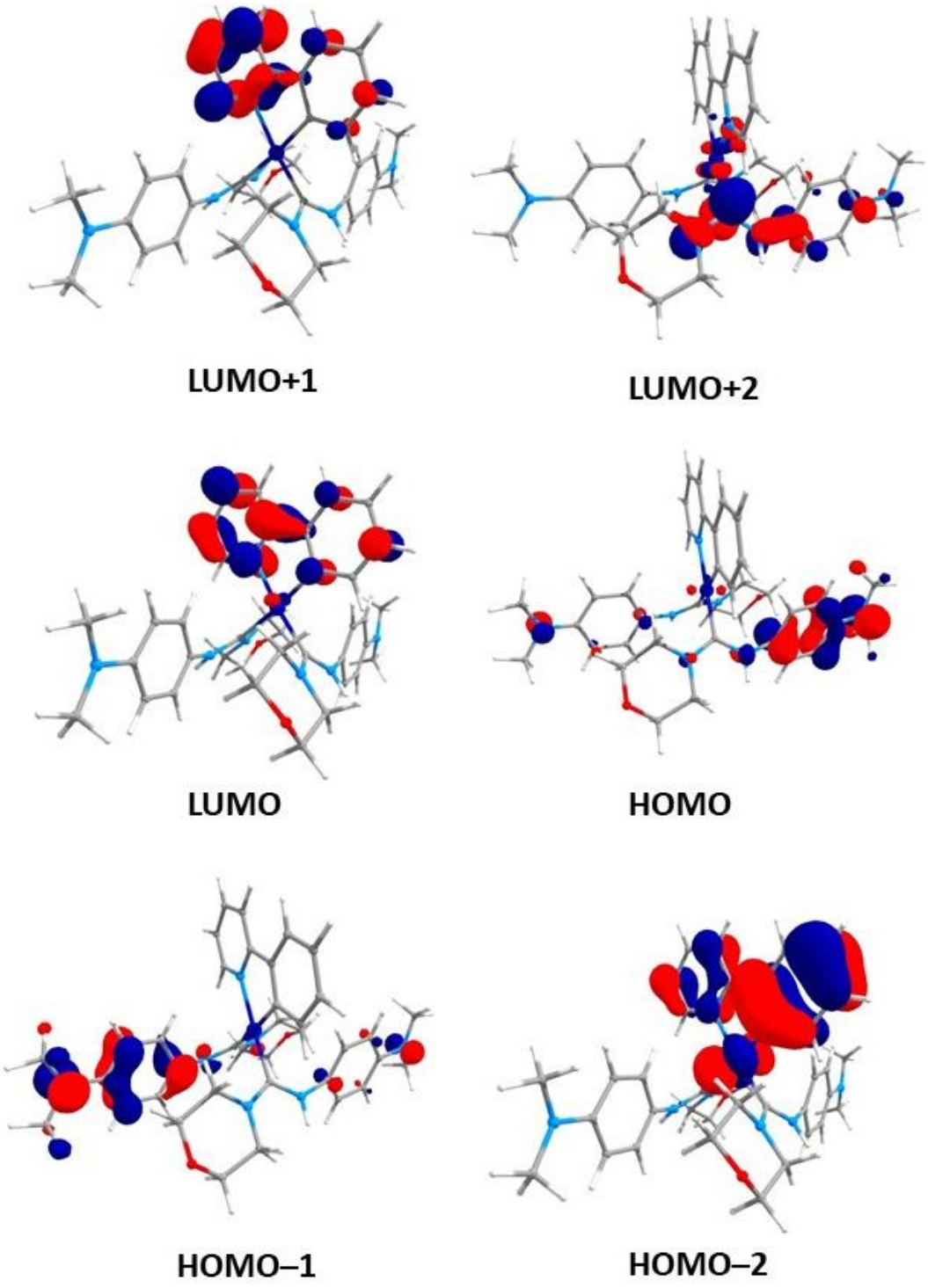

Figure S4.9. Selected frontier Molecular Orbitals for **2a** in the DCE.

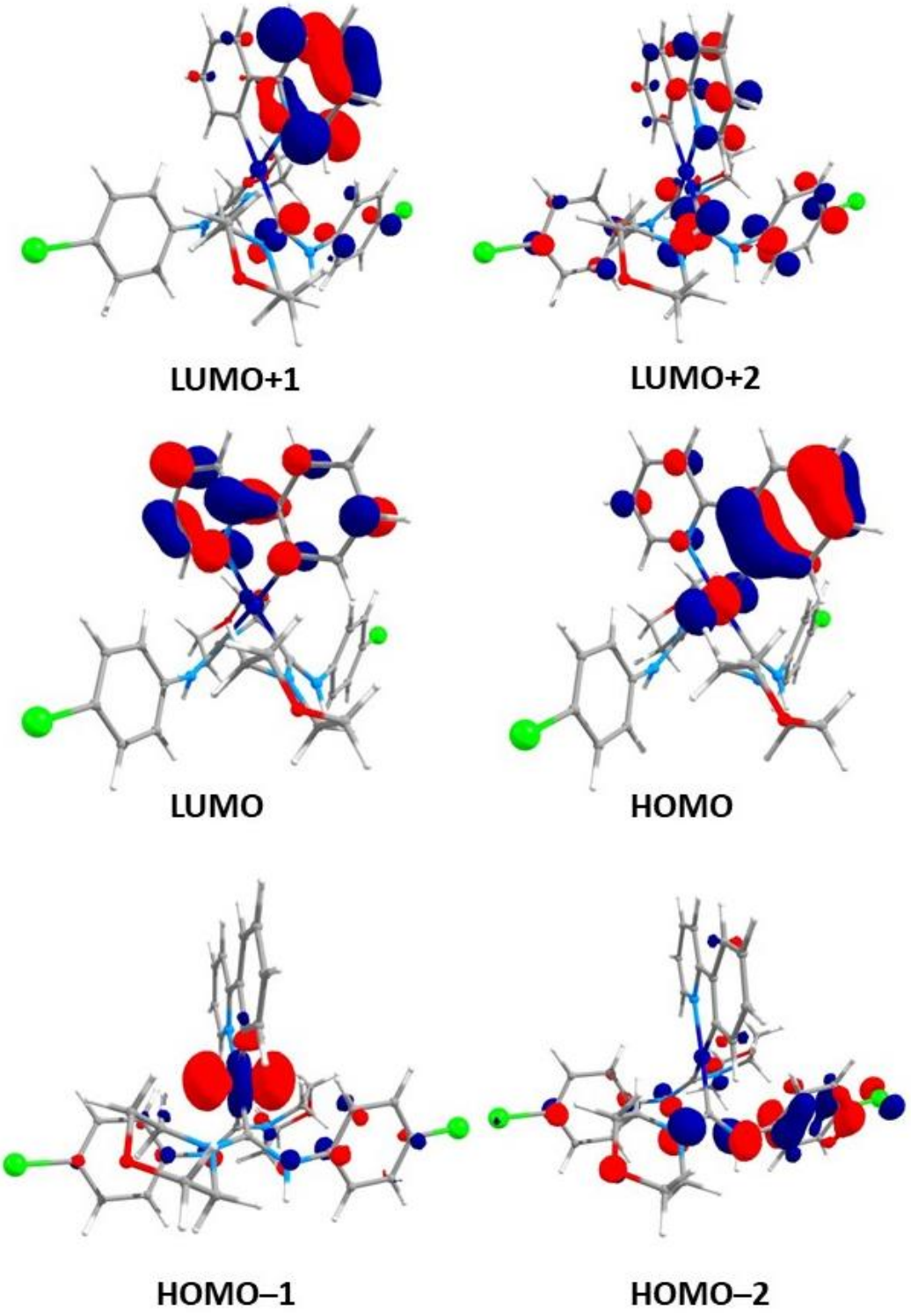

Figure S4.10. Selected frontier Molecular Orbitals for **2c** in the DCE.

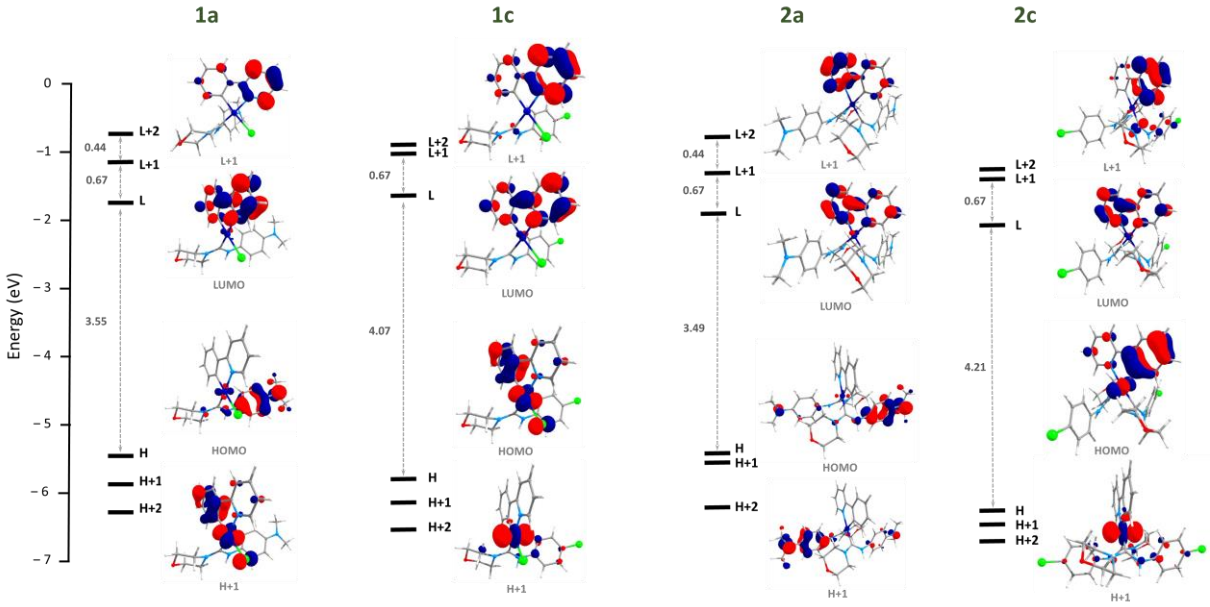

Figure S4.11. Molecular orbital patterns for **1a, 1c, 2a** and **2c** based on their optimized S_0 geometries.

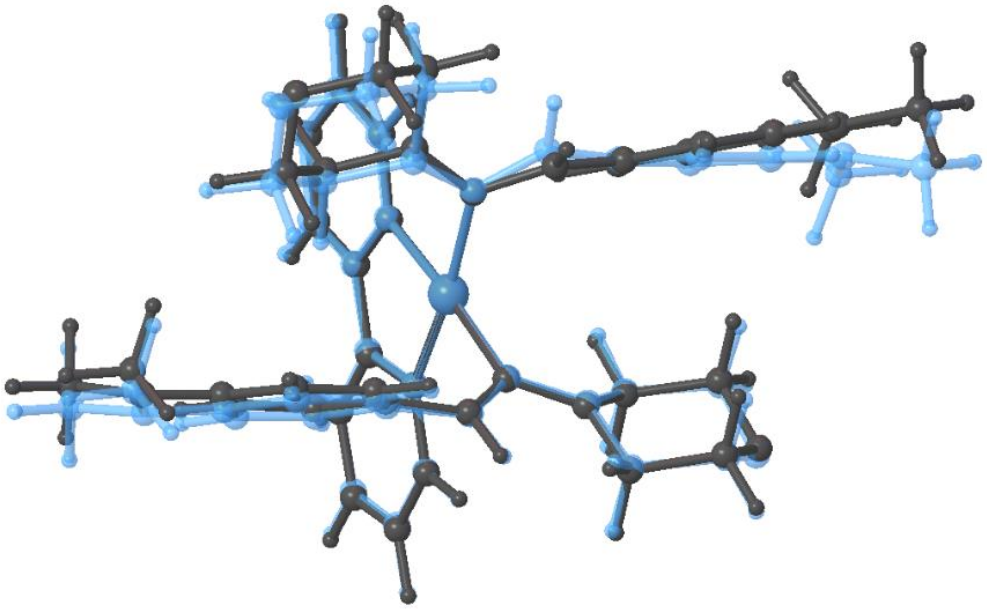

Figure S4.12. Comparison of DFT optimized geometries S1 (dark grey line) and triplet state T1 (blue line) of **2a** in DCE.

S5. OLED manufacturing

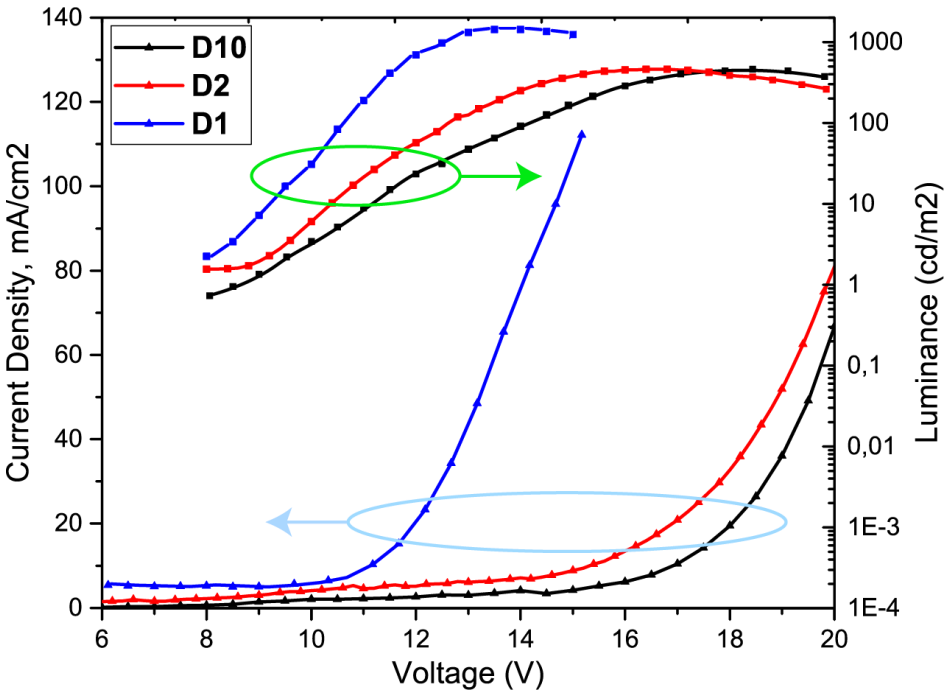

Figure S5.1. Current density and luminance versus applied voltage for devices **D1**–**D2**, **D10**.

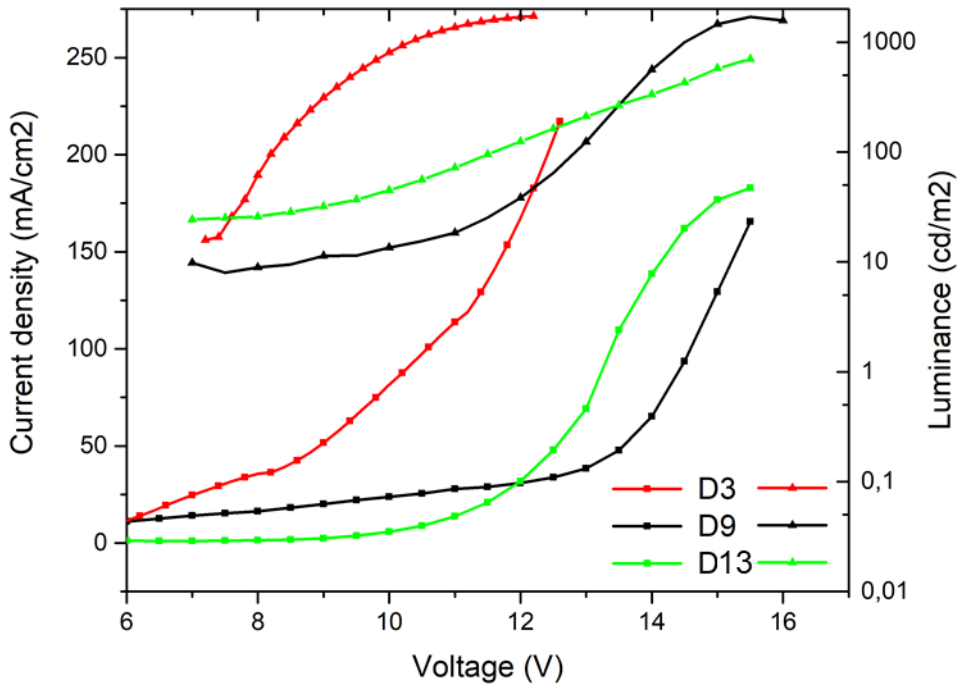

Figure S5.2. Current density and luminance versus applied voltage for devices **D3**, **D9**, **D13**.

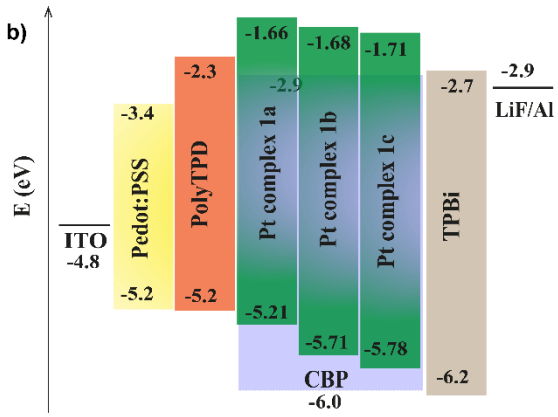

Figure S5.3. Energy level diagram of used materials for devices **D11**–**D13**.

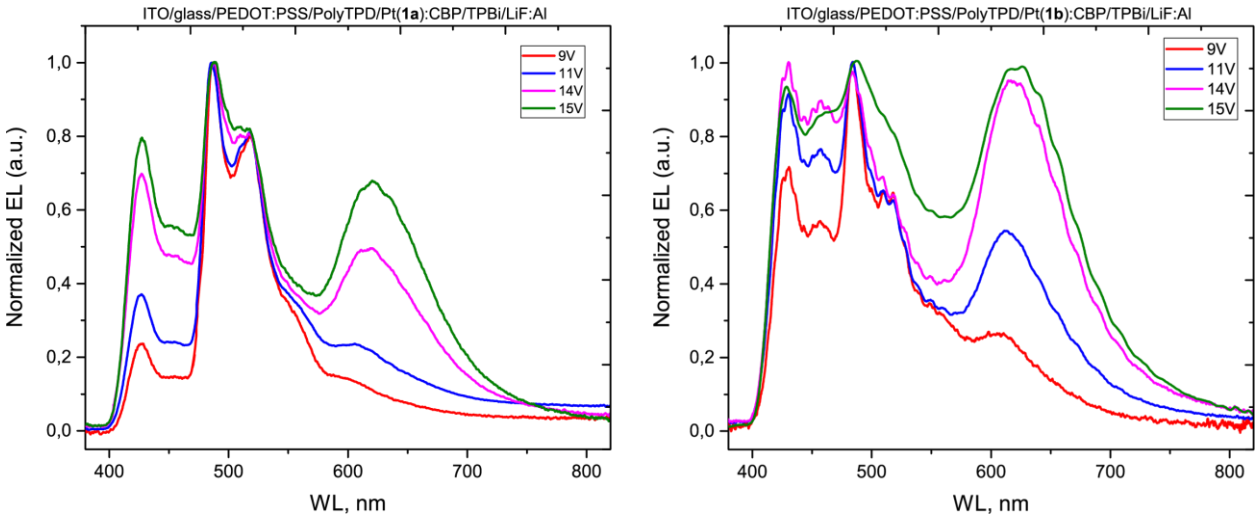

Figure S5.4. EL spectra developing of **D11** (right) and **D12** (left) under different applied bias.

Table S5.1. EL device performances reported for selected examples of luminescent platinum(II) diaminocarbene complexes.

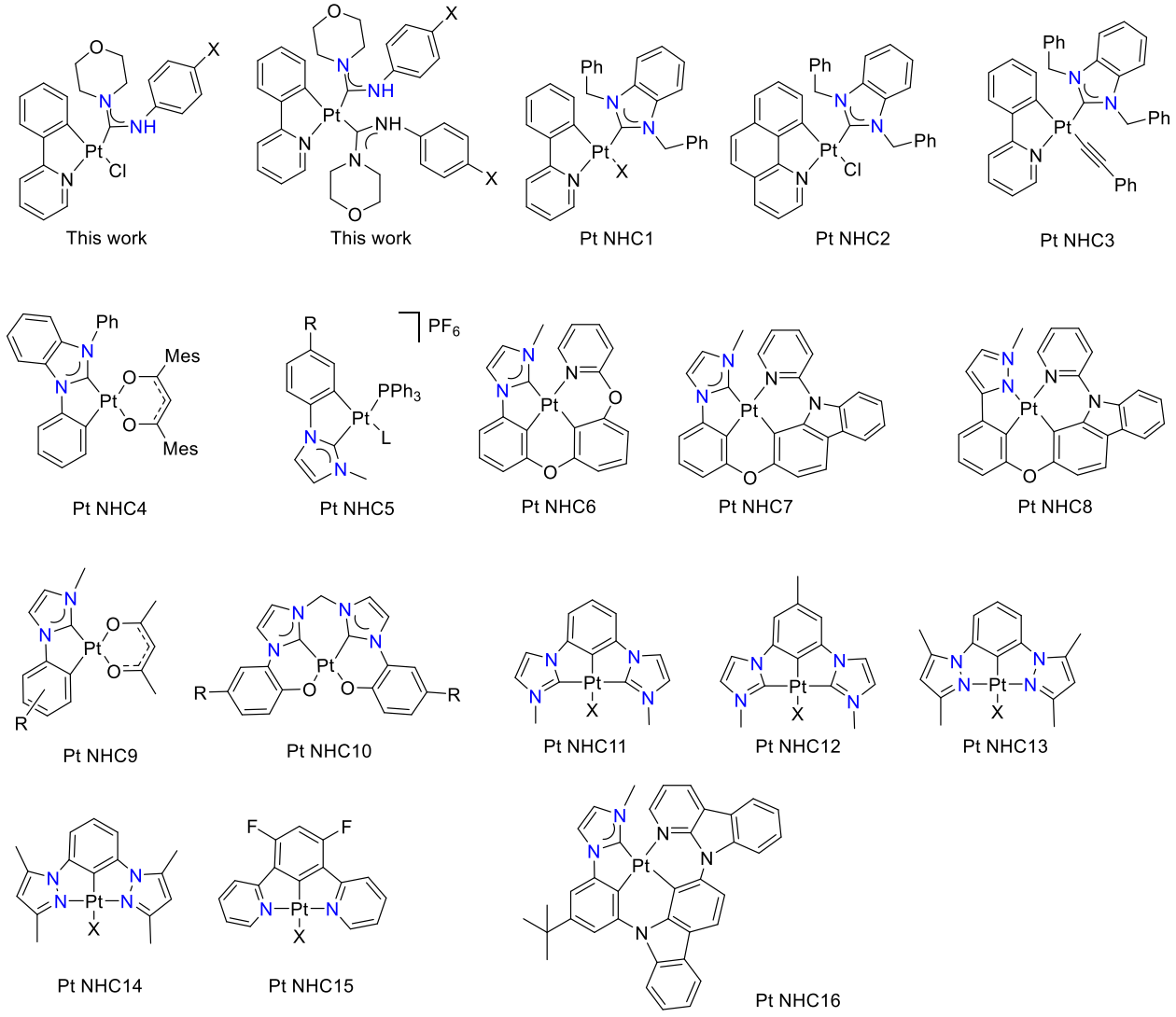

Pt NHC type structure	Device, doping concentration (%)	λ_{EL} (nm)	Luminance (cd·m^{-2})	Current efficiency, (cd·A^{-1})	Power efficiency, (lm·W^{-1})	CIE (x, y)	EML deposition technique	Ref.
Acyclic diaminocarbene Pt complex	Dev 5, 2%	482, 519	2435	2.93	1.02	0.245, 0.538	Spin-coating	This work
	Dev 6, 10%	482, 519	2728	2.17	0.65	0.249, 0.540		
	Dev 7, 2%	486, 519	1721	1.88	0.54	0.257, 0.489		
	Dev 8, 2%	485, 519	2436	1.46	0.34	0.240, 0.482		

	Dev 11, 2%	431, 484, 615	746	2.15	0.96	0.311, 0.320		
Pt NHC 1 Pt NHC 2 Pt NHC 3	Dev 1 (NHC 1), 10%	489, 521	963	1.75	0.5	0.219, 0.664	Spin-casting	18
	Dev 2 (NHC 1), 10%	488, 520	1896	3.18	0.9	0.202, 0.686		
	Dev 3 (NHC 3), 10%	491, 521	1561	2.36	0.67	0.210, 0.674		
	Dev 4 (NHC 2), 10%	503	705	1.23	0.35	0.223, 0.578		
	Dev 5 (NHC 1), 10%	490, 522	1729	2.81	0.8	0.208, 0.685		
	Dev 6 (NHC 1), 10%	494, 525	802	1.56	0.44	0.236, 0.676		
Pt NHC 9	Dev 1, 12%	530	4165	53	41.6	0.34, 0.53	Thermal vapor deposition	19
	Dev 2, 12%	510	2098	25.8	22.5	0.27, 0.50		
	Dev 1, 6%	480, 505, 540	4900	-	-	0.19, 0.19	Thermal vapor deposition	20
	Dev 2, 8%	480, 505, 540	5000	-	-	0.171, 0.163		
	Dev 3, 10%	480, 505, 540	5900	-	-	0.362, 0.469		
	Dev 4, 12%	480, 505, 540	6750	-	-	0.167, 0.157		
Pt NHC 4	Dev 1	-	-	5.91	1,67	0.191, 0.277	Doctor blade	21
	Dev 2	-	-	6.82	1.97	0.193, 0.290		
	Dev 3	-	-	9.34	2.91	0.203, 0.322		

	Dev 4	-	-	25.2	11.88	0.198, 0.310		
Pt NHC 4	Dev 5	-	-	19.9	11.61	0.194, 0.302	Doctor blade	[21]
	Dev 6	-	-	16.79	11.01	0.190, 0.289		
Pt NHC 10	Dev 1, 2%	455, 550	8700	19.1	13.3	0.19, 0.21	No info	[22]
	Dev 2, 4%	455, 550	9500	23.8	16.6	0.191, 0.217		
	Dev 3, 6%	455, 550	6500	14.9	13.3	0.189, 0.198		
	Dev 4, 8%	455, 550	6200	15.3	10.6	0.191, 0.207		
Pt NHC 5	Dev 1	450, 485	50	-	-	0.39, 0.53	Fully solution processed	[23]
	Dev 2	453, 487	101	-	-	0.38, 0.51		
	Dev 3	545	9	-	-	0.36, 0.50		
	Dev 4	565	5	-	-	0.31, 0.44		
	Dev 5	565	6	-	-	0.27, 0.37		
	Dev 6	570	4	-	-	0.27, 0.39		
NHC 11 NHC 13 NHC 14 NHC 15	Dev 1 (NHC 15), 2%	475, 513	-	-	17.4	0.13, 0.33	Thermal vapor deposition	[24]
	Dev 2 (NHC 14), 2%	475, 512	-	-	23.3	0.16, 0.36		
	Dev 3 (NHC 13), 2%	440, 475	-	-	0.16	0.17, 0.20		
	Dev 4 (NHC 11), 2%	450, 480	-	-	8.96	0.16, 0.15		
	Dev 5 (NHC 11), 2%	450, 480	-	-	19.3	0.16, 0.13		
NHC 11 NHC 12	Dev 1 (NHC 11), 2%	450, 480	150	-	10	0.18, 0.19	Thermal vapor	[25]

	Dev 2 (NHC 11), 10%	450, 480, 590	295	-	21	0.32, 0.32	deposition	
	Dev 3 (NHC 11), 14%	450, 480, 590	319	-	21.1	0.38, 0.37		
	Dev 4 (NHC 11), 18%	450, 480, 590	386	-	26.5	0.41, 0.39		
	Dev 5 (NHC 11), 10%	450, 480, 590	371	-	35.2	0.32, 0.33		
	Dev 6 (NHC 11), 10%	450, 480, 590	396	-	35.2	0.33, 0.33		
	Dev 1 (NHC 12), 2%	460, 490	249	-	16.3	0.18, 0.25		
	Dev 2 (NHC 12), 10%	460, 490	285	-	17.2	0.23, 0.30		
	Dev 3 (NHC 12), 14%	450, 480, 590	236	-	16	0.29, 0.33		
	Dev 4 (NHC 12), 18%	450, 480, 590	226	-	15.9	0.37, 0.38		
	Dev 5 (NHC 12), 18%	450, 480, 590	350	-	27.3	0.37, 0.40		
Pt NHC 6 Pt NHC 7 Pt NHC 8	Dev 1 (NHC 6), 2%	460	-	-	0.25	0.15, 0.10	No info	[26]
	Dev 2 (NHC 7), 2%	460	-	-	6.6	0.14, 0.19		
	Dev 3 (NHC 7), 6%	460	-	-	10.2	0.15, 0.14		

	Dev 4 (NHC 8), 6%	460	-	-	11.7	0.15, 0.13		
Pt NHC	Dev 1 (NHC 16), 10%	512	60275	-	-	0.288, 0.588	Thermal vapor deposition	[27]
	Dev 2 (NHC), 10 %	509	64416	-	-	0.261, 0.575		

S6. NMR and HR ESI$^+$-MS Spectra

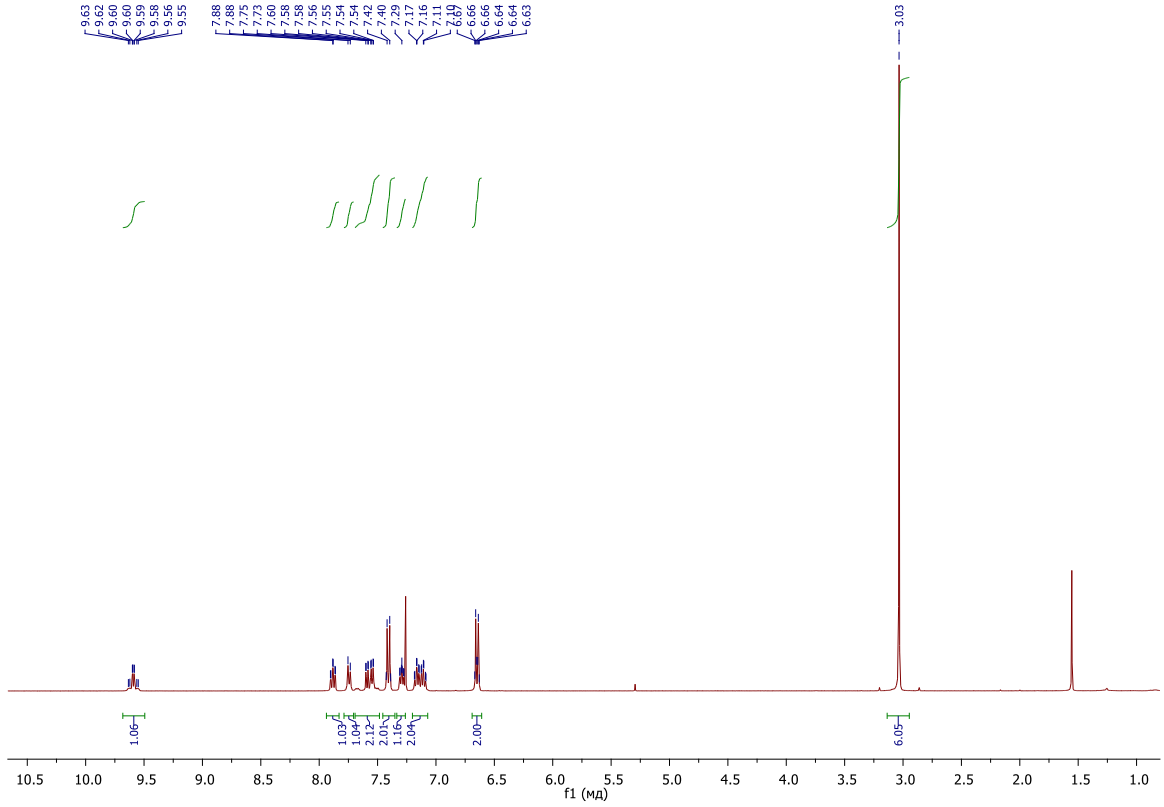

Figure S6.1. ^{1}H NMR spectrum of [Pt(ppy)Cl{$CNC_6H_4N(Me)_2$}] S**1a** ($CDCl_3$, 400 MHz).

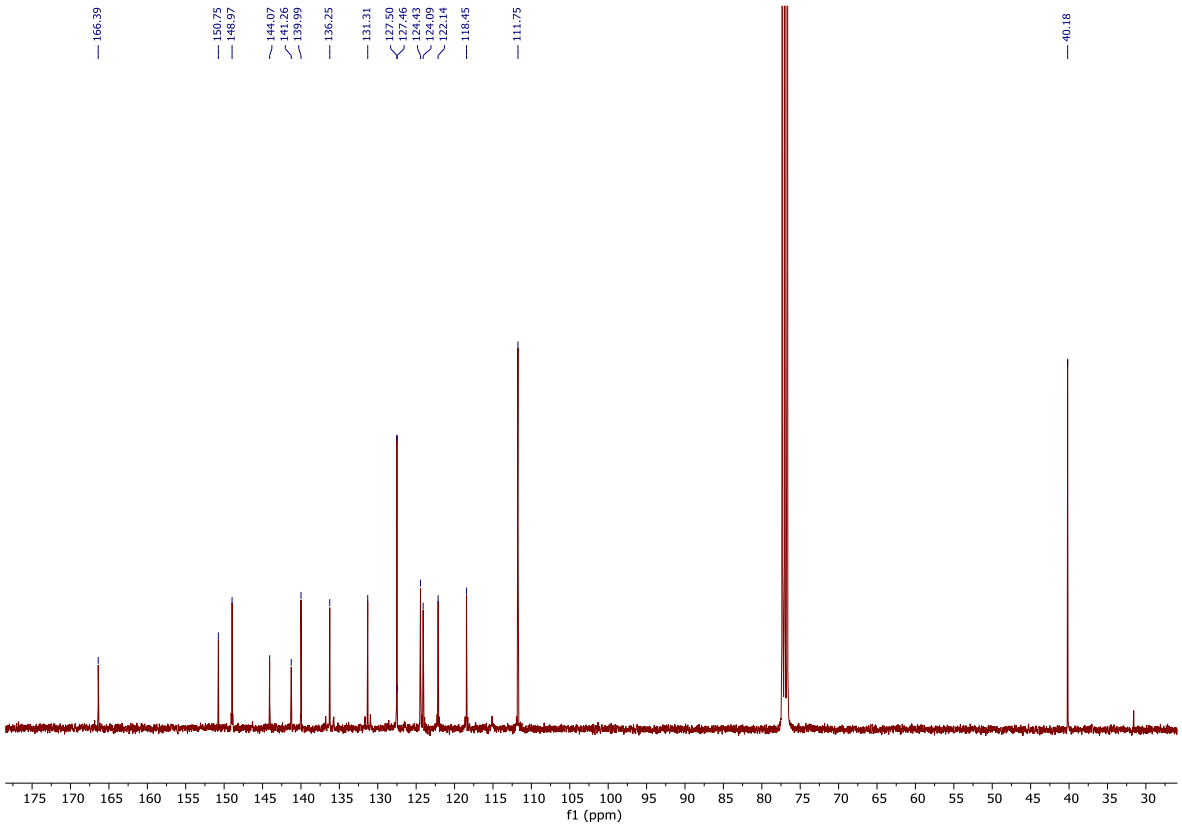

Figure S6.2. $^{13}C\{^1H\}$ NMR of [Pt(ppy)Cl{$CNC_6H_4N(Me)_2$}] **S1a** ($CDCl_3$, 100 MHz).

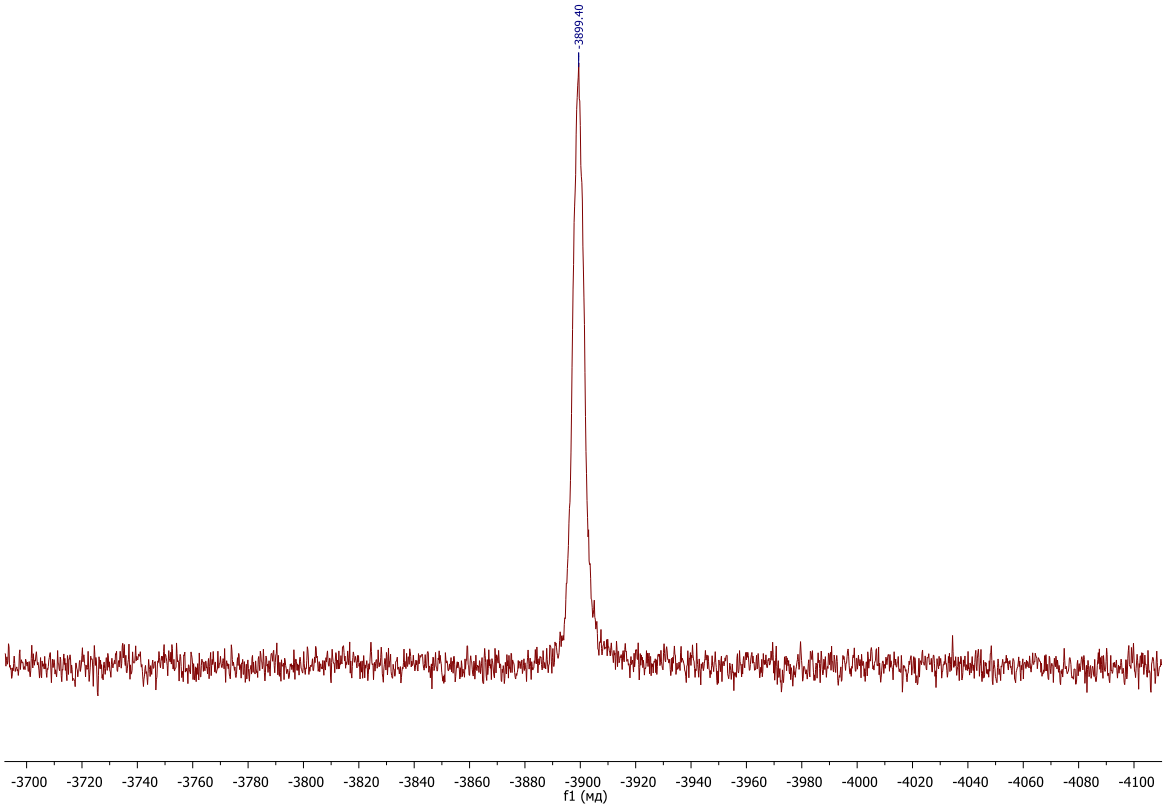

Figure S6.3. ^{195}Pt NMR of [Pt(ppy)Cl{$CNC_6H_4N(Me)_2$}] **S1a** ($CDCl_3$, 100 MHz).

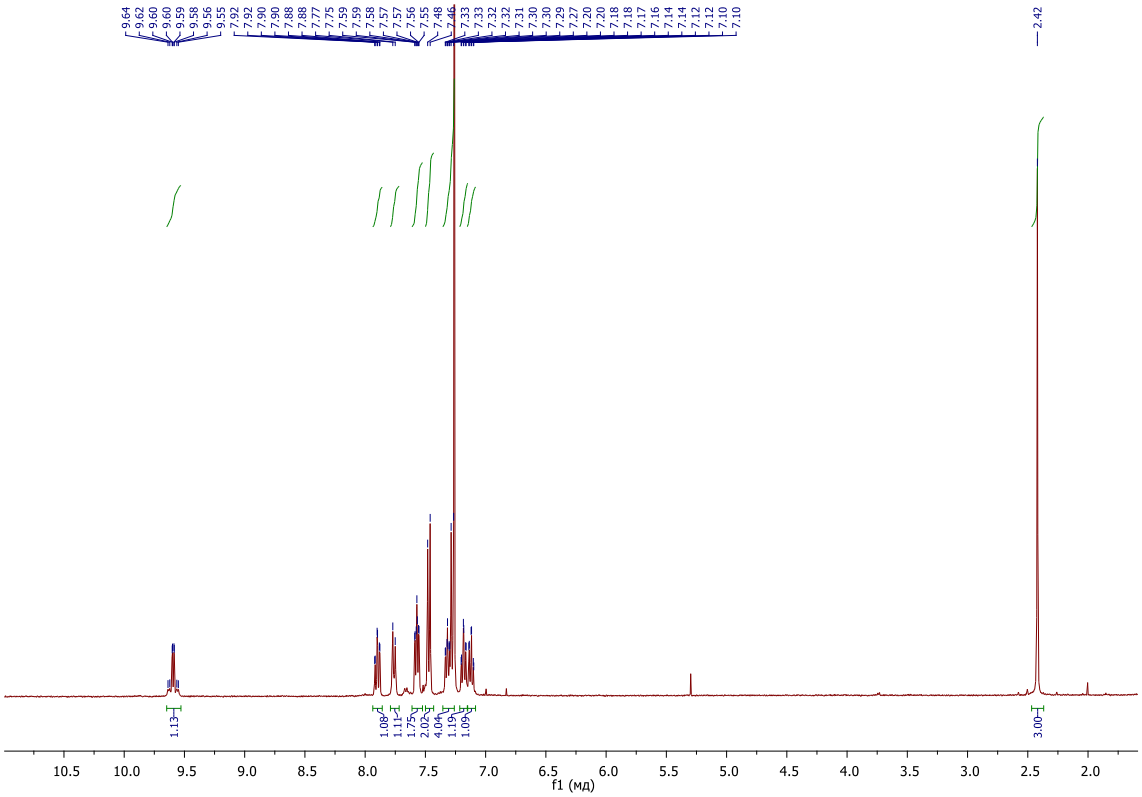

Figure S6.4. ^{1}H NMR spectrum of Pt(ppy){CN(*p*-Tol)}Cl] **S1b** ($CDCl_3$, 400 MHz).

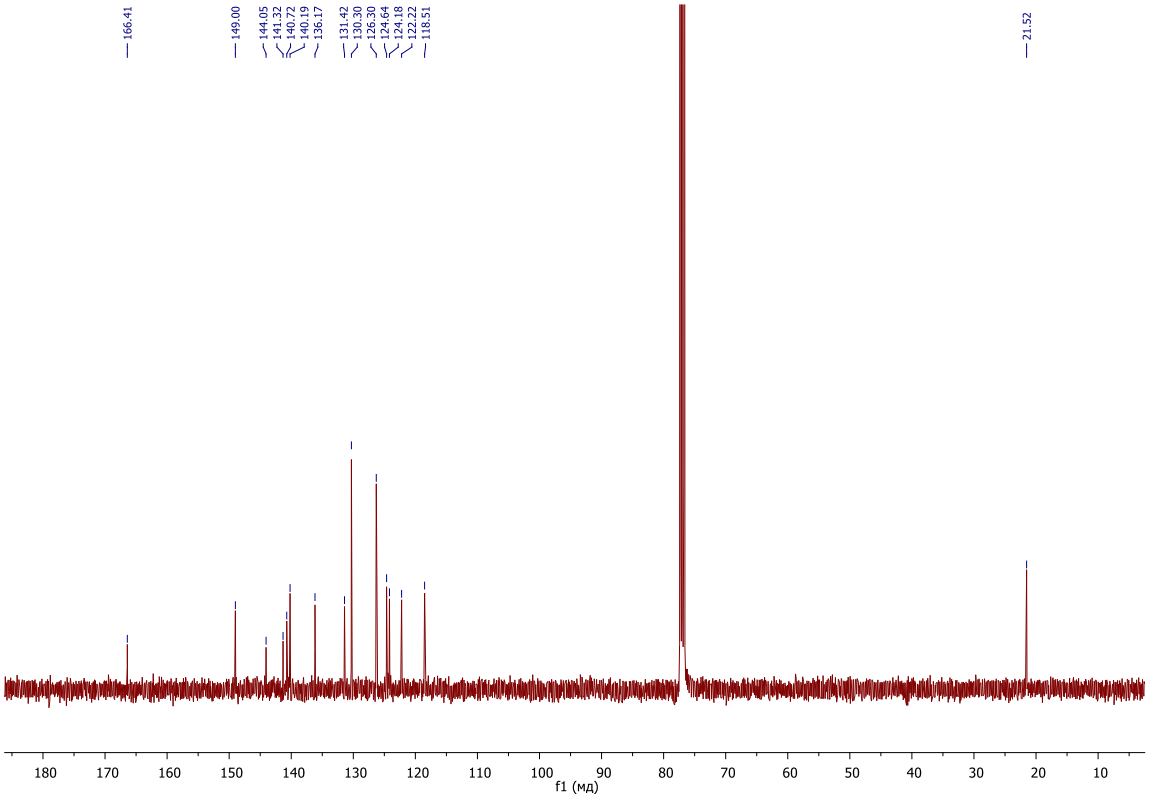

Figure S6.5. $^{13}C\{^{1}H\}$ NMR of Pt(ppy){CN(*p*-Tol)}Cl] **S1b** ($CDCl_3$, 100 MHz).

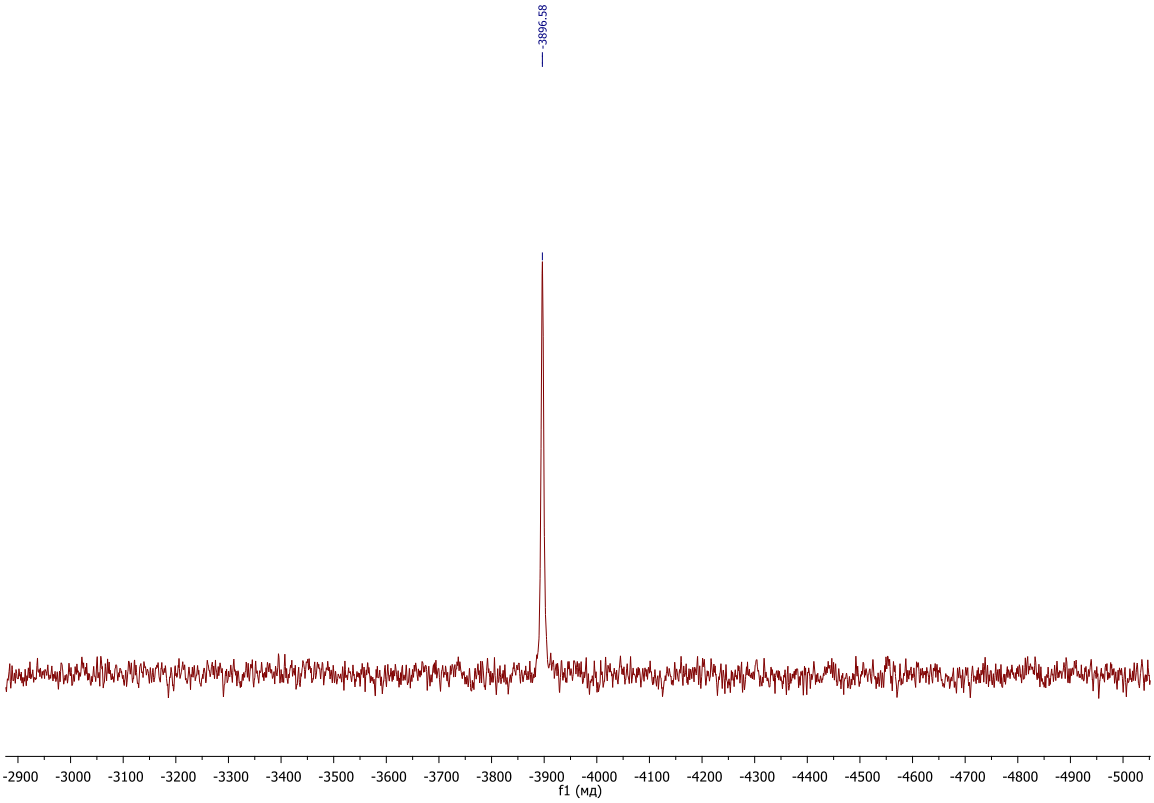

Figure S6.6. ^{195}Pt NMR of Pt(ppy){CN(*p*-Tol)}Cl] **S1a** ($CDCl_3$, 100 MHz).

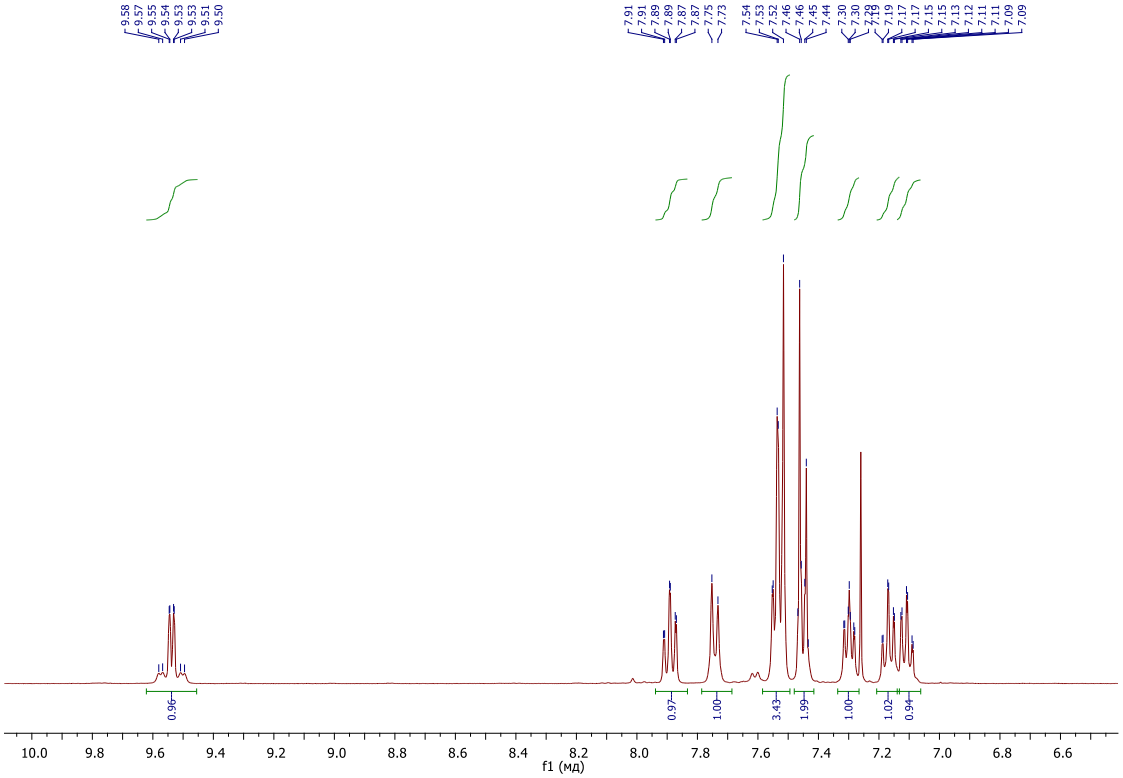

Figure S6.7. ^{1}H NMR spectrum of [Pt(ppy)Cl{CNC_6H_4Cl}] **S1c** ($CDCl_3$, 400 MHz).

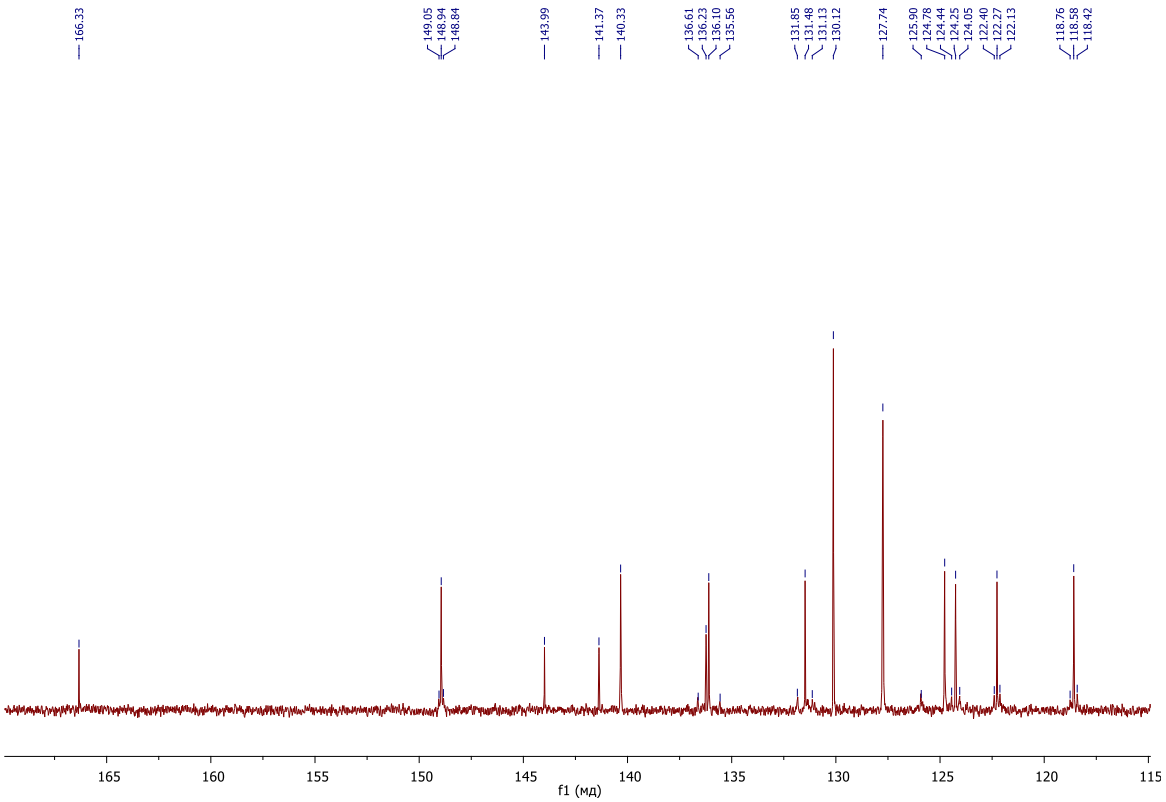

Figure S6.8. $^{13}C\{^{1}H\}$ NMR of [Pt(ppy)Cl{CNC_6H_4Cl}] **S1c** ($CDCl_3$, 100 MHz).

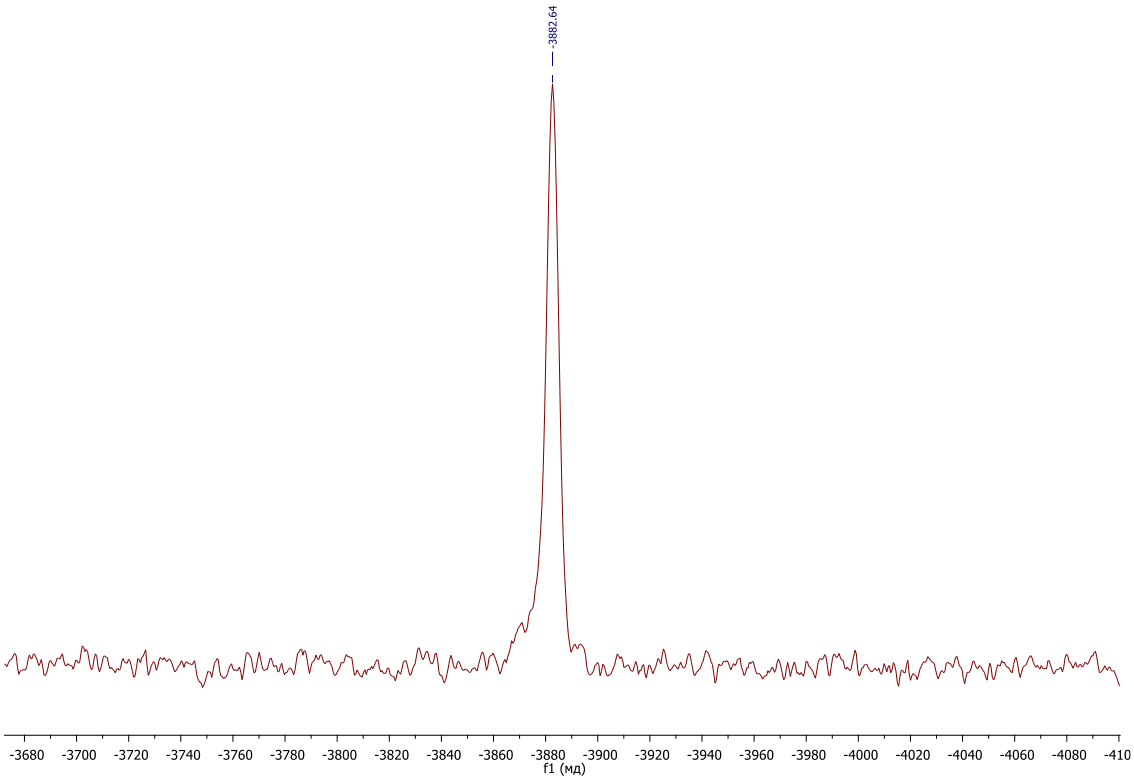

Figure S6.9. ^{195}Pt NMR of [Pt(ppy)Cl{CNC_6H_4Cl}] **S1c** ($CDCl_3$, 100 MHz)

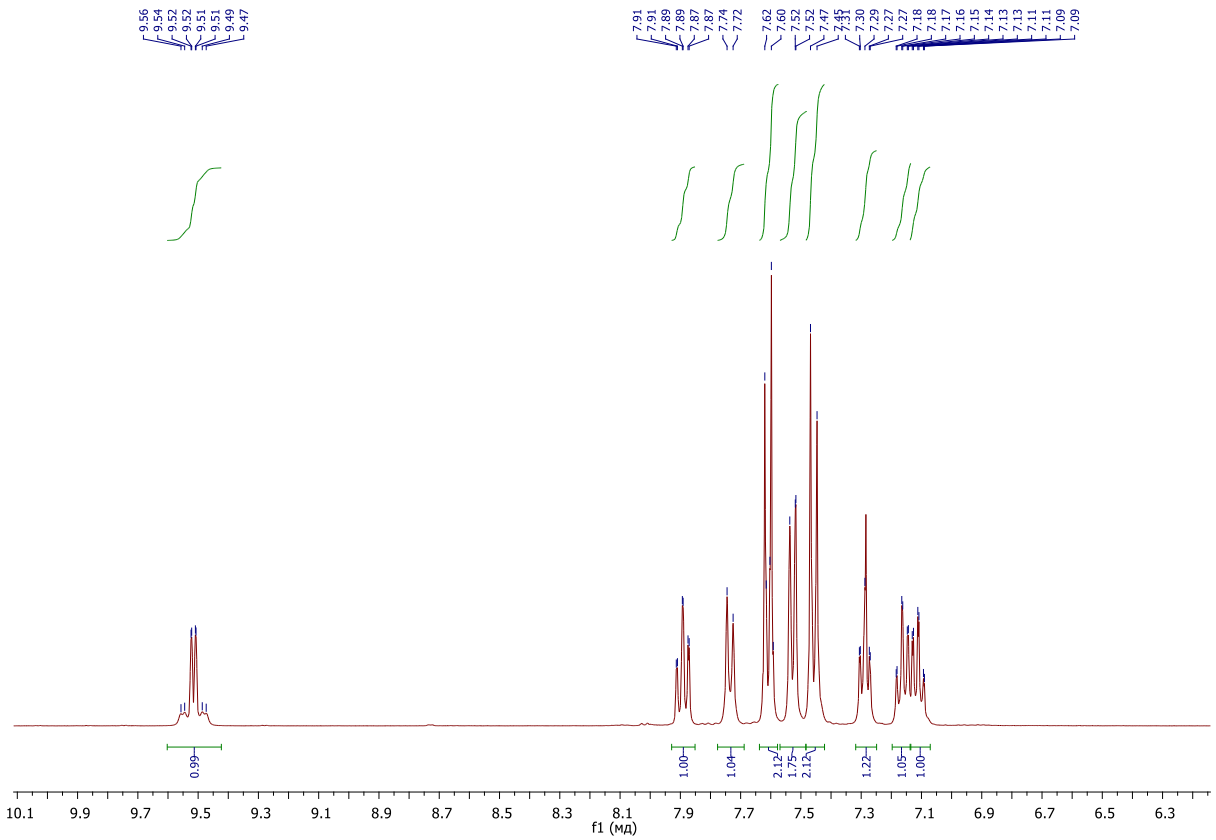

Figure S6.10. ^{1}H NMR spectrum of [Pt(ppy)Cl{CNC_6H_4Br}] **S1d** ($CDCl_3$, 400 MHz).

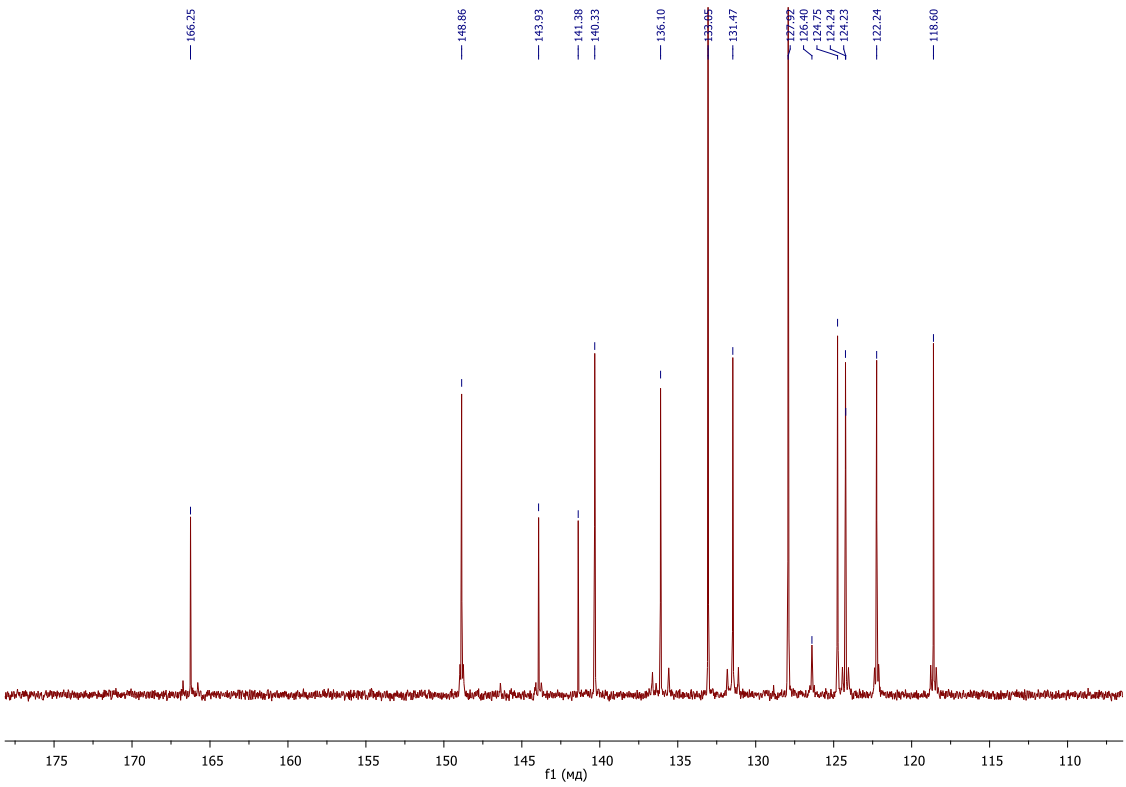

Figure S6.12. $^{13}C\{^{1}H\}$ NMR of [Pt(ppy)Cl{CNC_6H_4Brl}] **S1d** ($CDCl_3$, 100 MHz)

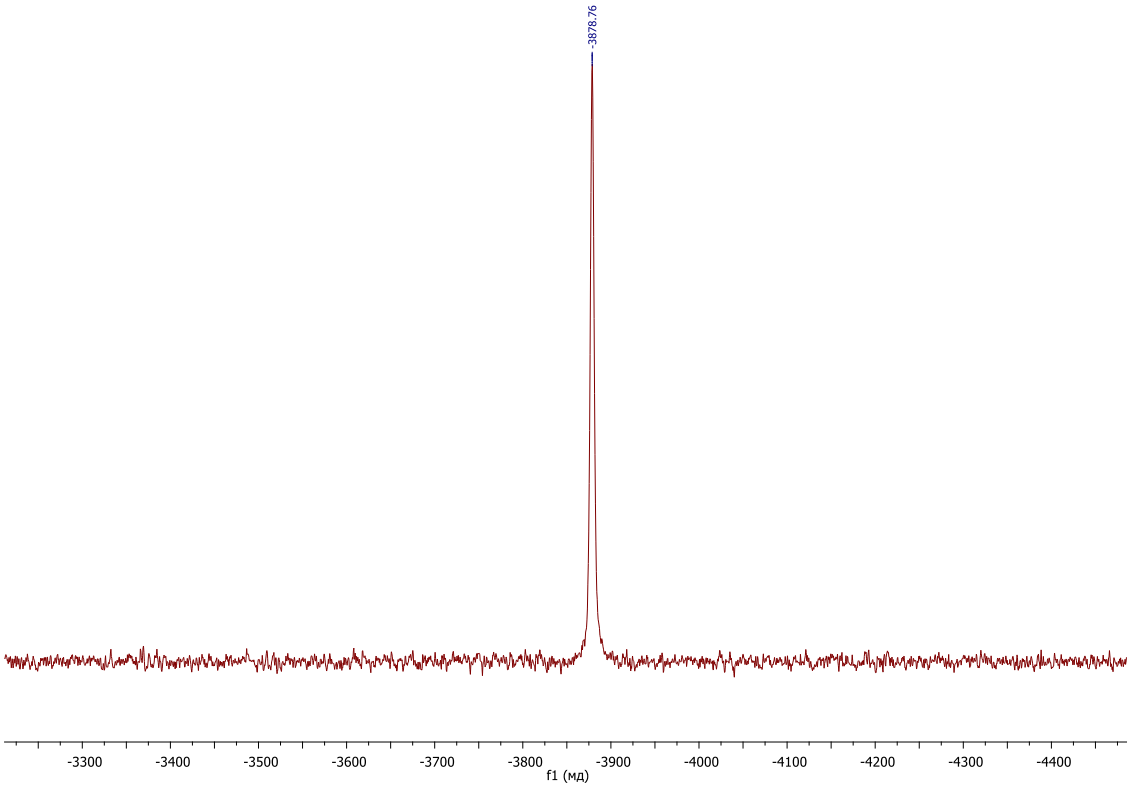

Figure S6.13. ^{195}Pt NMR of [Pt(ppy)Cl{CNC_6H_4Br}] **S1d** ($CDCl_3$, 100 MHz)

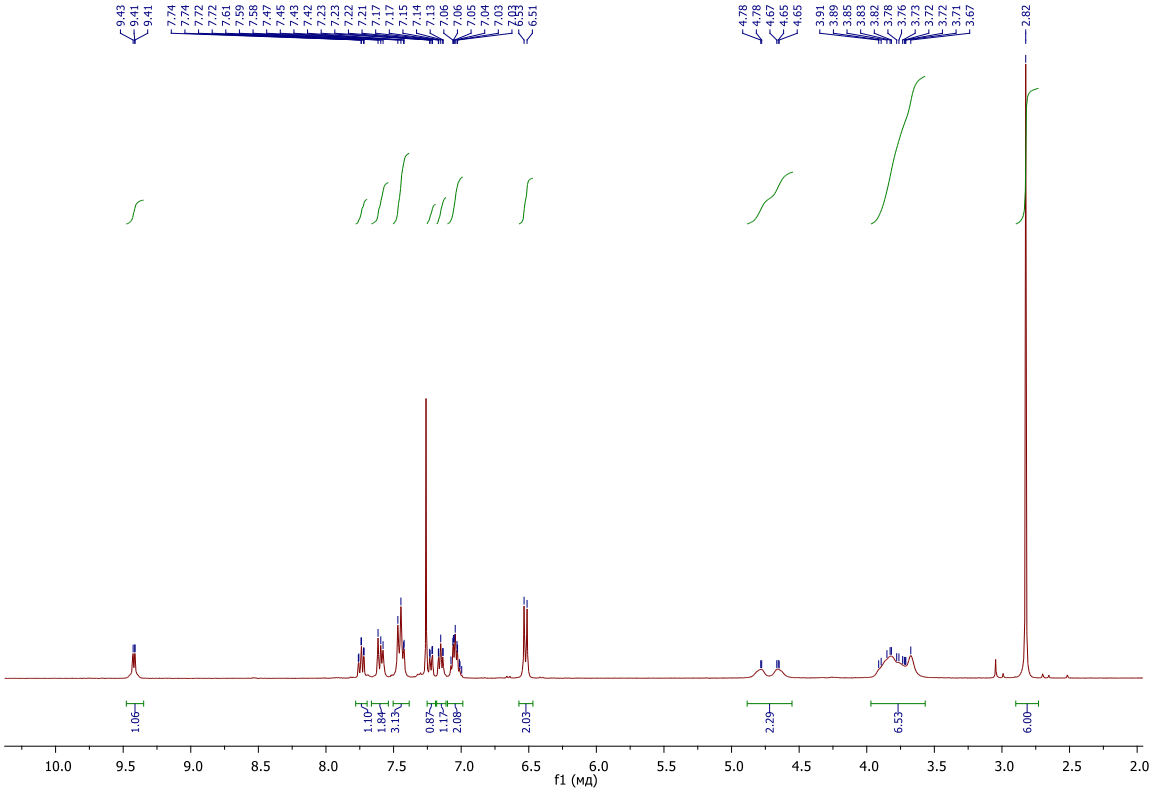

Figure S6.14. ^{1}H NMR spectrum of **1a** ($CDCl_3$, 400 MHz).

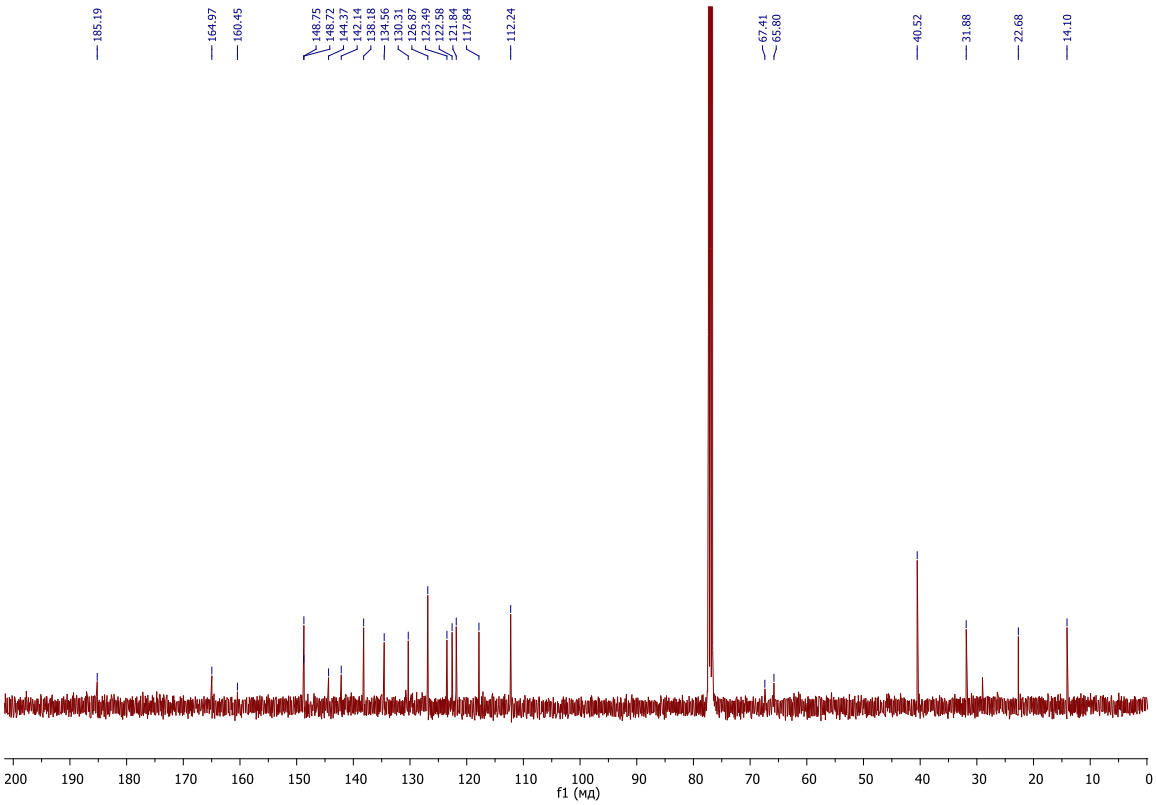

Figure S6.15. ^{13}C{^{1}H} NMR of **1a** ($CDCl_3$, 100 MHz).

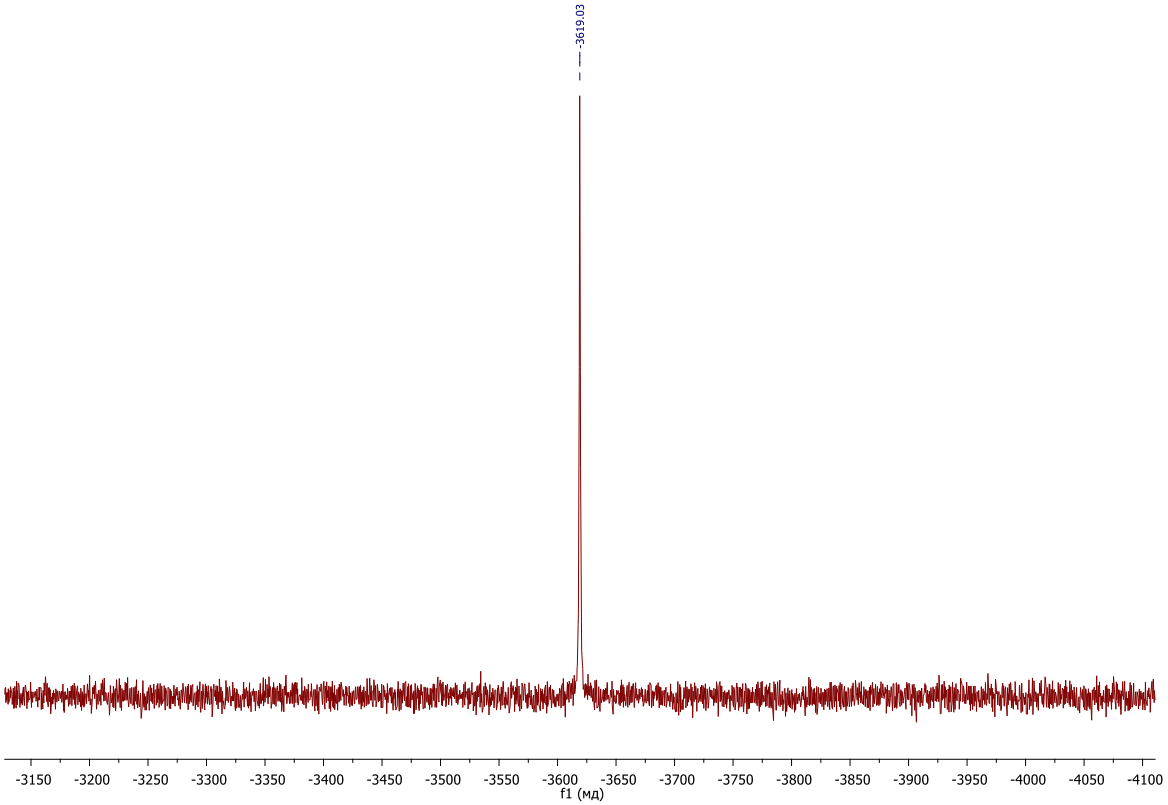

Figure S6.16. ^{195}Pt NMR of **5a** ($CDCl_3$, 100 MHz).

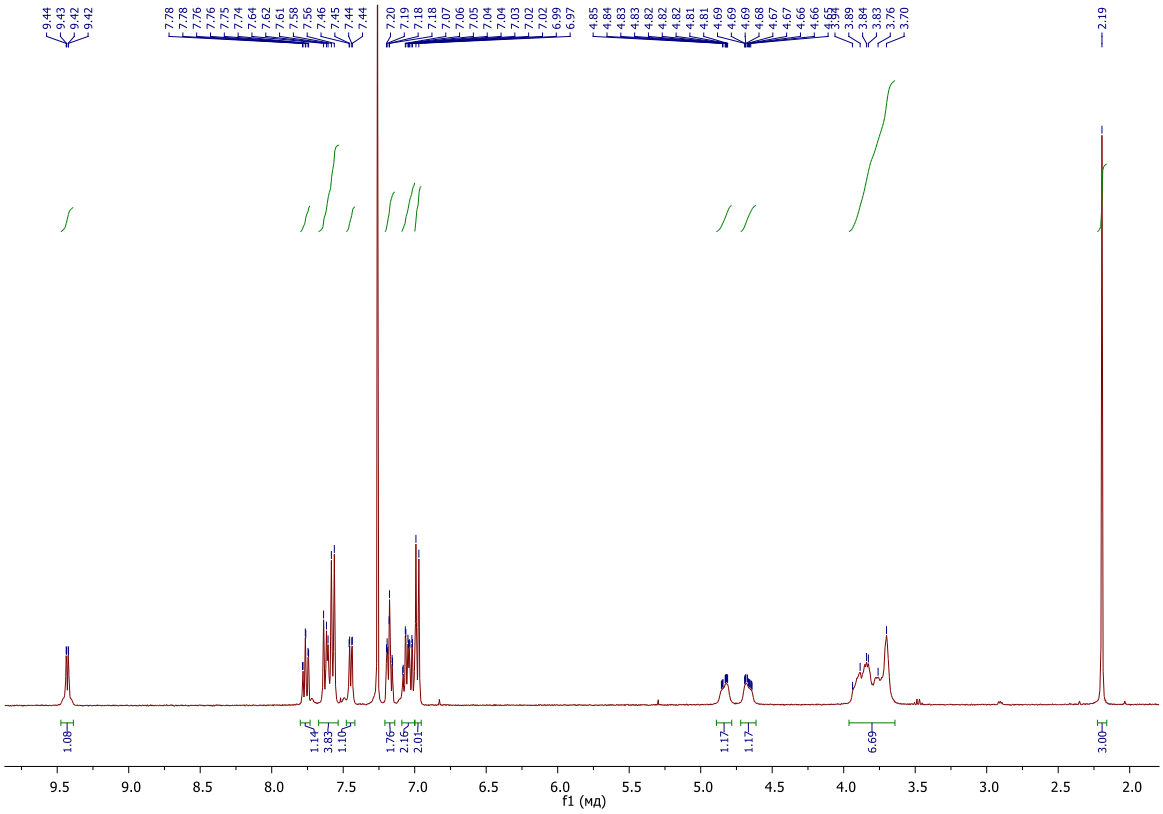

Figure S6.17. ^{1}H NMR spectrum of **1b** ($CDCl_3$, 400 MHz).

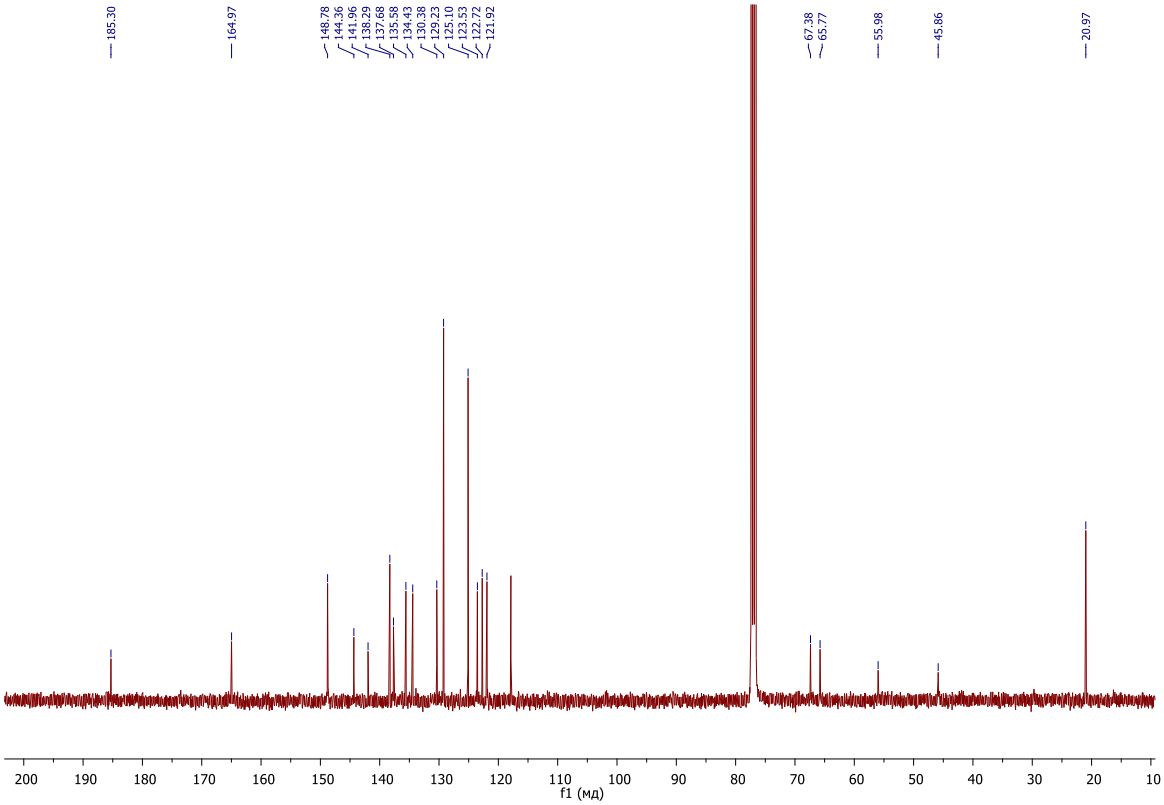

Figure S6.18. $^{13}C\{^{1}H\}$ NMR of **1b** ($CDCl_3$, 100 MHz).

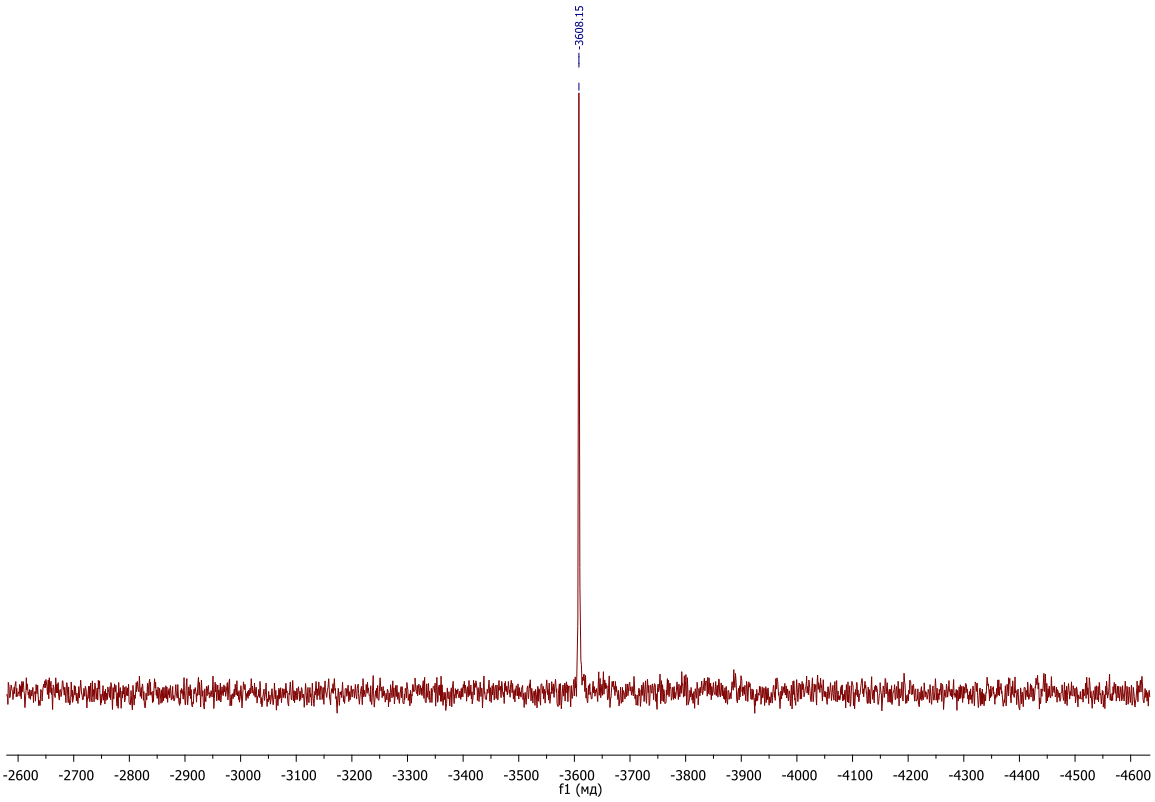

Figure S6.19. ^{195}Pt NMR of **1b** ($CDCl_3$, 100 MHz).

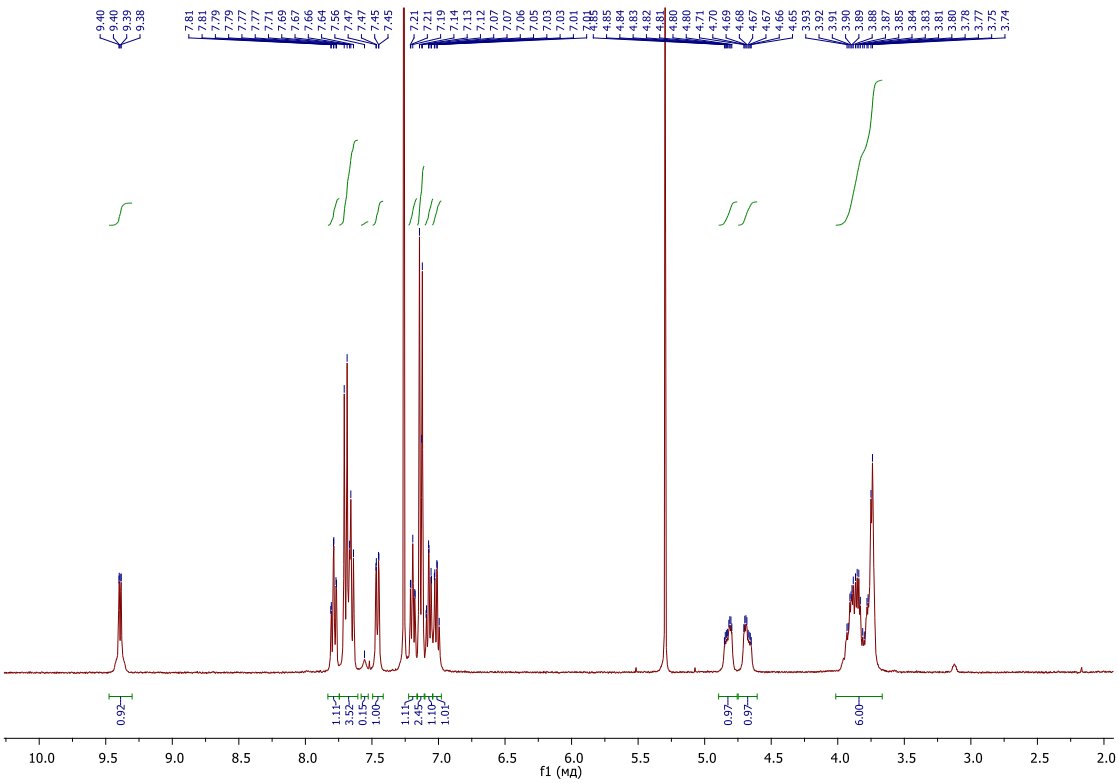

Figure S6.20. ^{1}H NMR spectrum of **1c** ($CDCl_3$, 400 MHz).

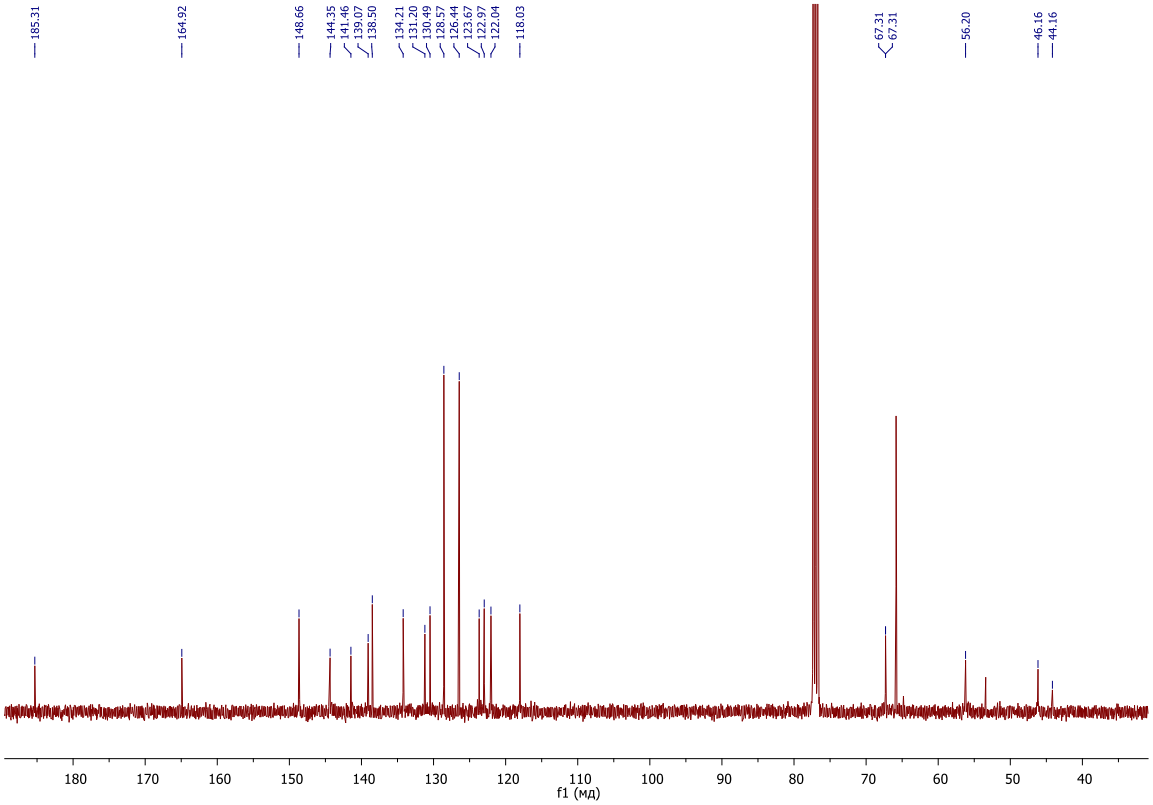

Figure S6.21. $^{13}C\{^{1}H\}$ NMR of **1c** ($CDCl_3$, 100 MHz).

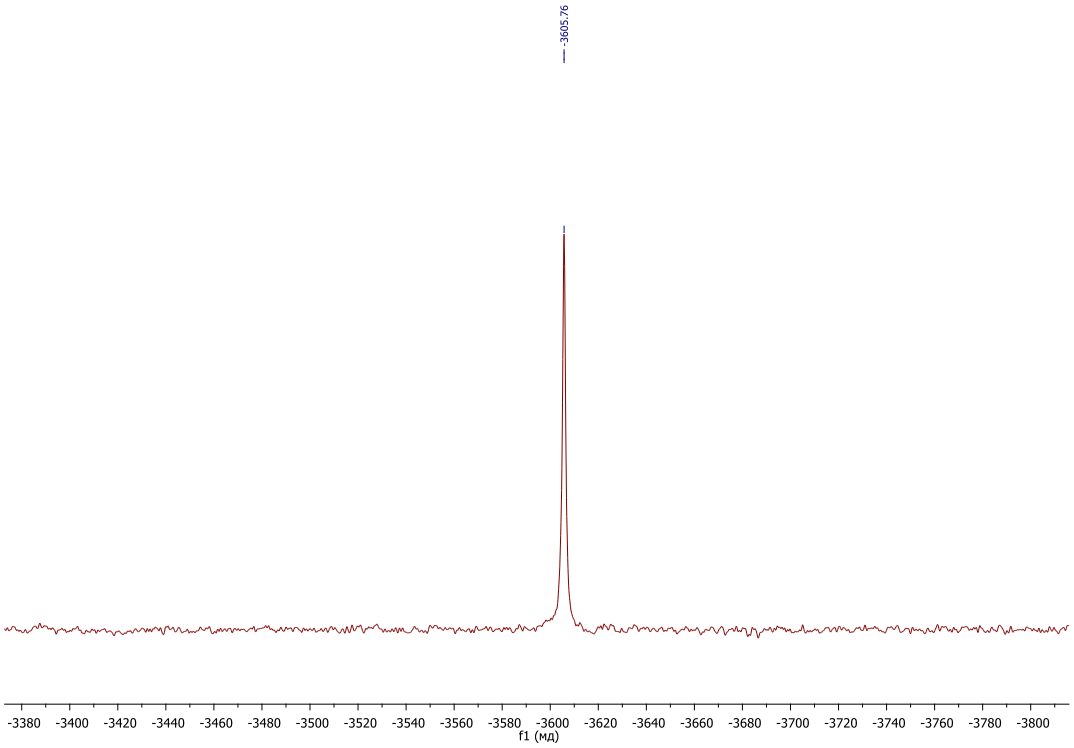

Figure S6.22. ^{195}Pt NMR of **1c** ($CDCl_3$, 100 MHz).

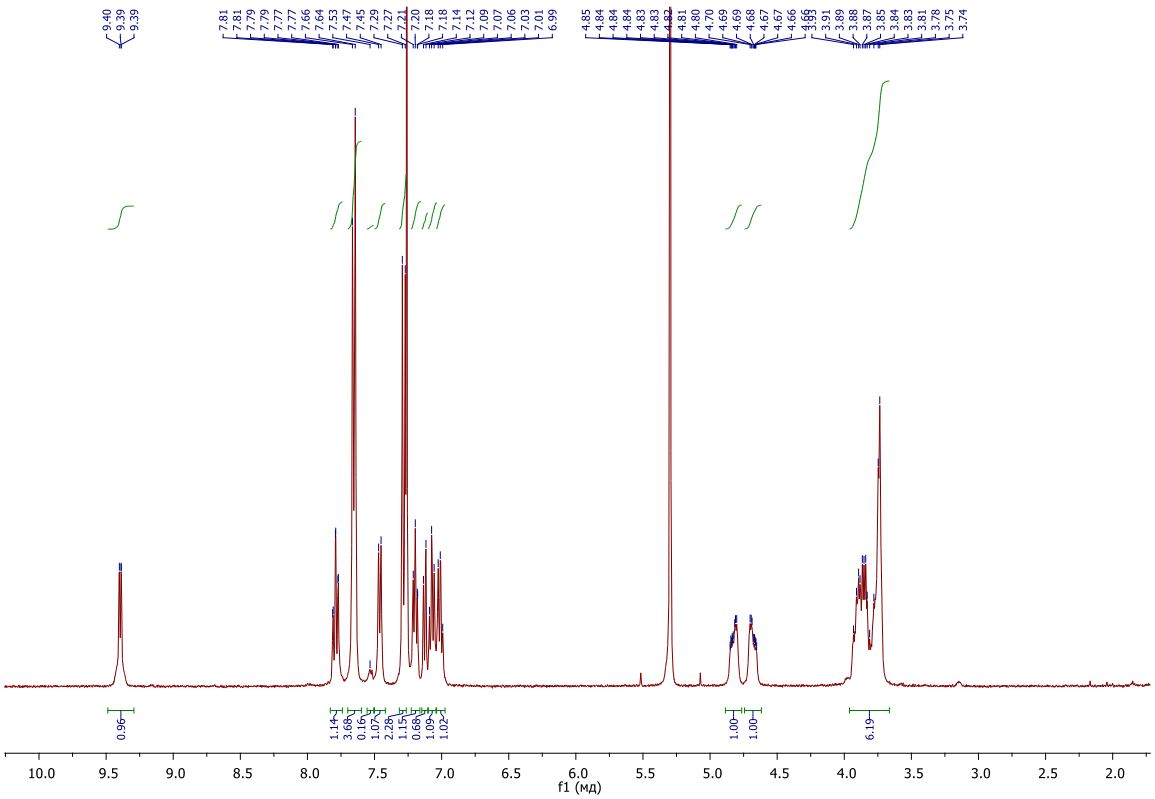

Figure S6.23. ^{1}H NMR spectrum of **1d** ($CDCl_3$, 400 MHz).

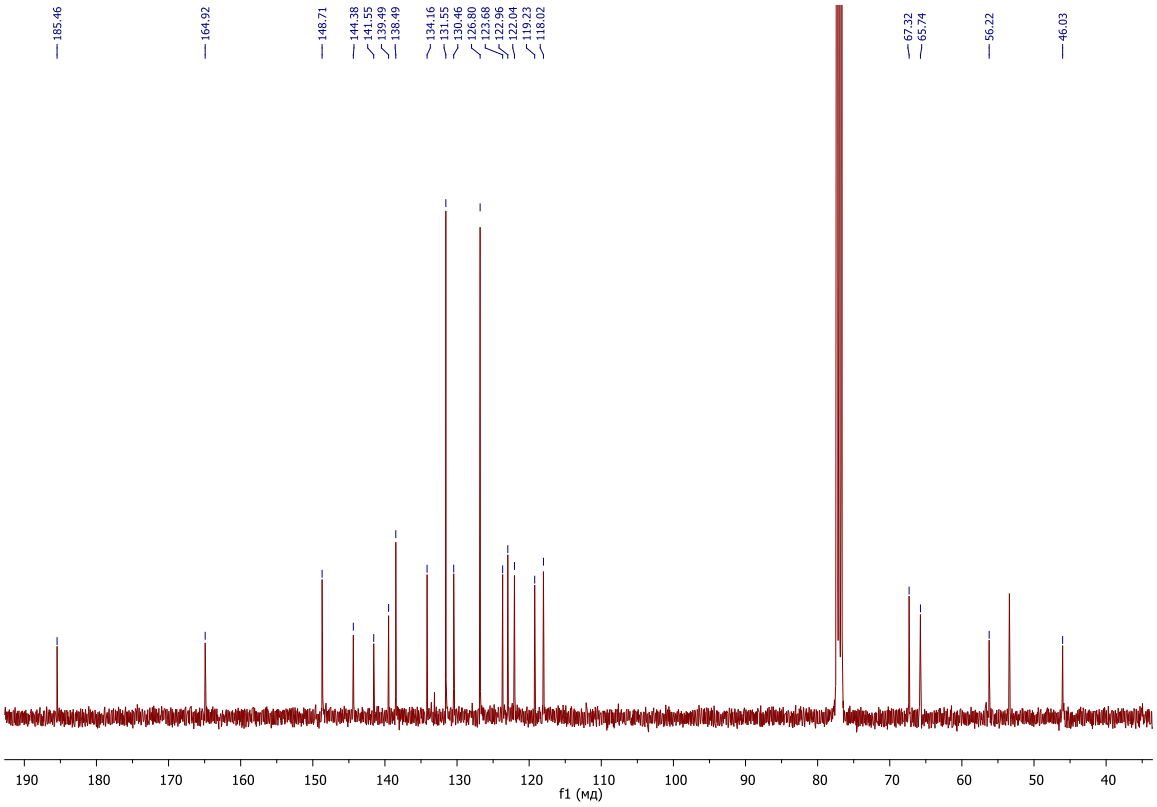

Figure S6.24. $^{13}C\{^{1}H\}$ NMR of **1d** ($CDCl_3$, 100 MHz).

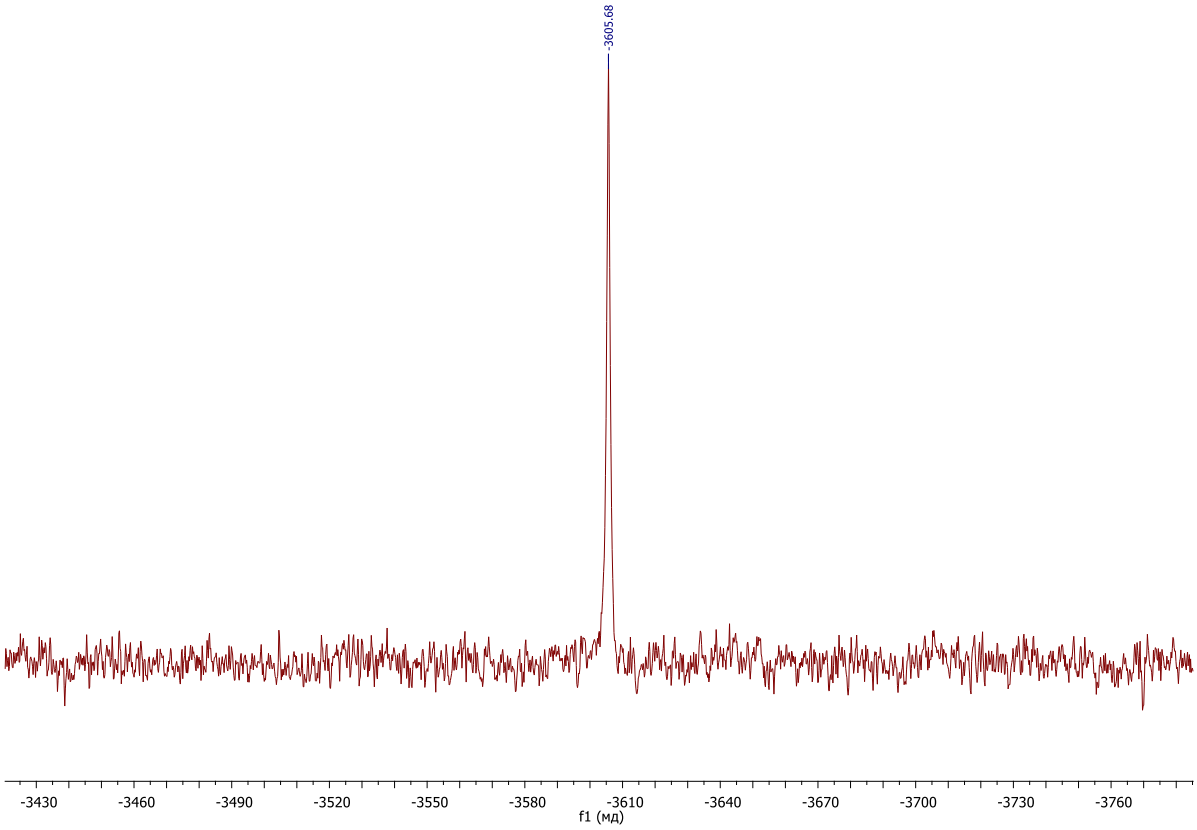

Figure S6.25. ^{195}Pt NMR of **1c** ($CDCl_3$, 86.015 MHz).

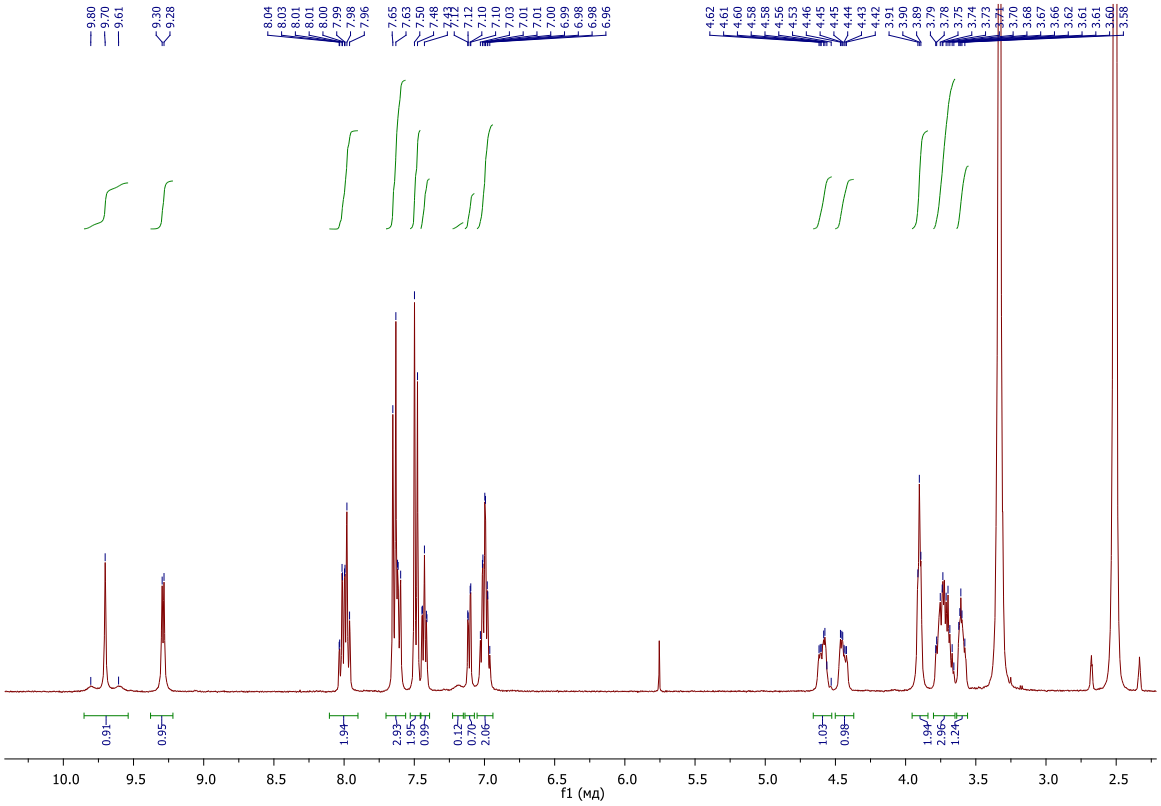

Figure S6.26. ^{1}H NMR spectrum of **1e** (DMSO-d$_6$, 400 MHz).

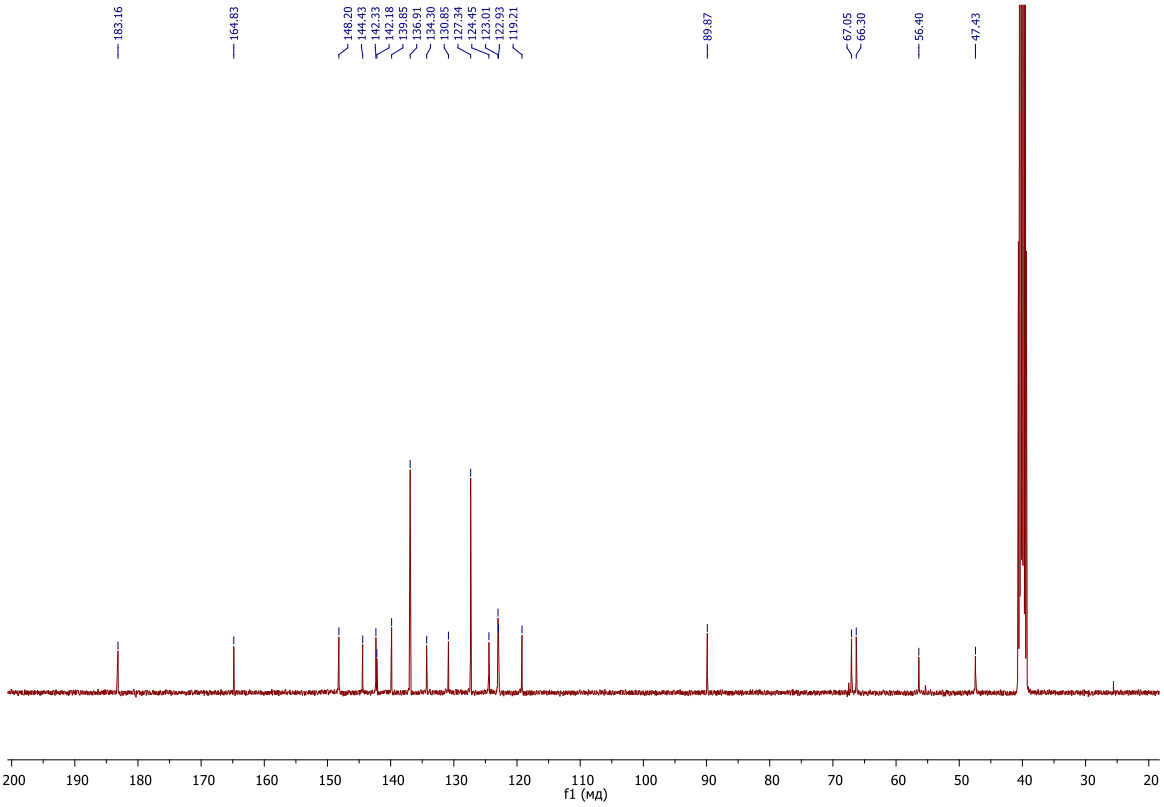

Figure S6.27. ^{13}C{^{1}H} NMR of **1e** (DMSO-d$_6$, 100 MHz).

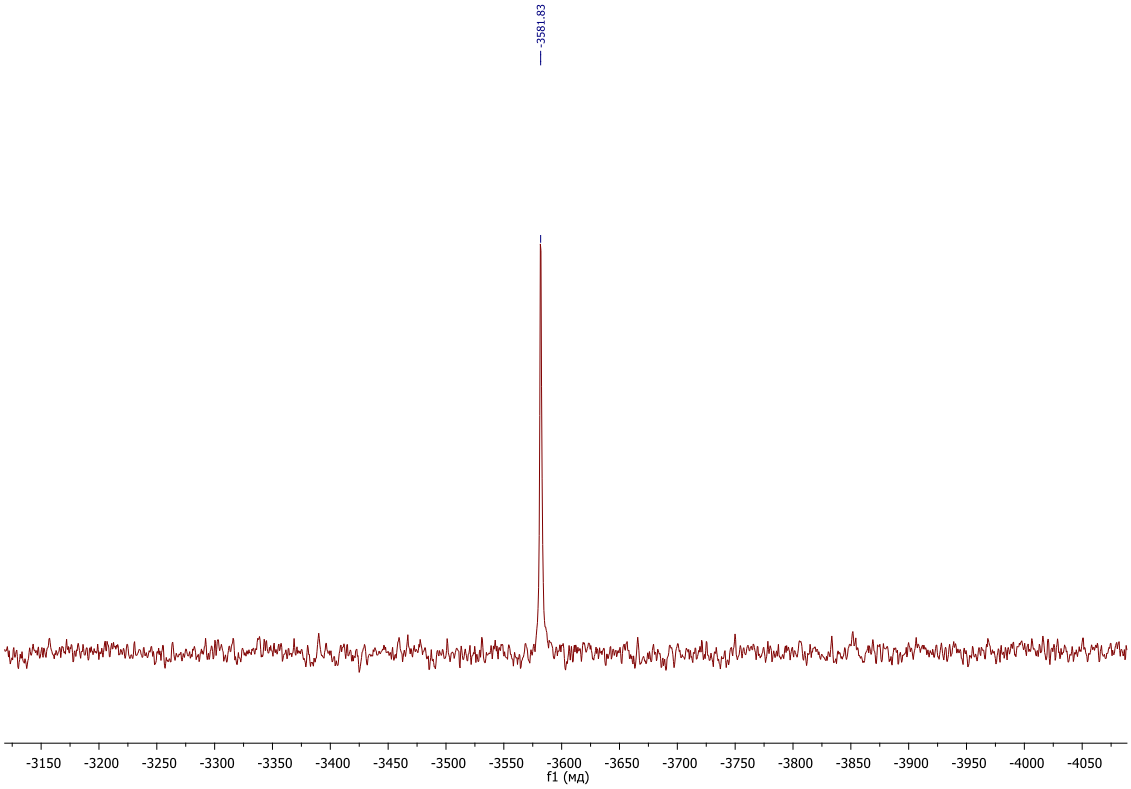

Figure S6.28. ^{195}Pt NMR of **1e** (DMSO-d_6, 86.015 MHz).

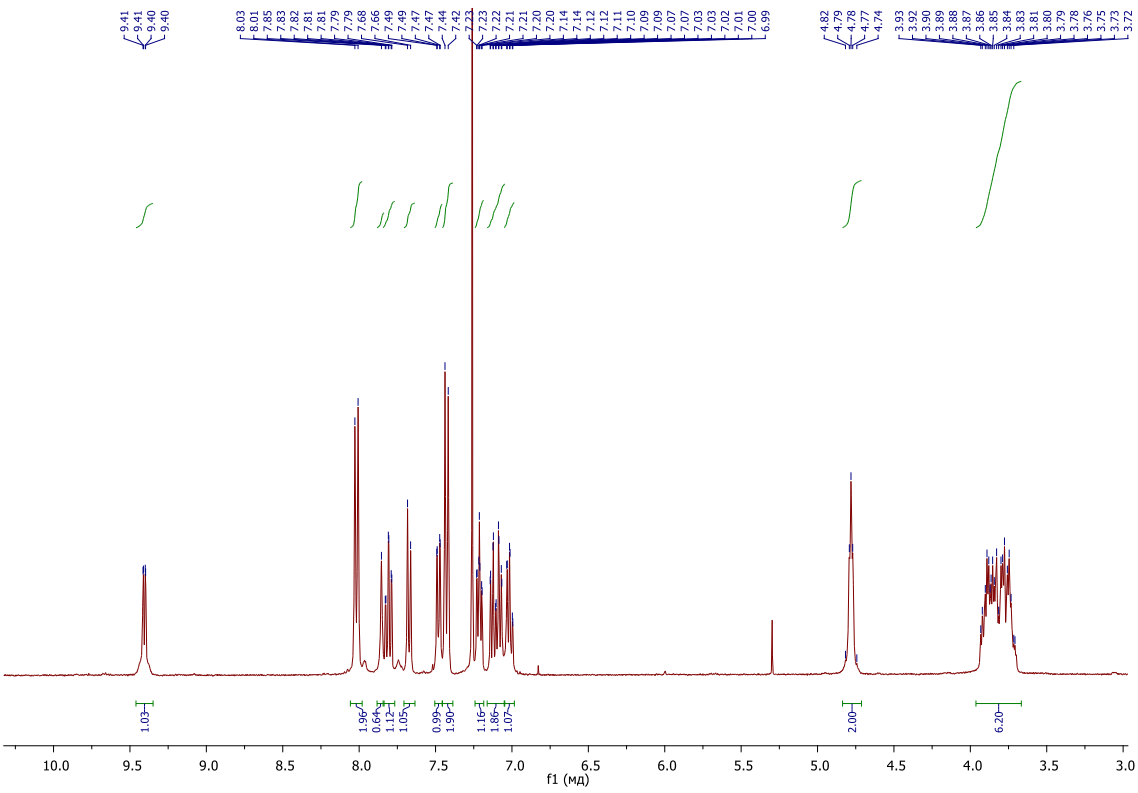

Figure S6.29. ^{1}H NMR spectrum of **1f** ($CDCl_3$, 400 MHz).

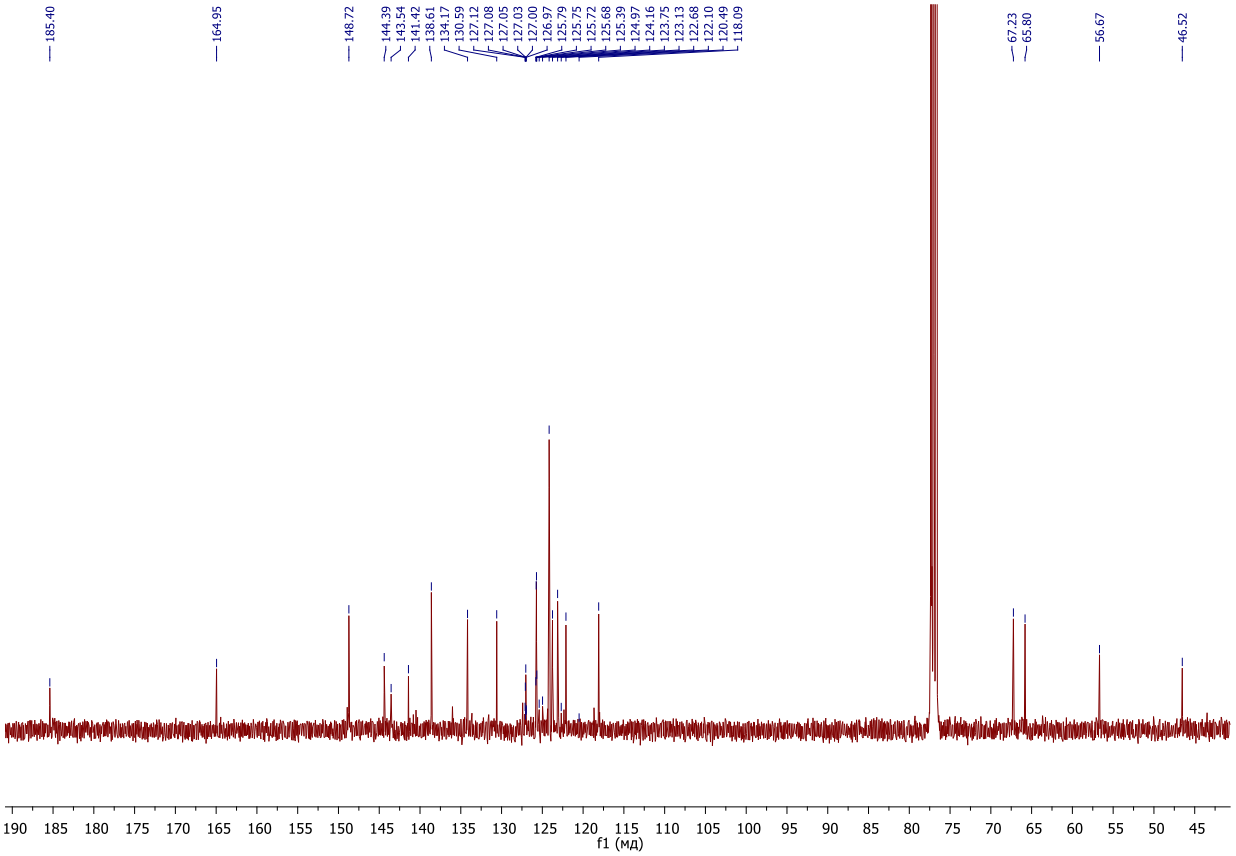

Figure S6.30. $^{13}C\{^{1}H\}$ NMR spectrum of **1f** ($CDCl_3$, 376.50 MHz).

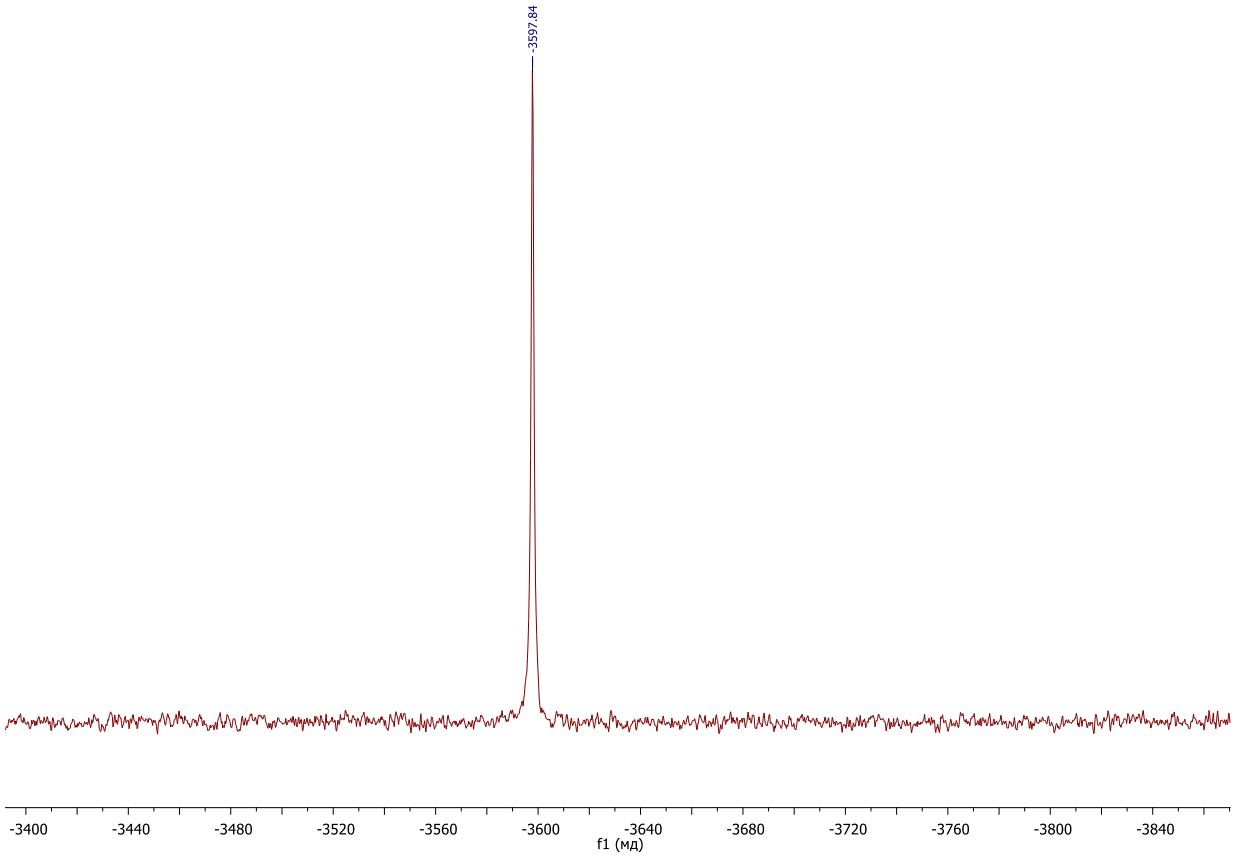

Figure S6.31. ^{195}Pt NMR of **1f** ($CDCl_3$, 86.015 MHz).

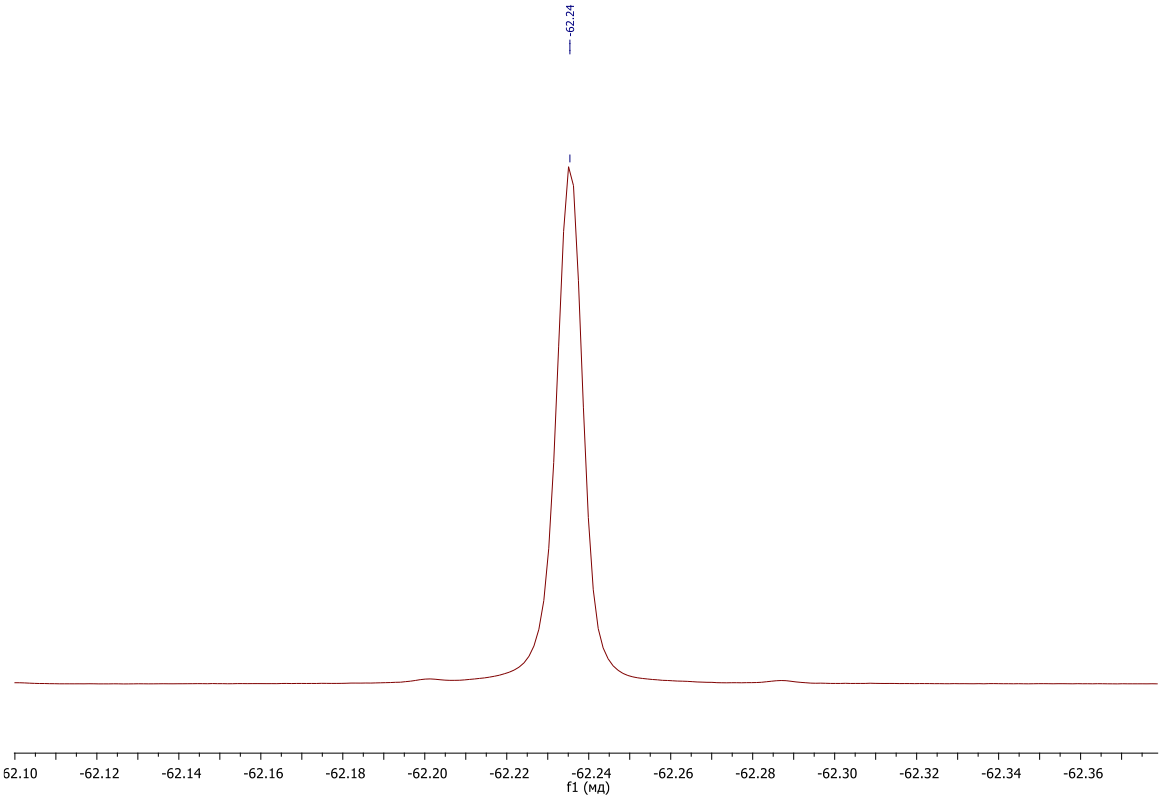

Figure S6.32. ^{19}F NMR of **1f** ($CDCl_3$, 376.50 MHz).

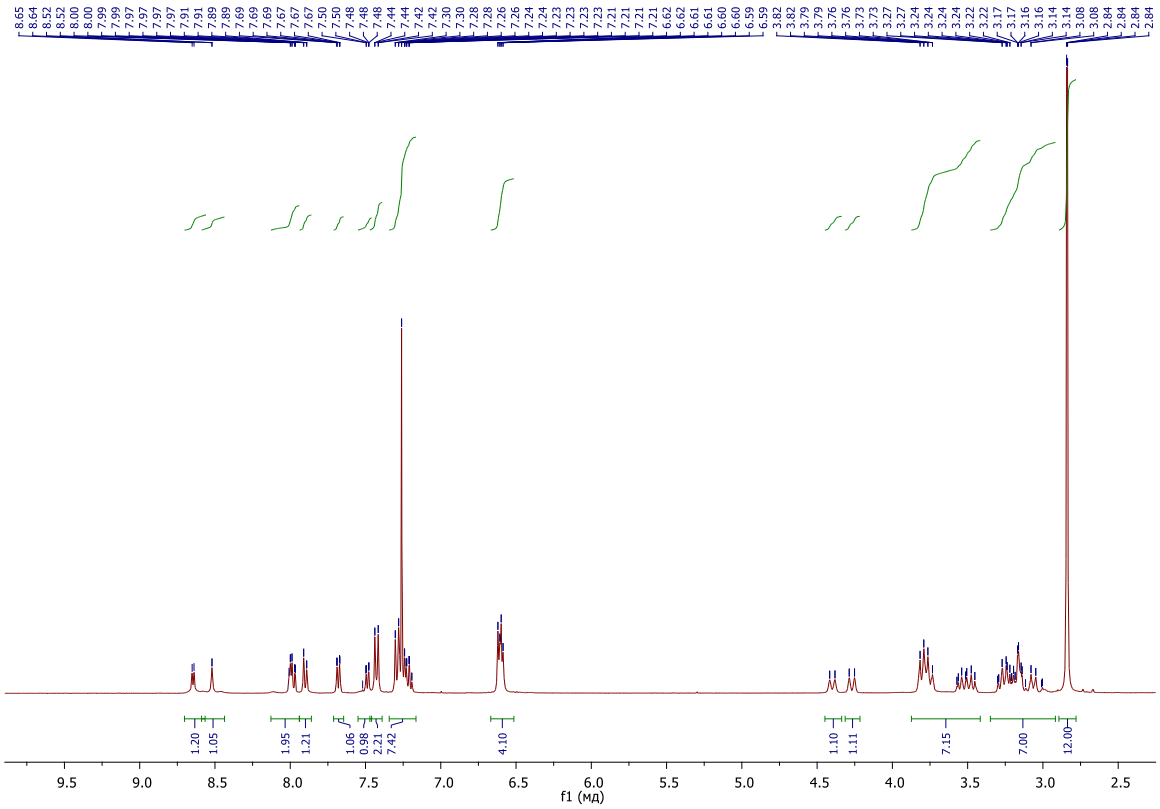

Figure S6.33. ^{1}H NMR spectrum of **2a** ($CDCl_3$, 400 MHz).

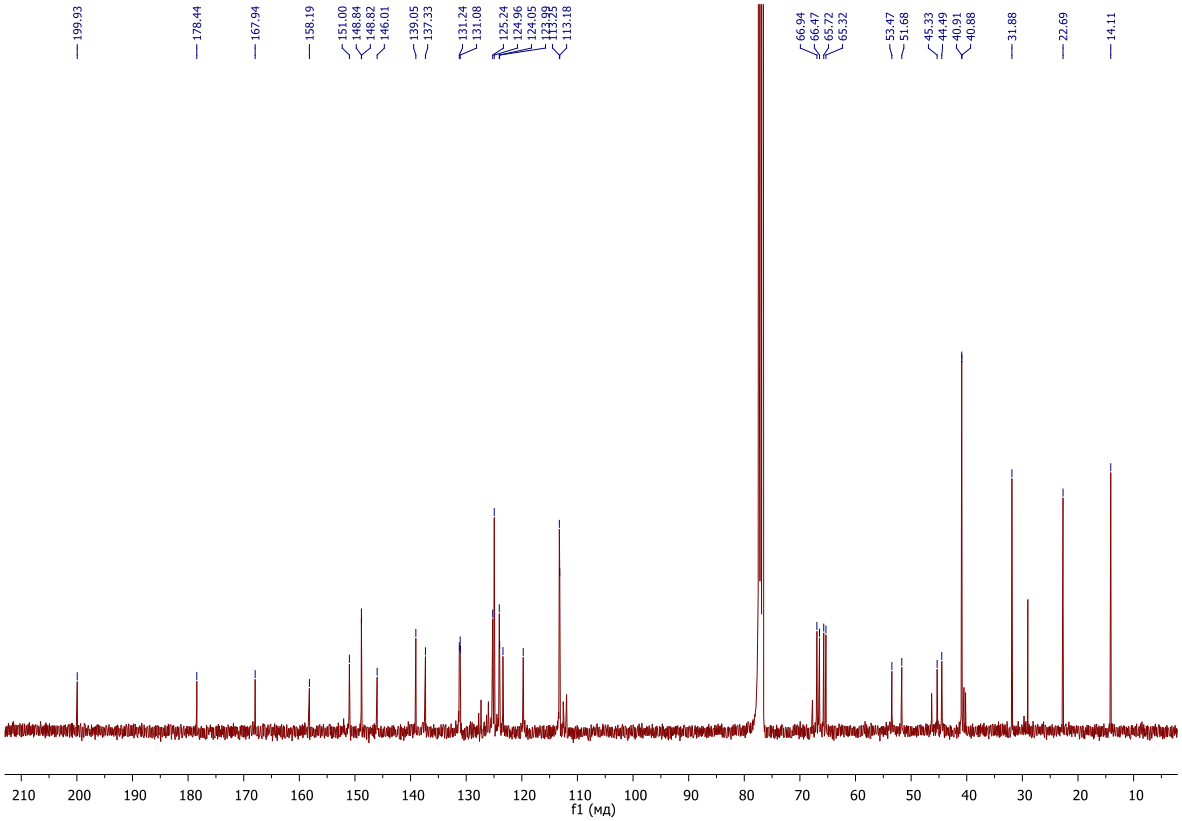

Figure S6.34. $^{13}C\{^{1}H\}$ NMR of **2a** ($CDCl_3$, 100 MHz).

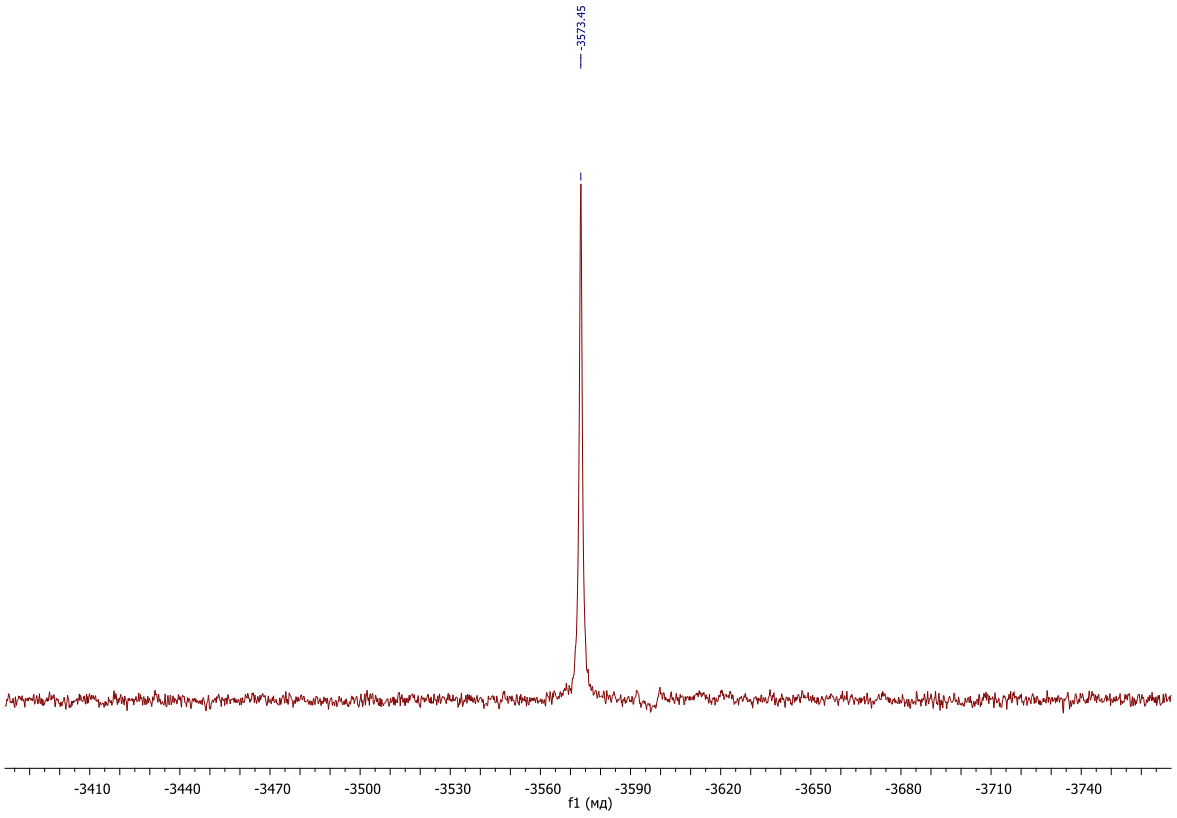

Figure S6.35. ^{195}Pt NMR of **2a** ($CDCl_3$, 86.015 MHz).

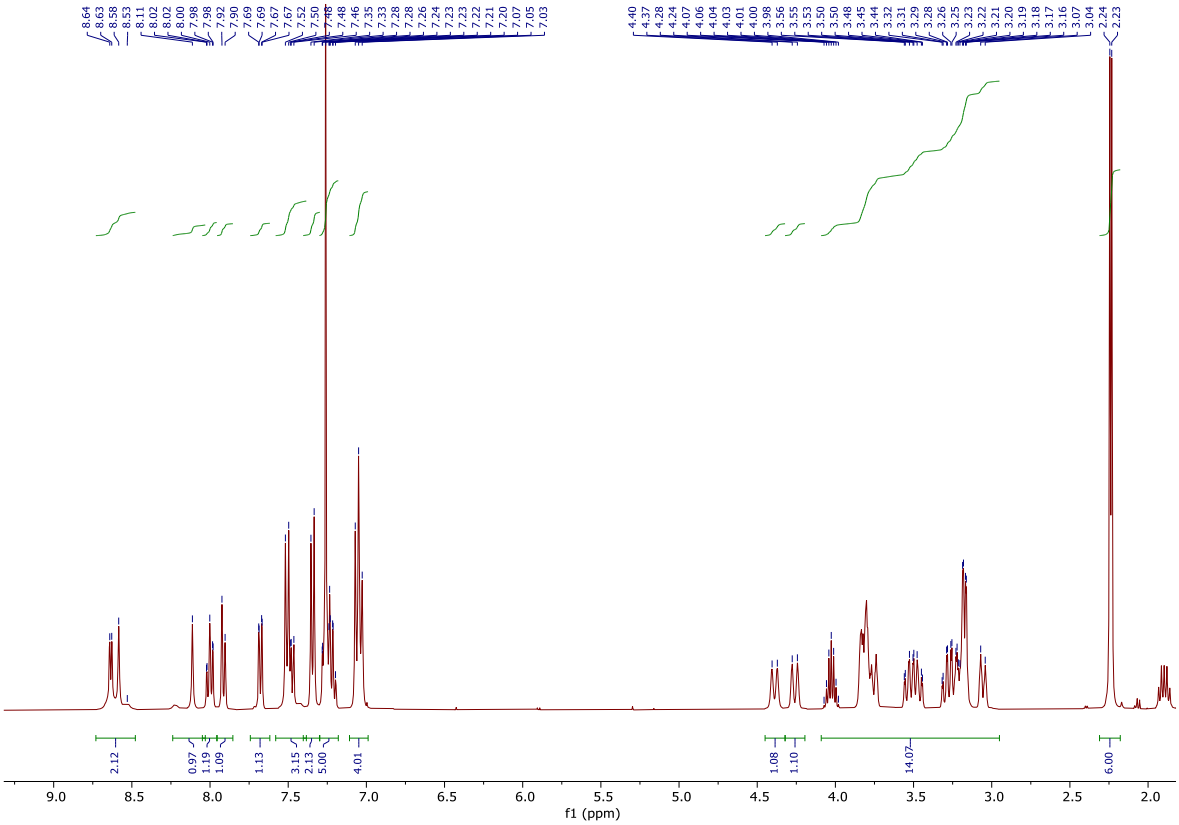

Figure S6.36. $^{13}C\{^{1}H\}$ NMR of **2b** ($CDCl_3$, 100 MHz).

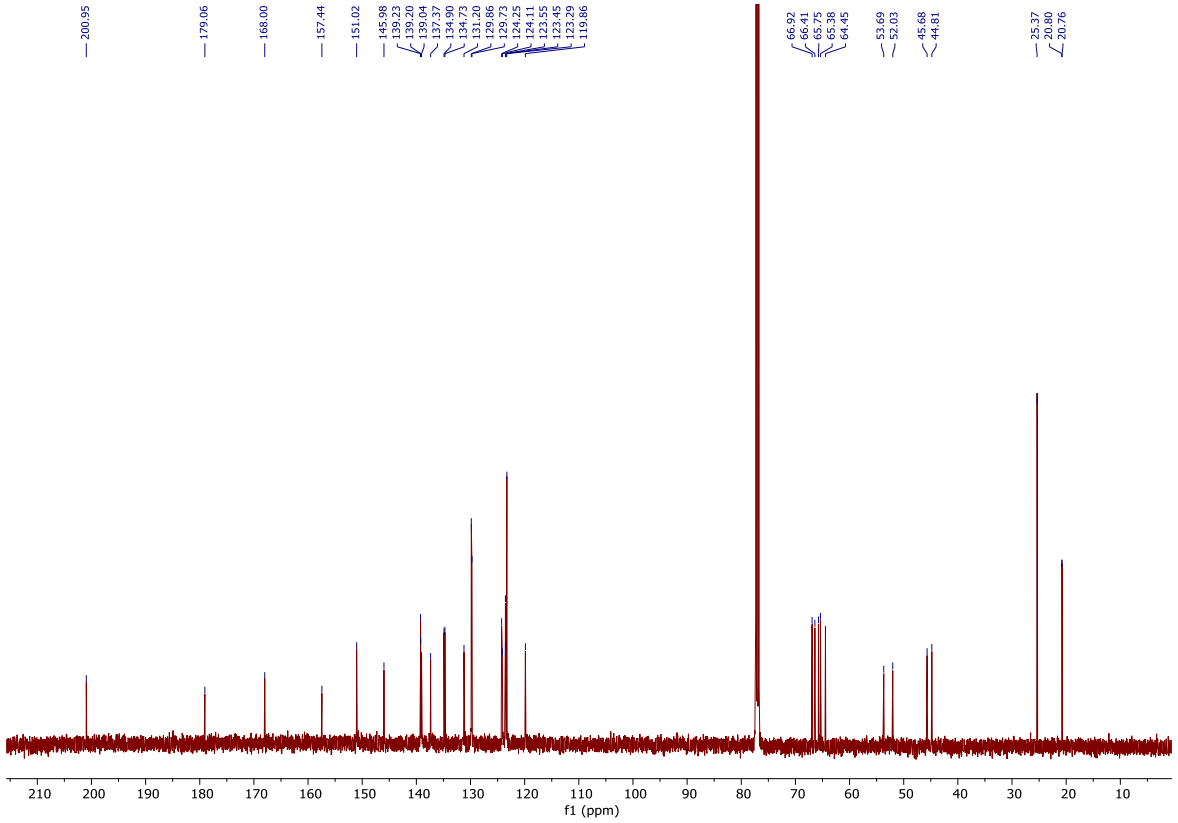

Figure S6.37. $^{13}C\{^{1}H\}$ NMR of **2b** ($CDCl_3$, 100 MHz).

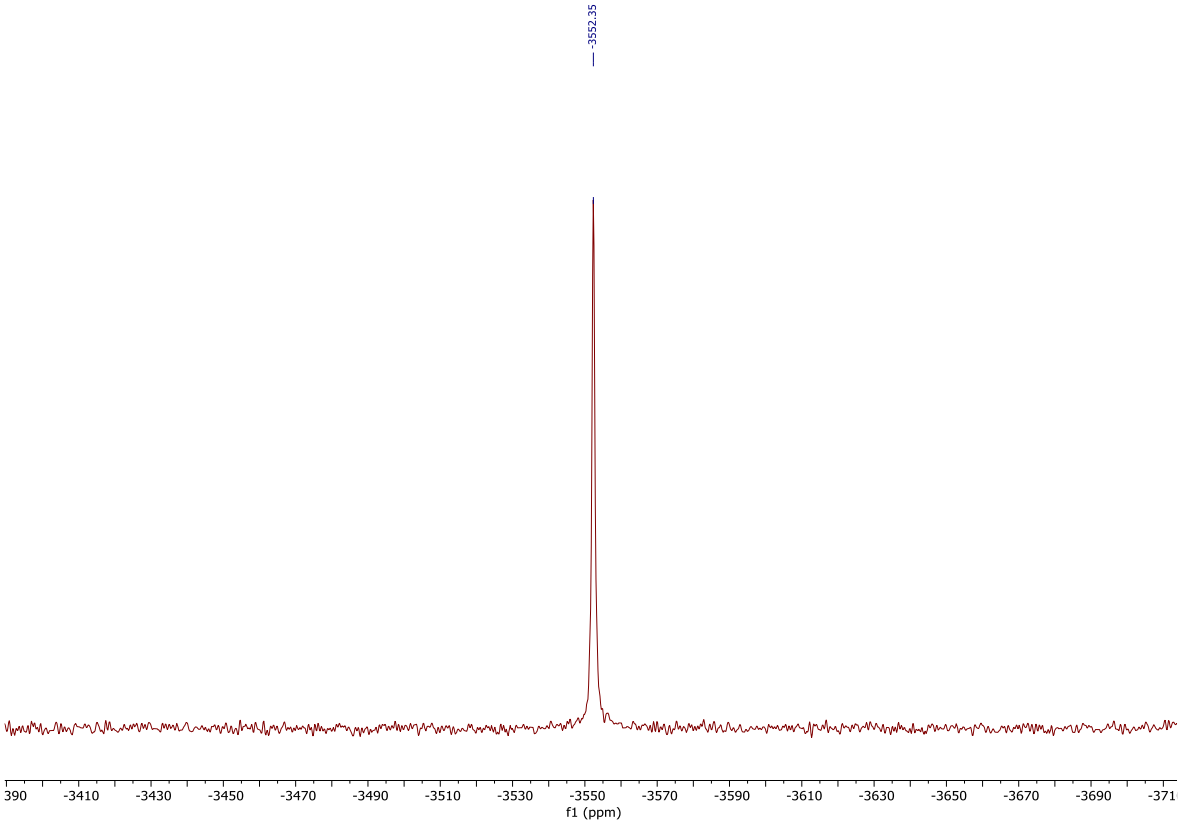

Figure S6.38. ^{195}Pt NMR of **2b** ($CDCl_3$, 86.015 MHz).

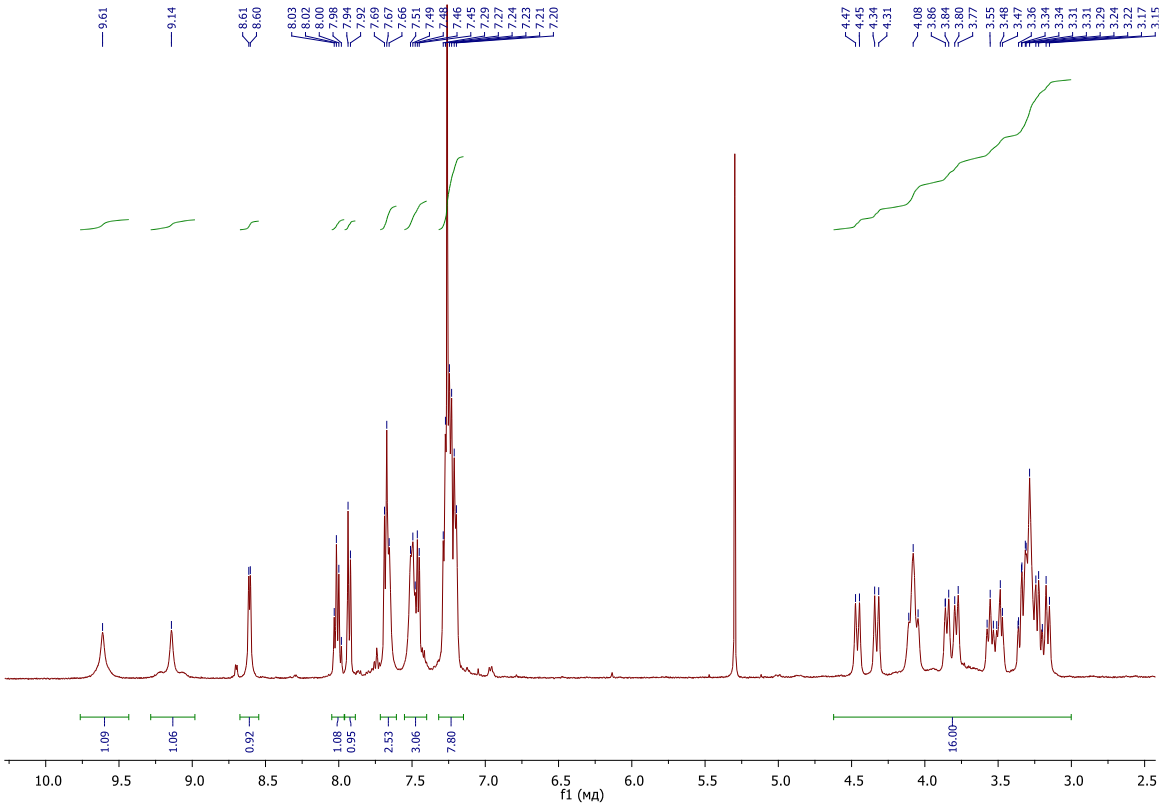

Figure S6.39. ^{1}H NMR spectrum of **2c** ($CDCl_3$, 400 MHz).

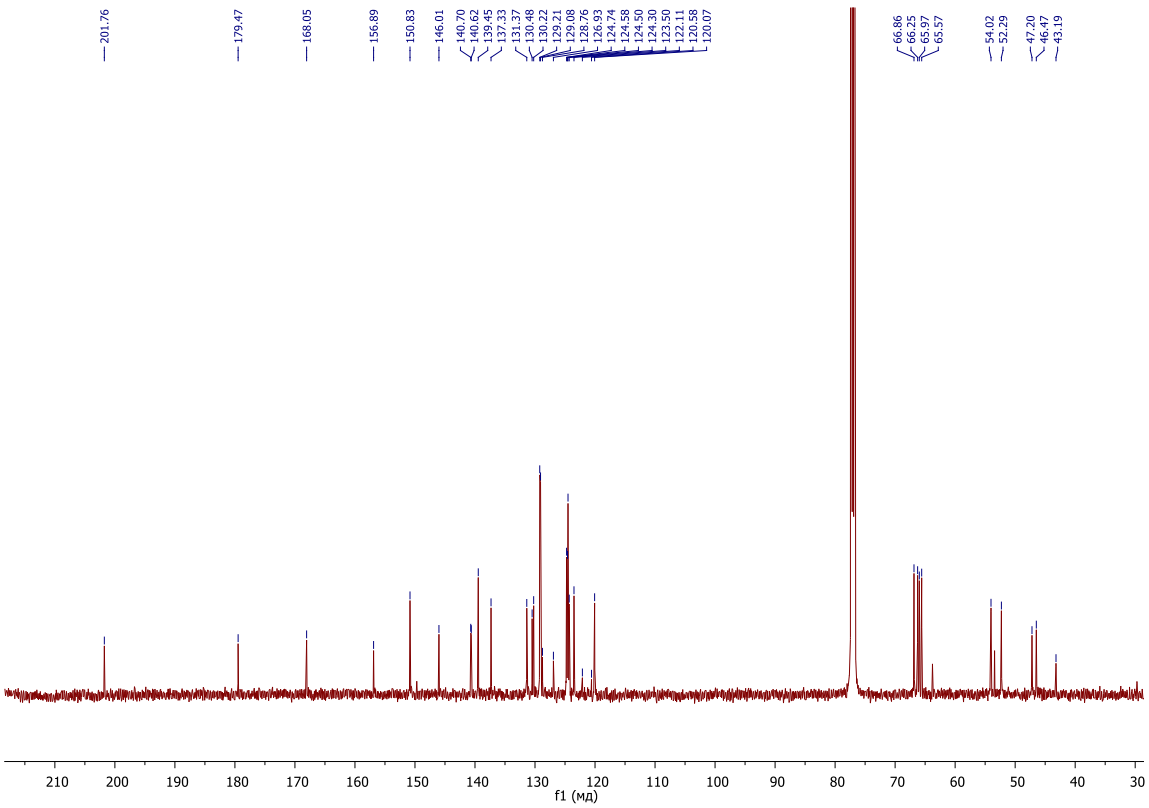

Figure S6.40. $^{13}C\{^{1}H\}$ NMR of **2c** ($CDCl_3$, 100 MHz).

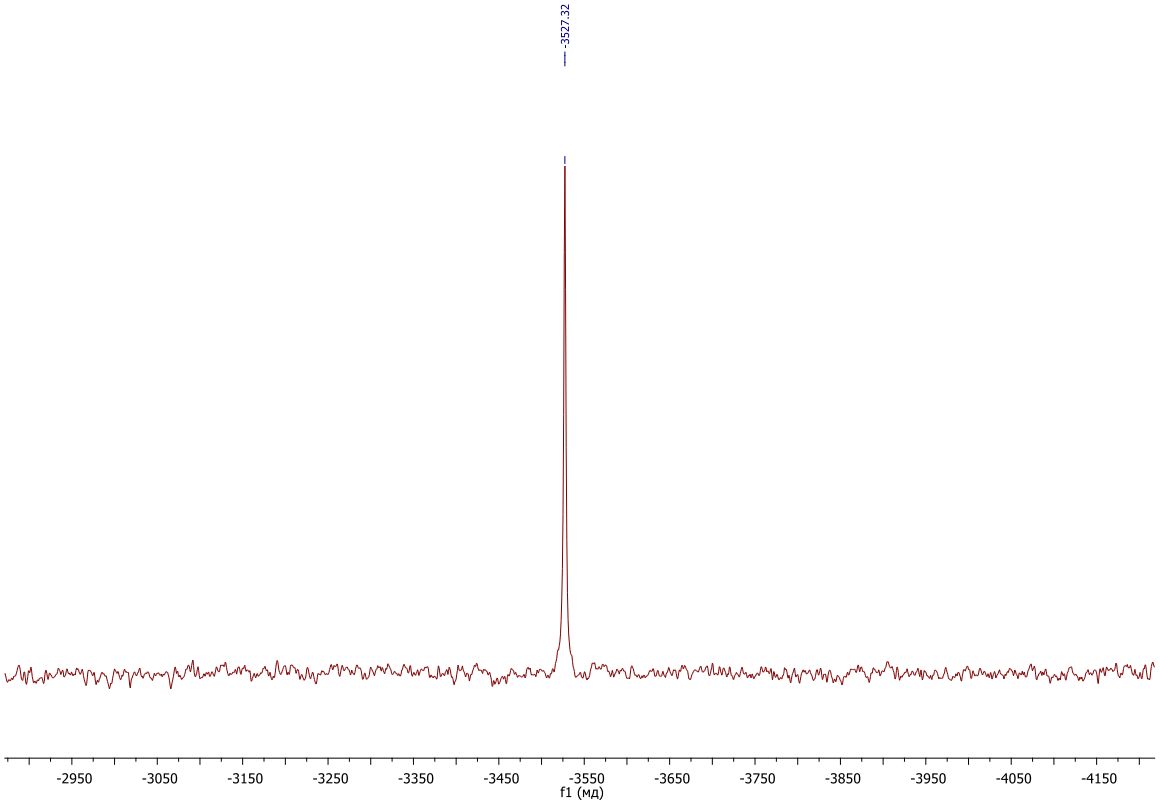

Figure S6.41. ^{195}Pt NMR of **2c** ($CDCl_3$, 86.015 MHz).

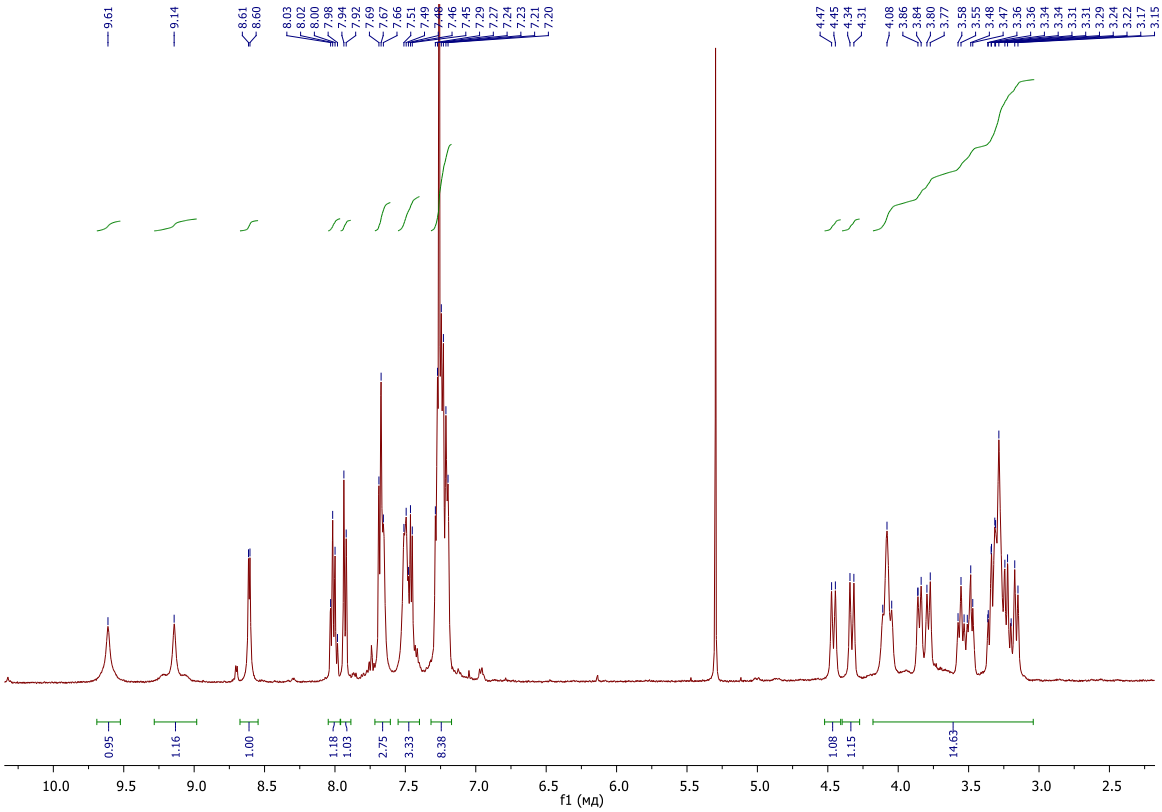

Figure S6.42. ^{1}H NMR spectrum of **2d** ($CDCl_3$, 400 MHz).

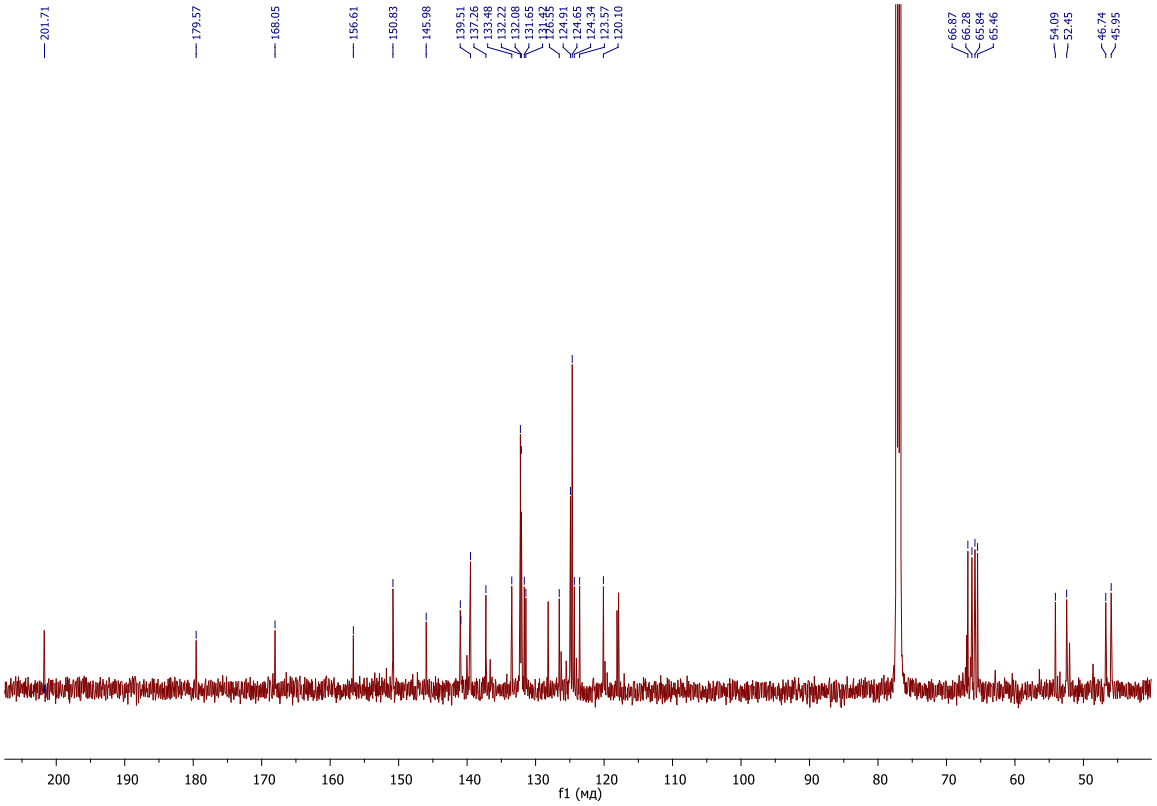

Figure S6.43. $^{13}C\{^{1}H\}$ NMR of **2d** ($CDCl_3$, 100 MHz).

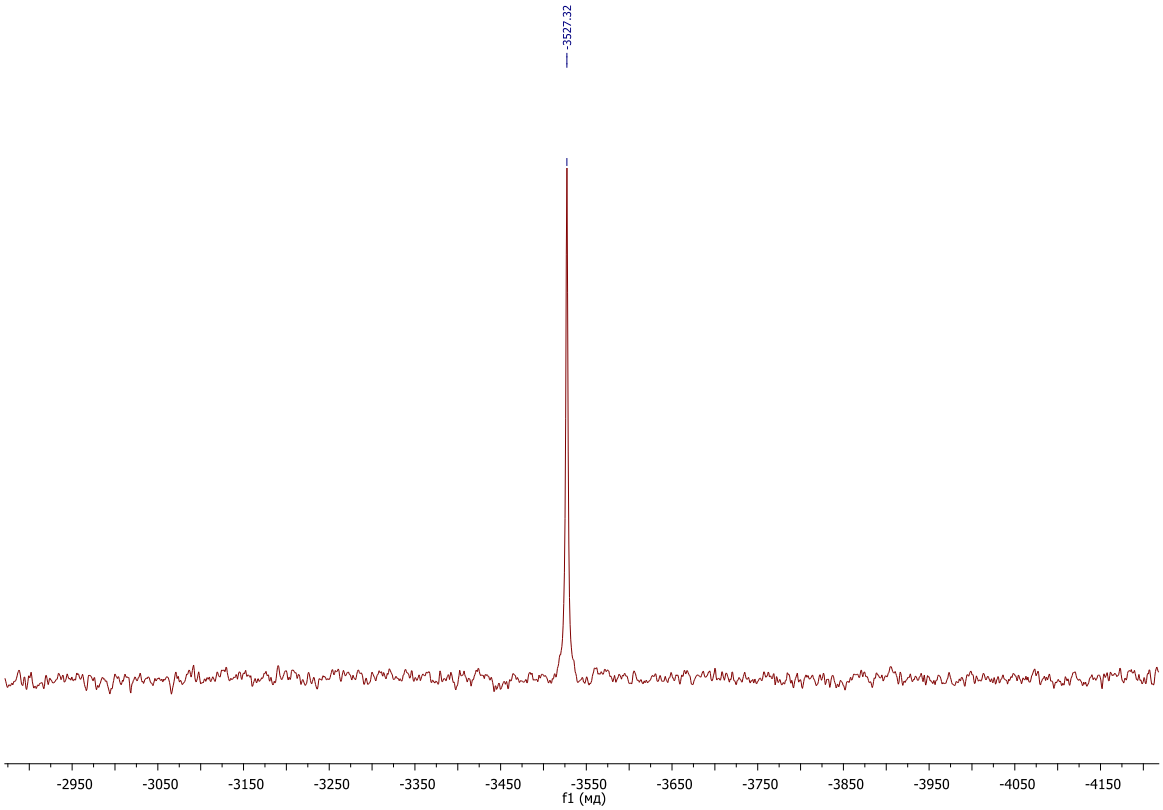

Figure S6.44. ^{195}Pt NMR of **2d** ($CDCl_3$, 86.015 MHz).

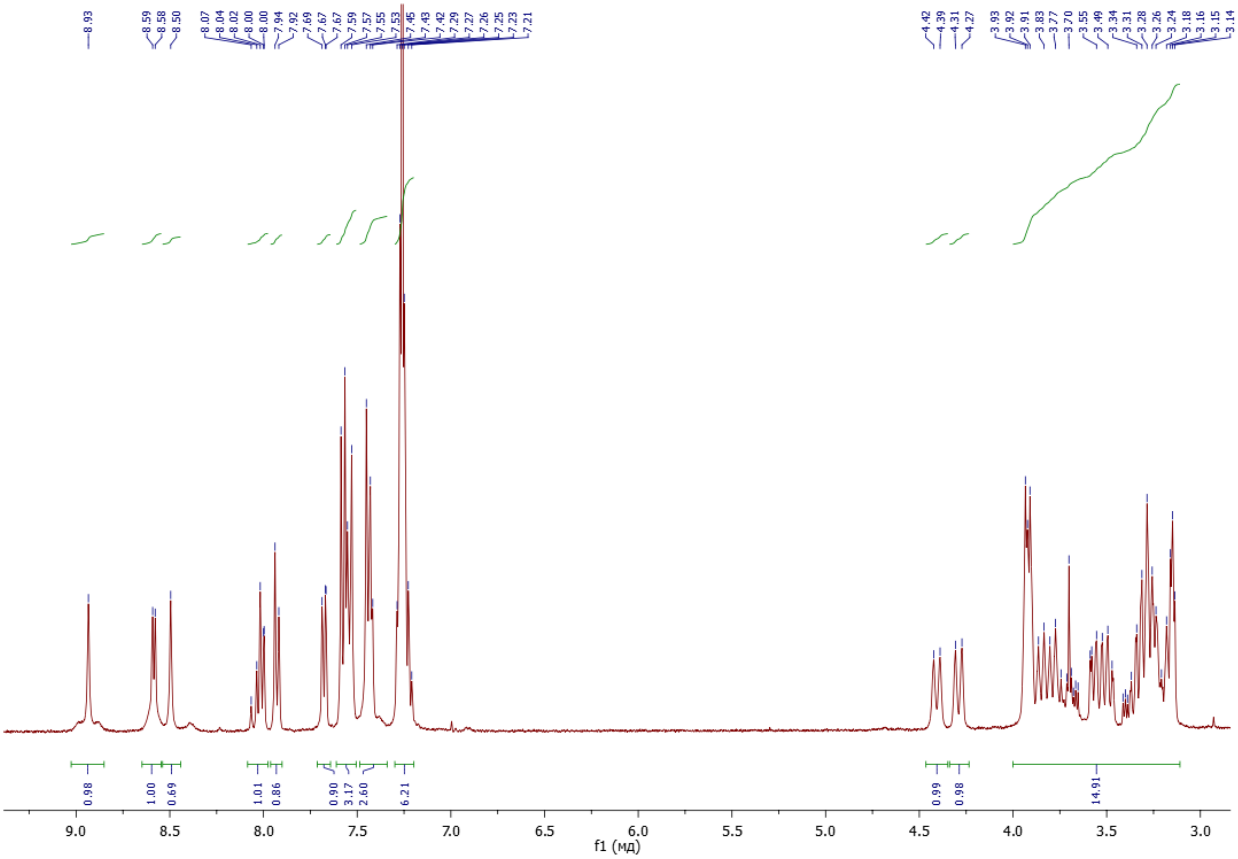

Figure S6.45. ^{1}H NMR spectrum of **2e** ($CDCl_3$, 400 MHz).

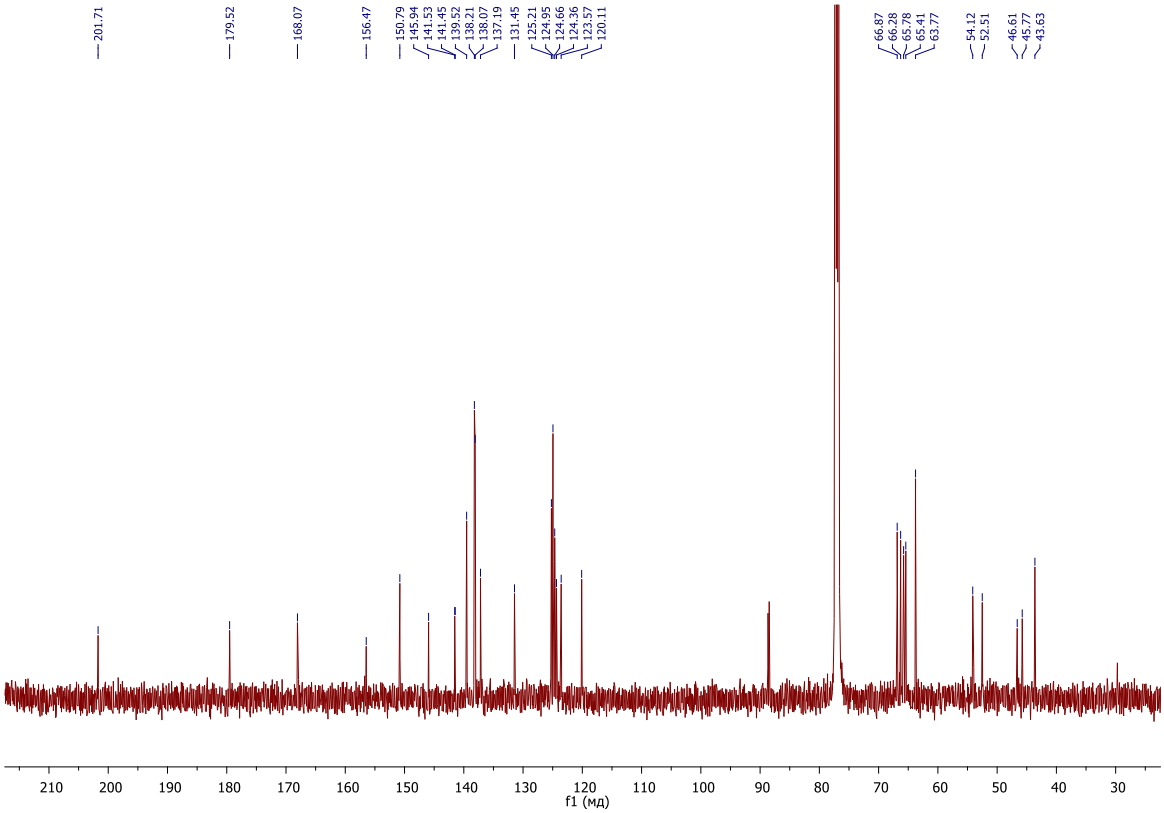

Figure S6.46. $^{13}C\{^{1}H\}$ NMR of **2e** ($CDCl_3$, 100 MHz).

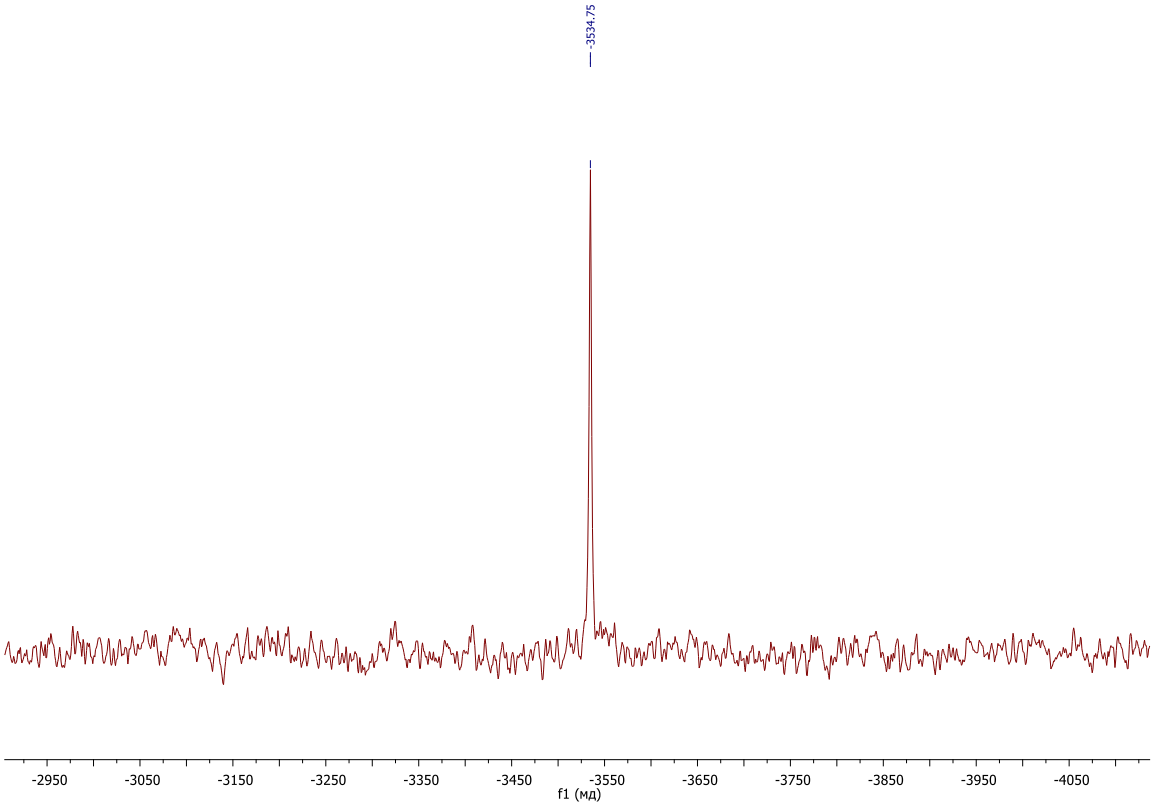

Figure S6.47. ^{195}Pt NMR of **2e** ($CDCl_3$, 86.015 MHz).

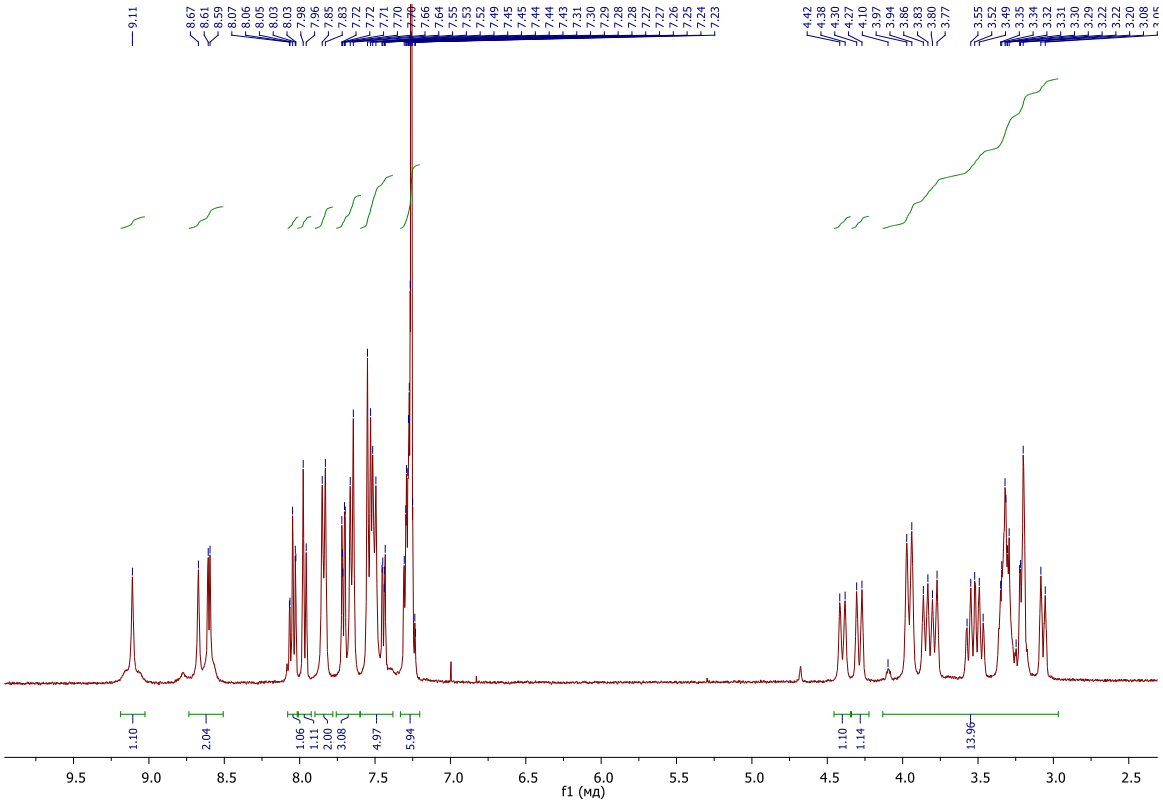

Figure S6.48. $^{13}C\{^{1}H\}$ NMR of **2f** ($CDCl_3$, 100 MHz).

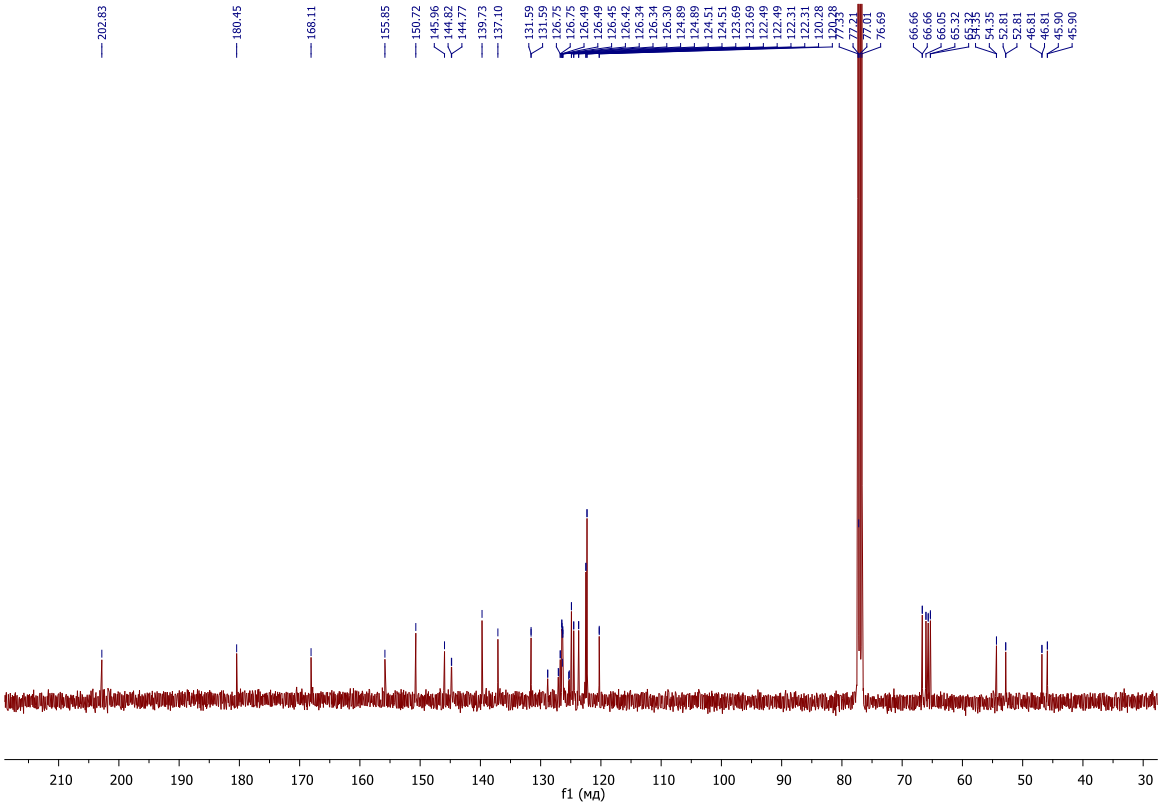

Figure S6.49. $^{13}C\{^{1}H\}$ NMR of **2f** ($CDCl_3$, 100 MHz).

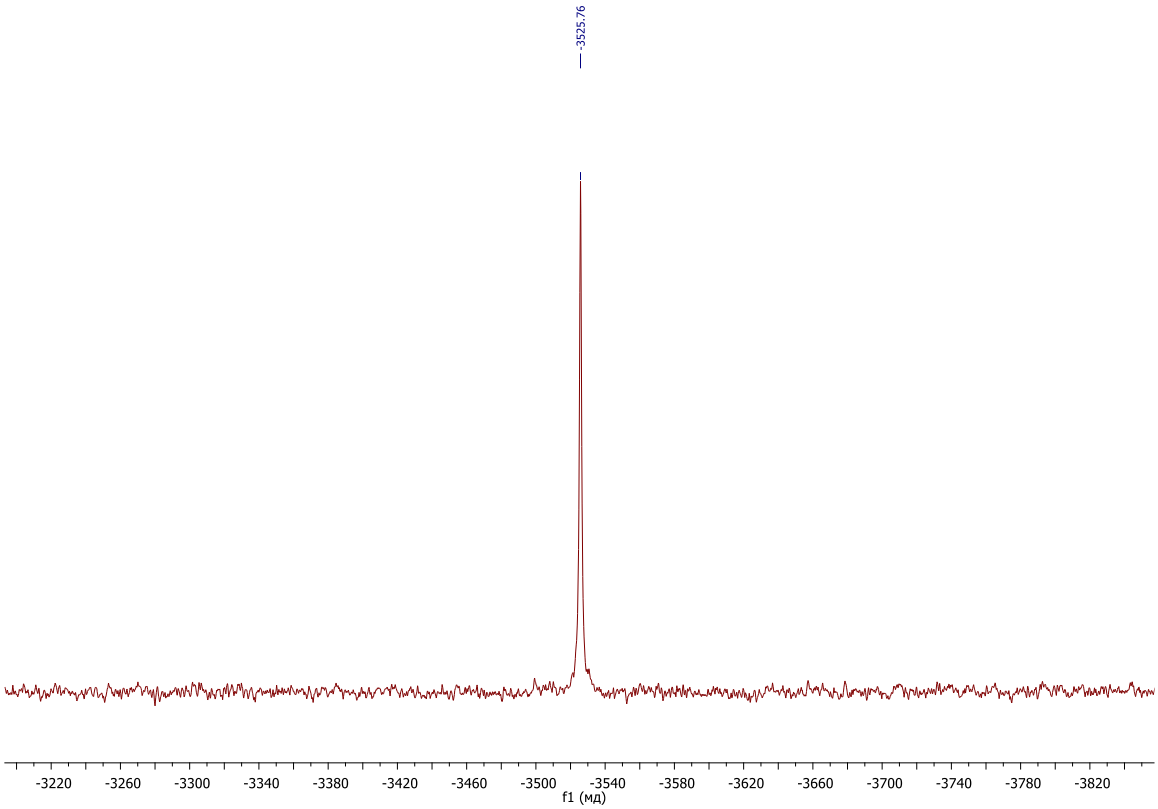

Figure S6.50. ^{195}Pt NMR of **2f** ($CDCl_3$, 86.015 MHz).

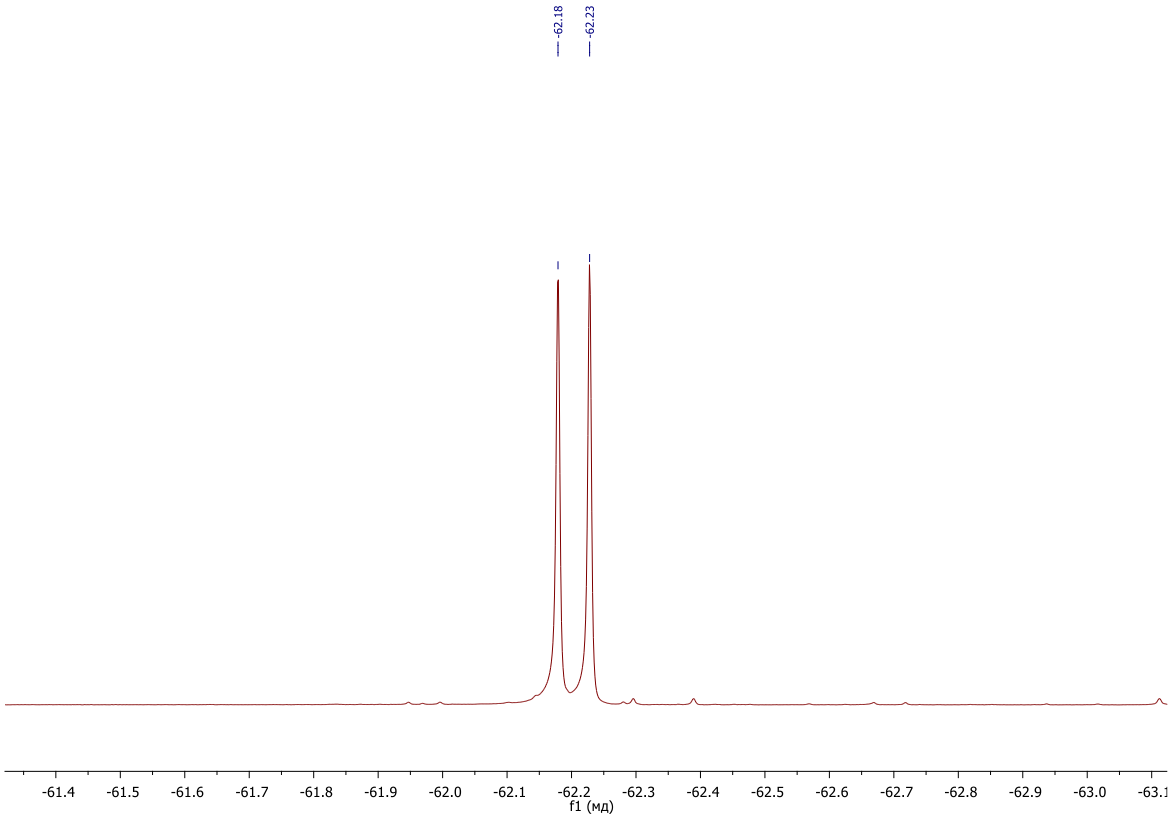

Figure S6.51. ^{19}F NMR of **2f** ($CDCl_3$, 376.50 MHz).

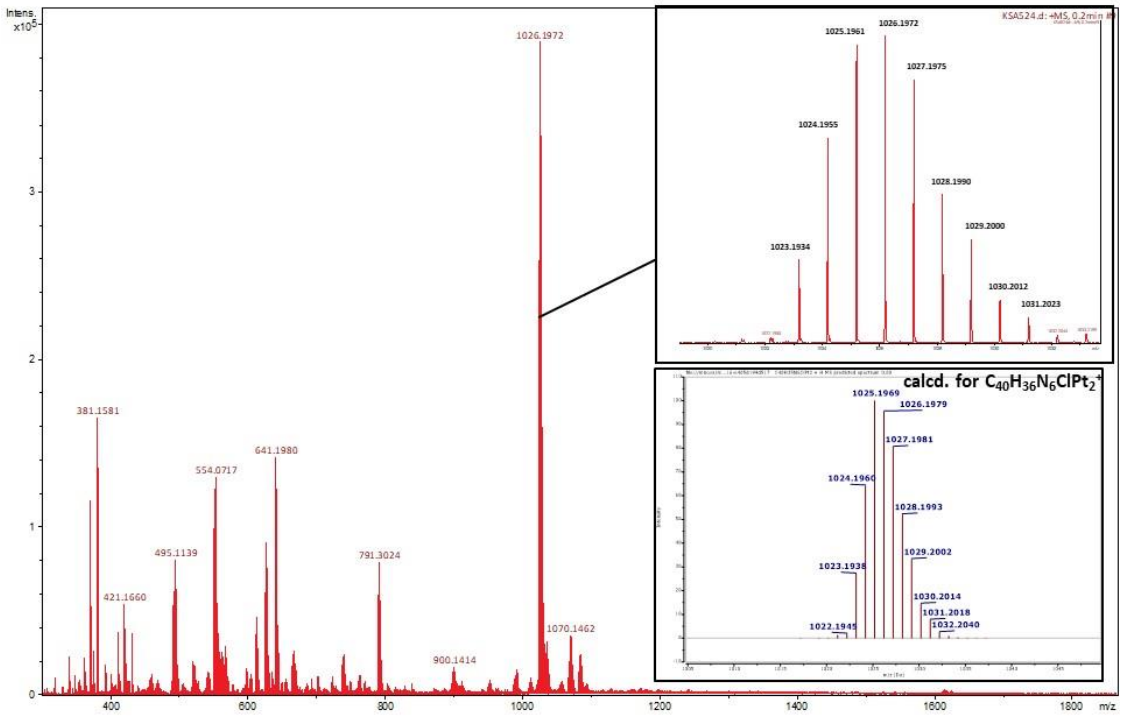

Figure S6.52. HRESI$^+$-MS of **S1a** with calculated isotopic distribution for $C_{40}H_{36}N_6ClPt_2^+$.

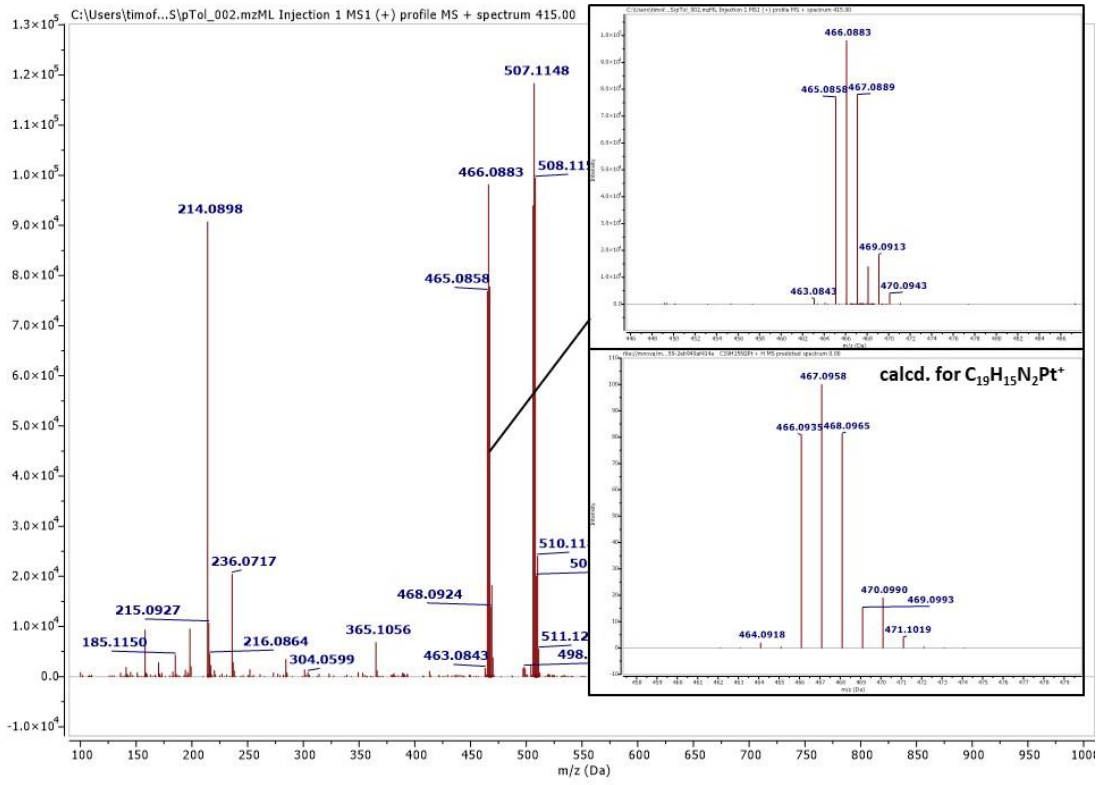

Figure S6.53. HRESI$^+$-MS of **S1b** with calculated isotopic distribution for $C_{19}H_{15}N_2Pt^+$.

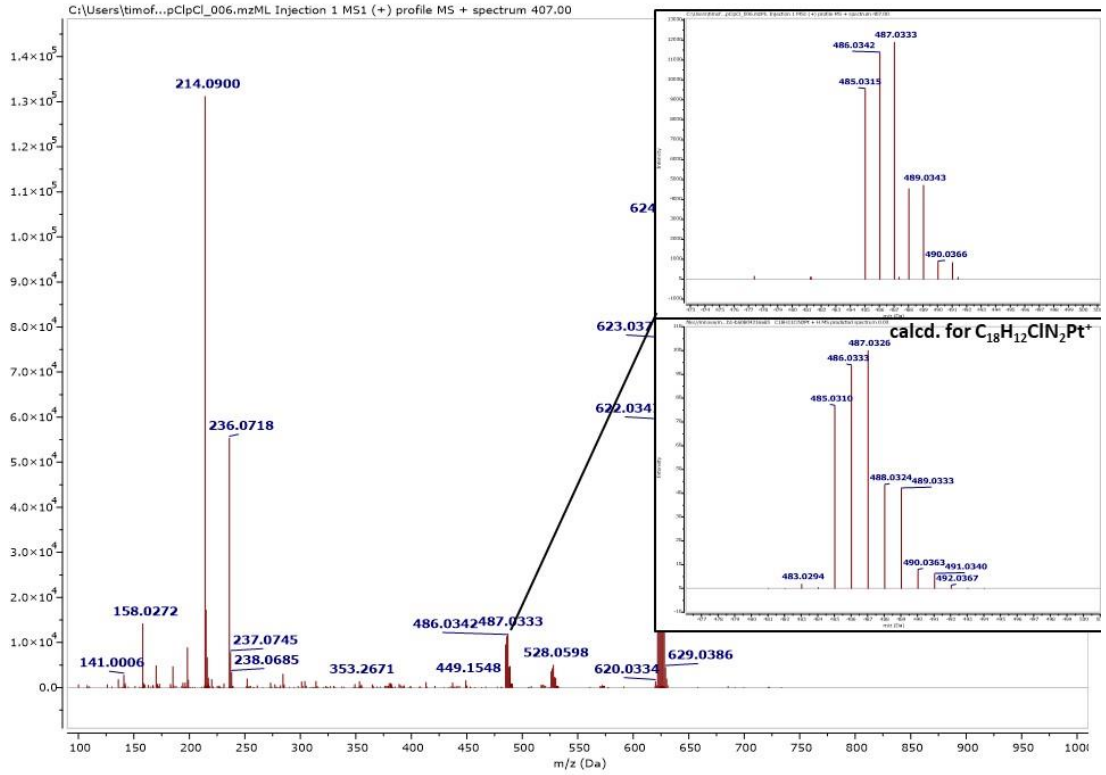

Figure S6.54. HRESI$^+$-MS of **S1c** with calculated isotopic distribution for $C_{18}H_{12}ClN_2Pt^+$.

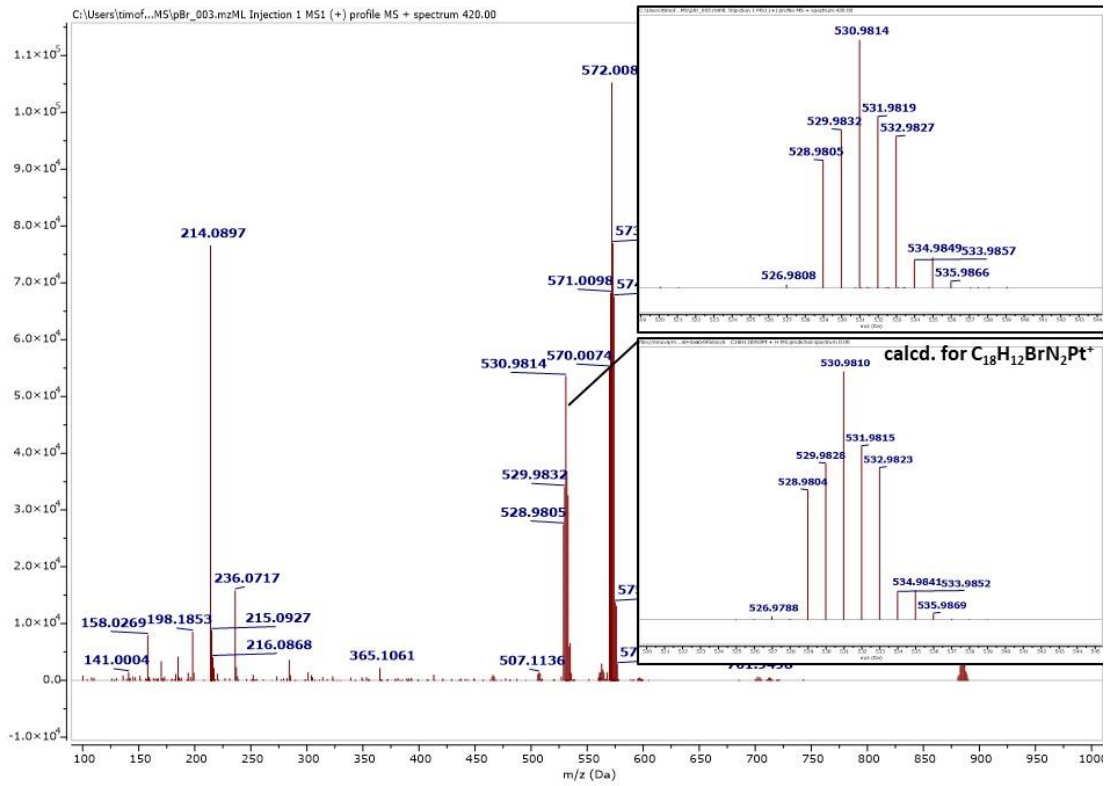

Figure S6.55. HRESI$^+$-MS of **S1d** with calculated isotopic distribution for $C_{18}H_{12}BrN_2Pt^+$.

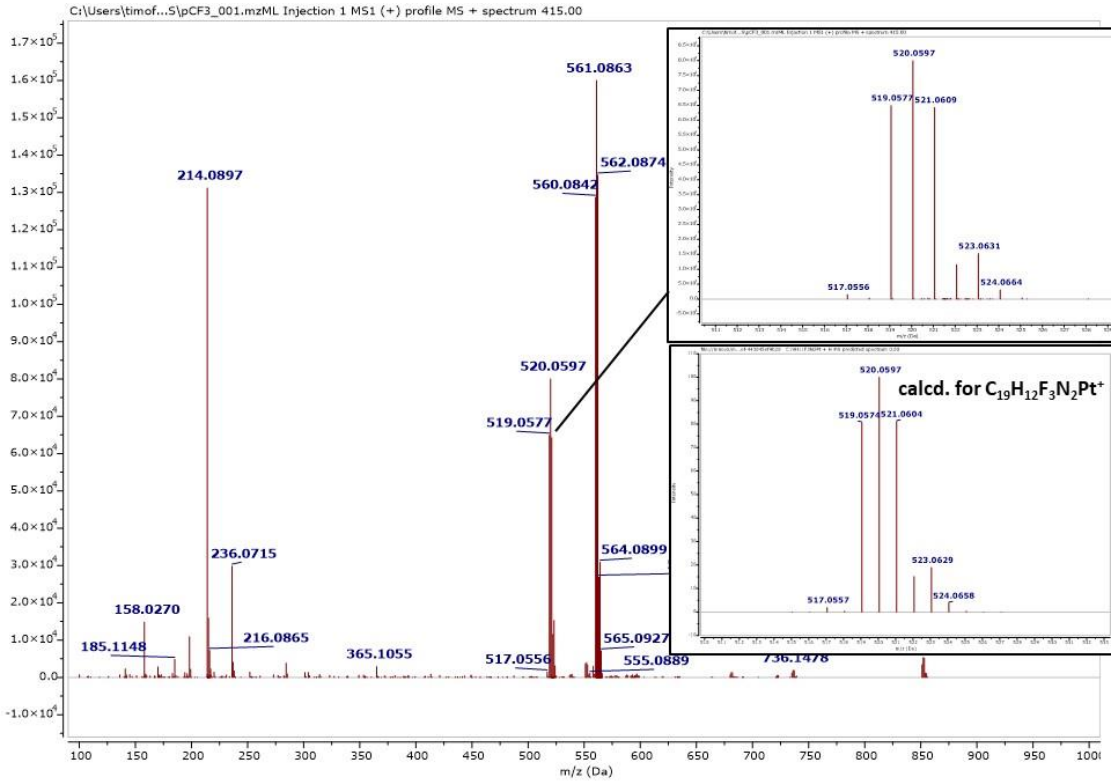

Figure S6.56. HRESI$^+$-MS of **S3f** with calculated isotopic distribution for $C_{19}H_{12}F_3N_2Pt^+$.

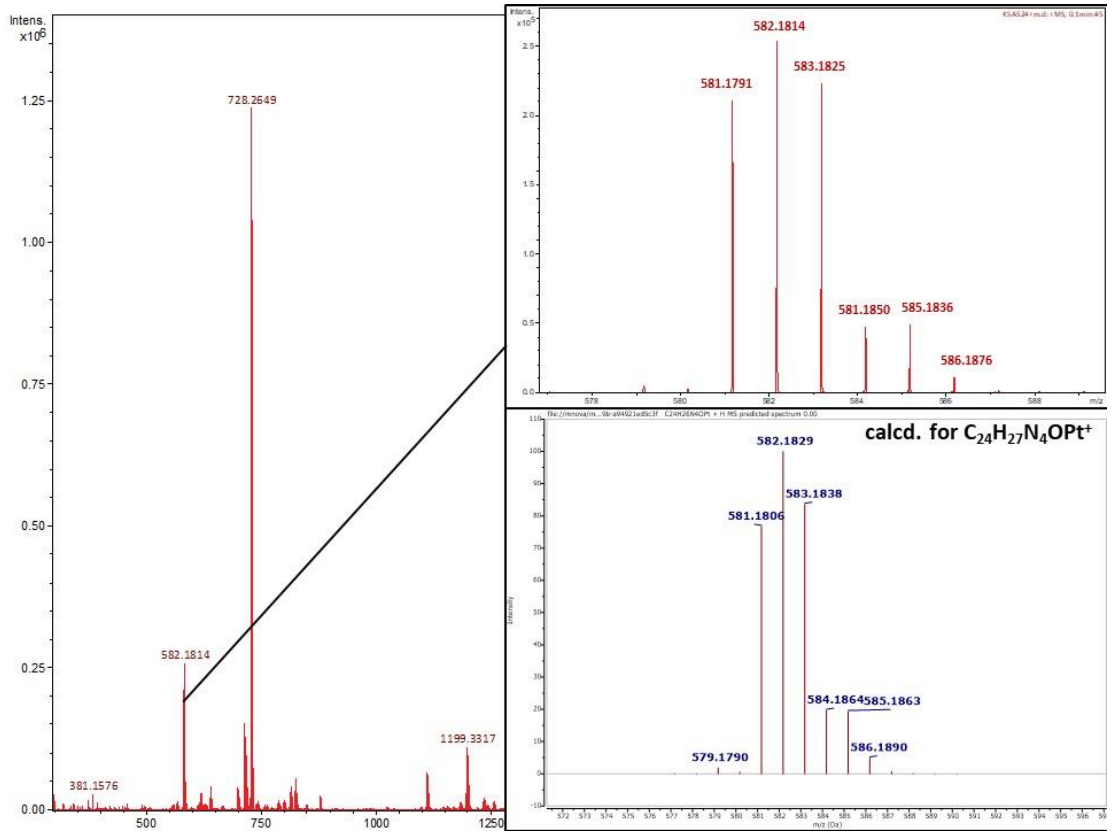

Figure S6.57. HRESI$^+$-MS of **1a** with calculated isotopic distribution for $C_{24}H_{27}N_4OPt^+$.

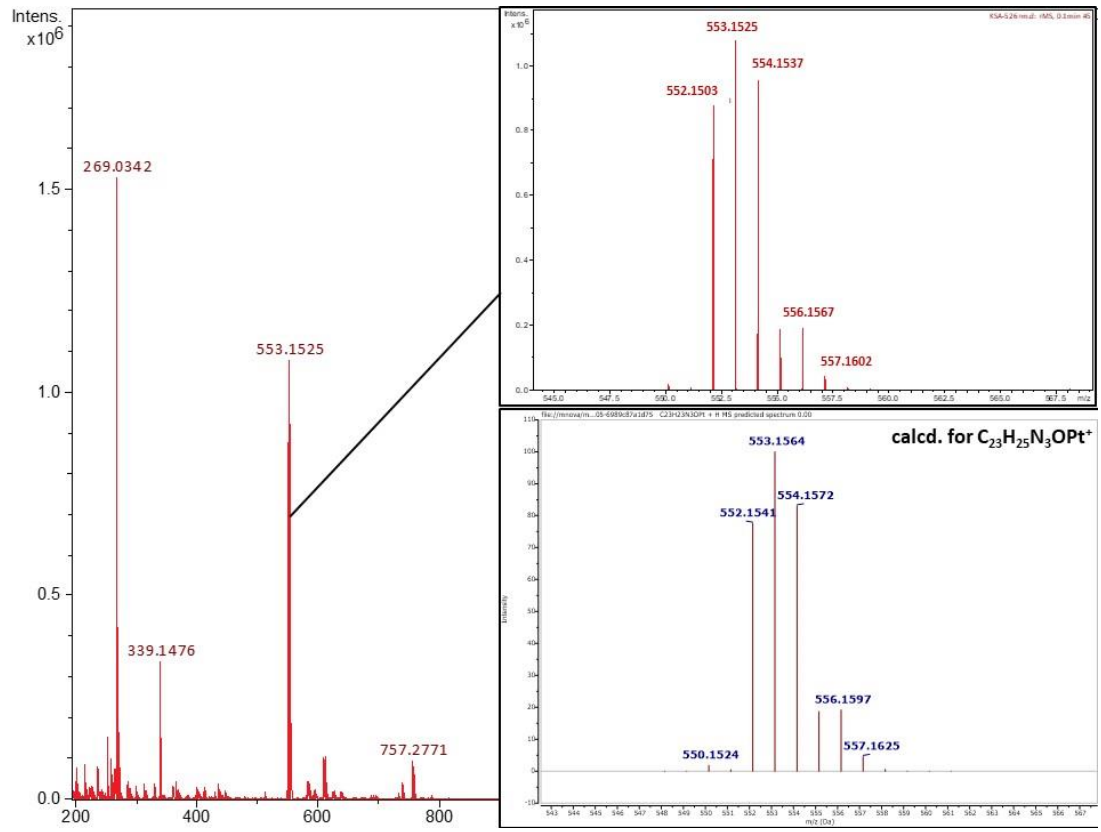

Figure S6.58. HRESI$^+$-MS of **1b** with calculated isotopic distribution for $C_{23}H_{25}N_3OPt^+$.

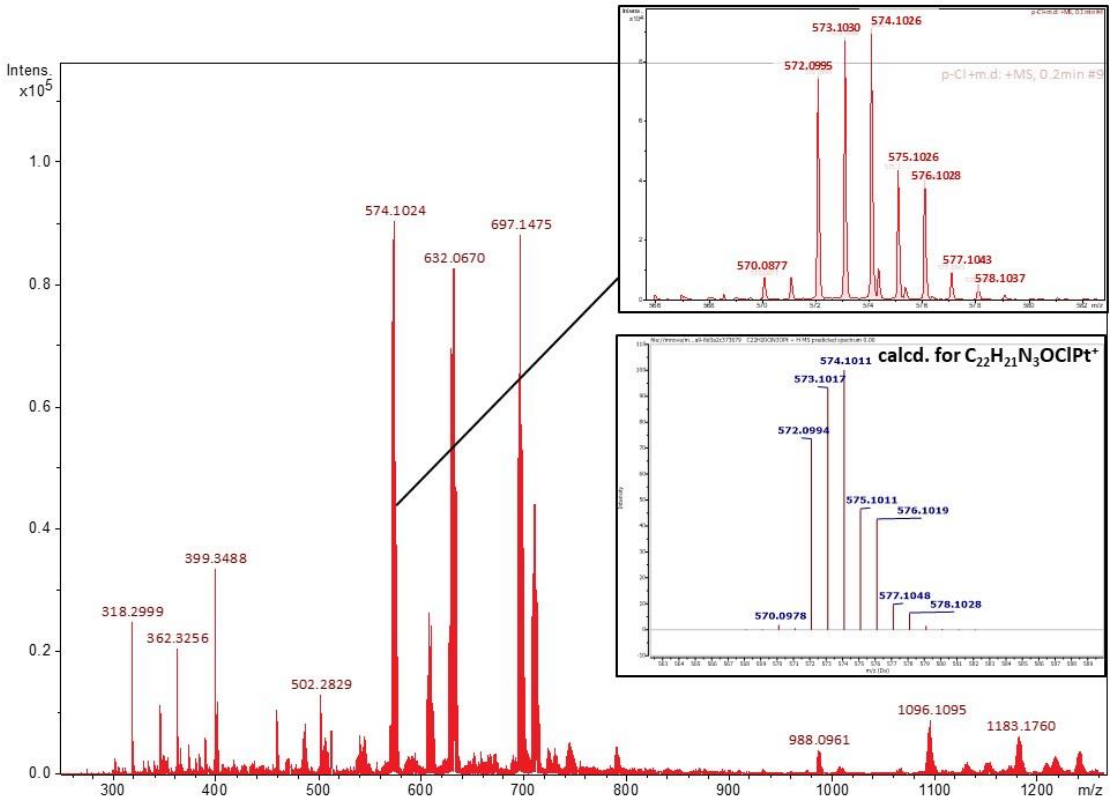

Figure S6.59. HRESI$^+$-MS of **1c** with calculated isotopic distribution for $C_{23}H_{21}N_3OClPt^+$.

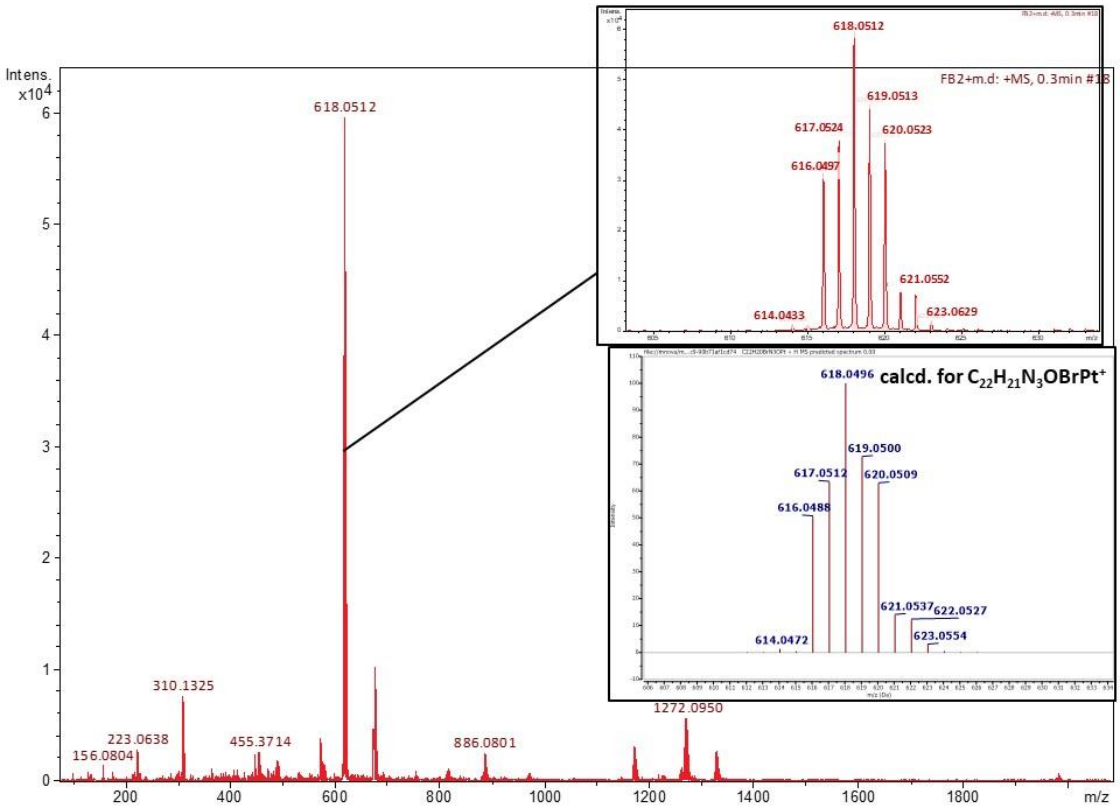

Figure S6.60. HRESI$^+$-MS of **1d** with calculated isotopic distribution for $C_{22}H_{21}N_3OBrPt^+$.

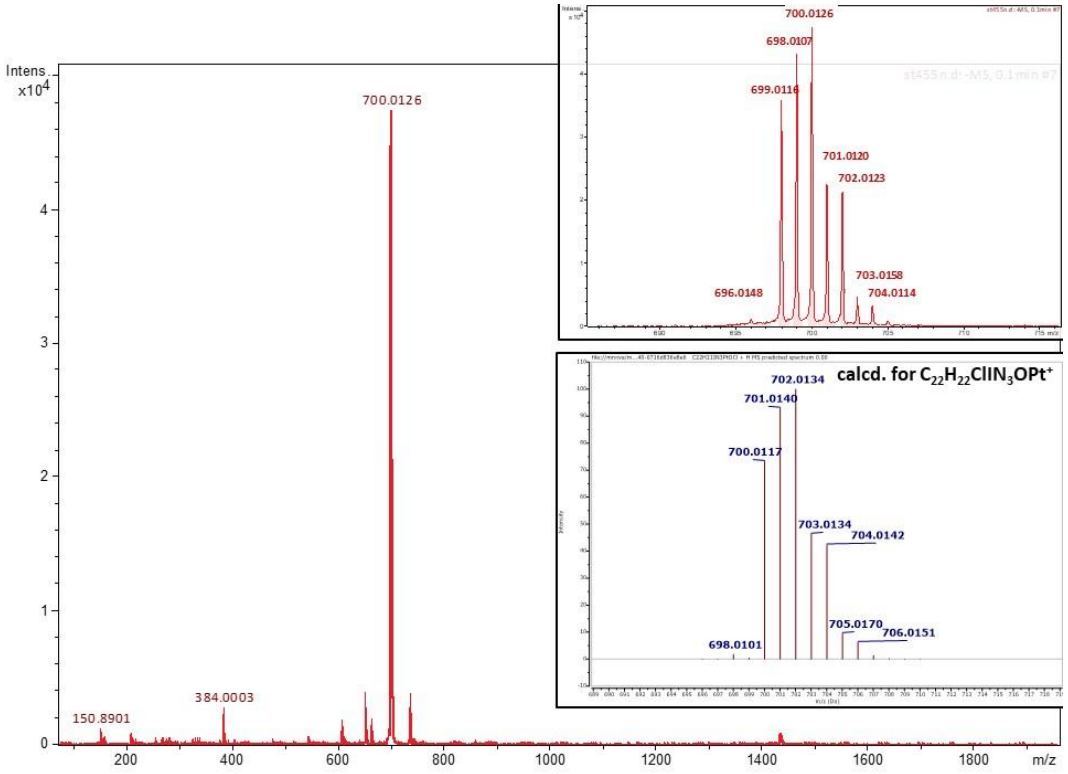

Figure S6.61. HRESI$^+$-MS of **1e** with calculated isotopic distribution for $C_{22}H_{22}N_3OClIPt^+$.

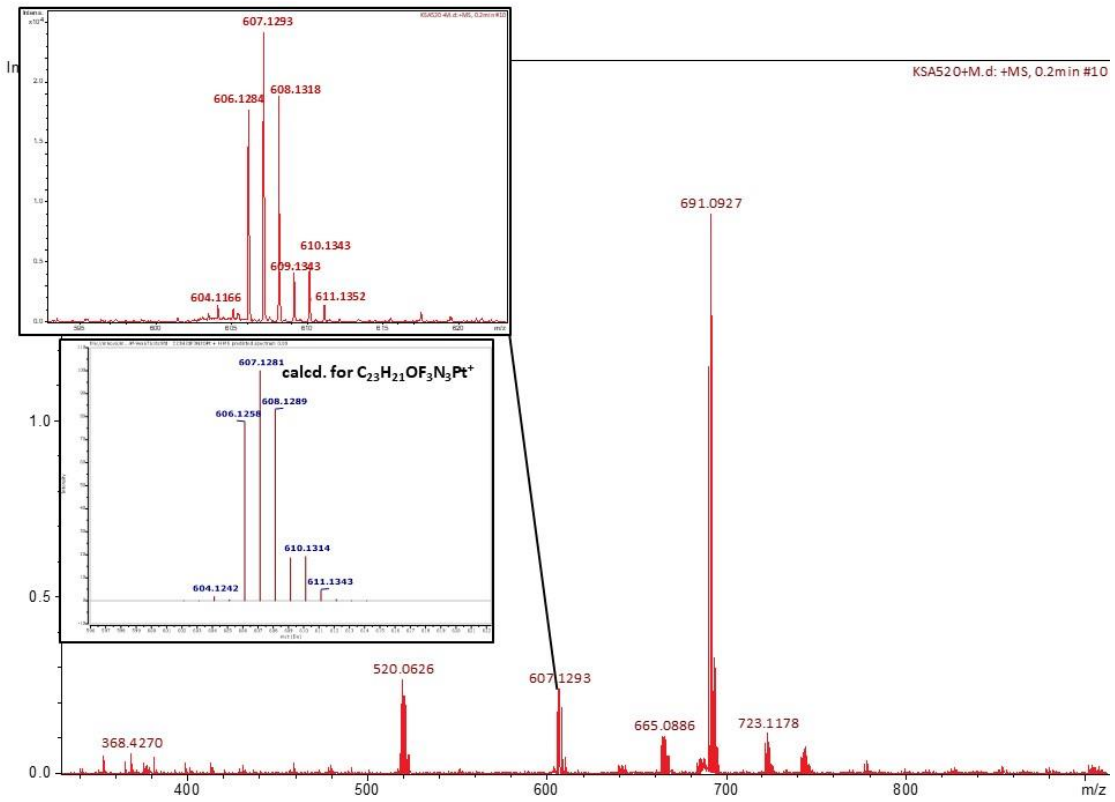

Figure S6.62. HRESI$^+$-MS of **1f** with calculated isotopic distribution for $C_{23}H_{21}N_3OF_3Pt^+$.

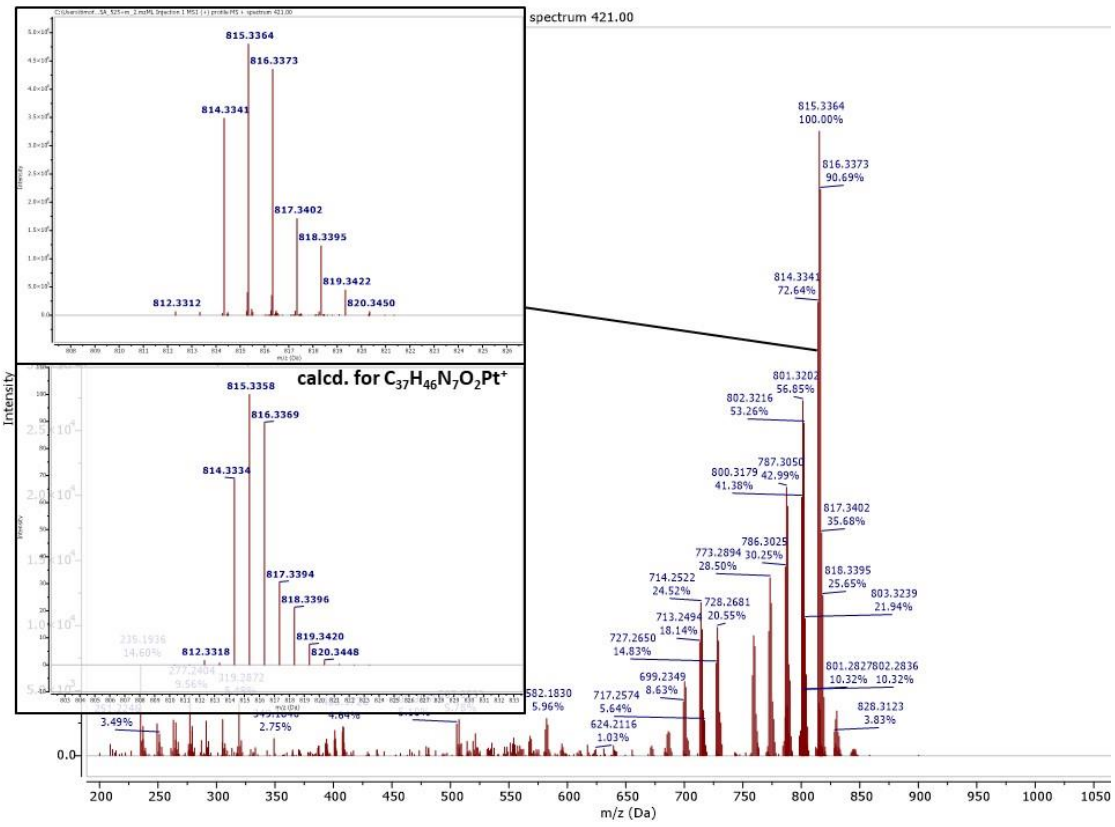

Figure S6.63. HR ESI$^+$-MS of **2a** with calculated isotopic distribution for $C_{23}H_{21}N_3OF_3Pt^+$.

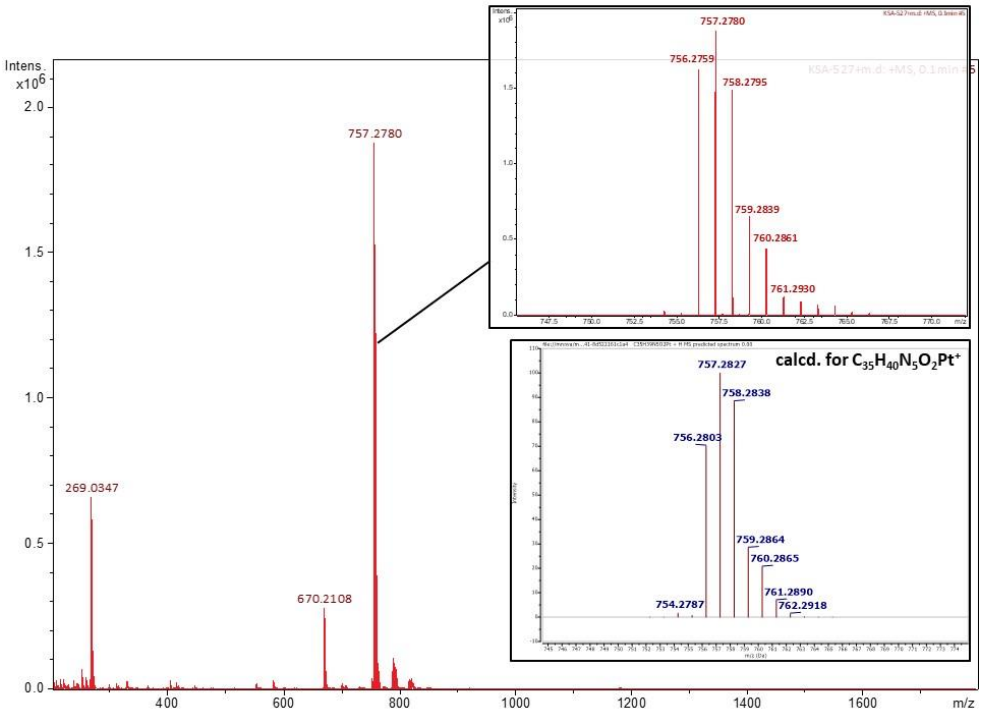

Figure S6.64. HR ESI$^+$-MS of **2b** with calculated isotopic distribution for $C_{35}H_{40}N_5O_2Pt^+$.

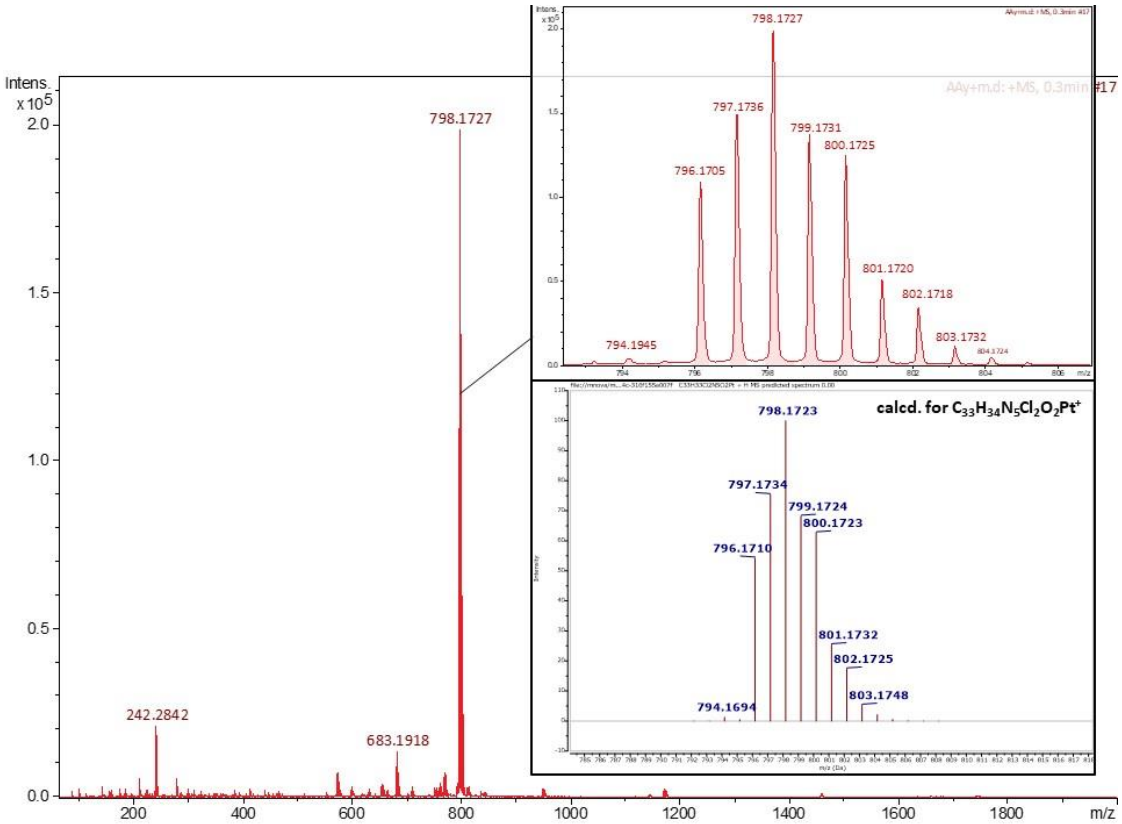

Figure S6.65. HRESI$^+$-MS of **2c** with calculated isotopic distribution for $C_{33}H_{34}N_5Cl_2O_2Pt^+$.

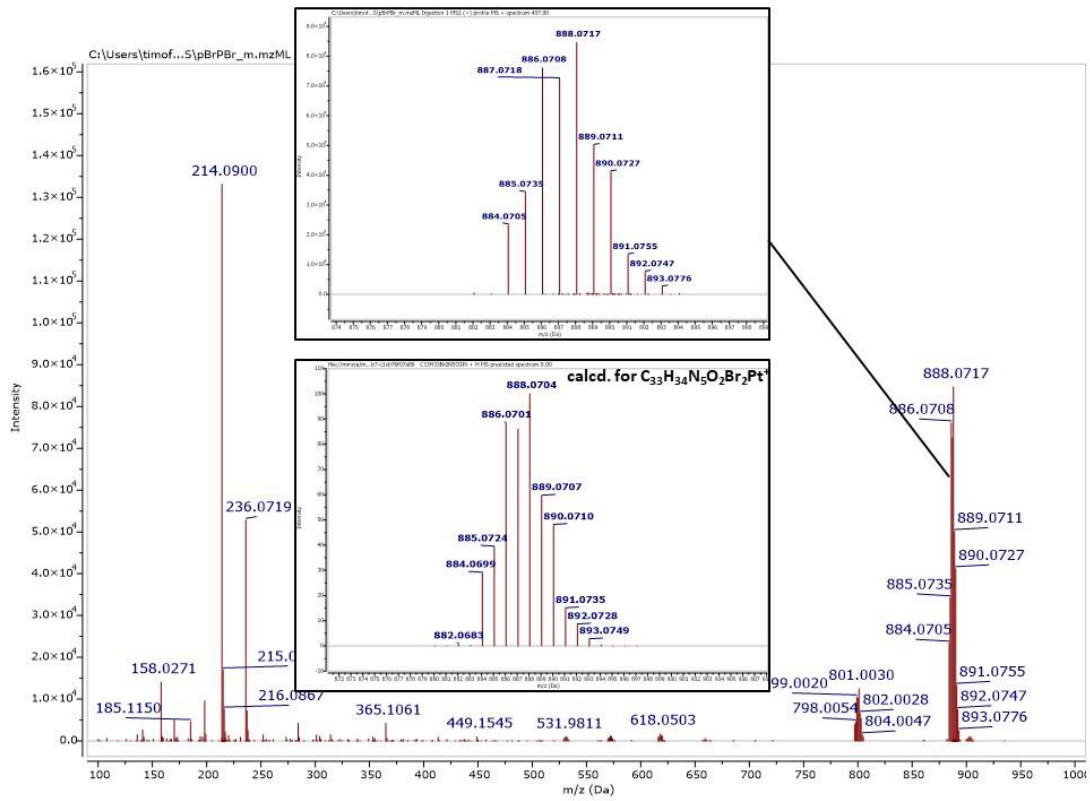

Figure S6.66. HRESI$^+$-MS of **2d** with calculated isotopic distribution for $C_{33}H_{34}N_5Br_2O_2Pt^+$.

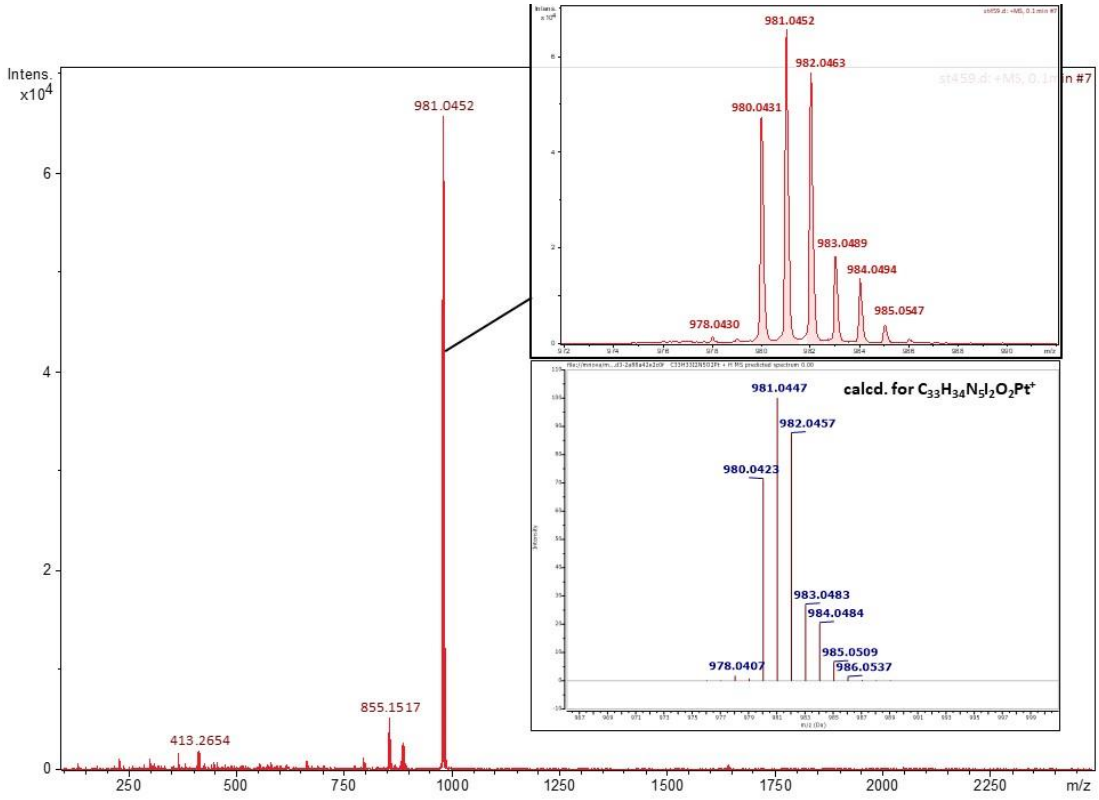

Figure S6.67. HRESI$^+$-MS of **2e** with calculated isotopic distribution for $C_{33}H_{34}N_5I_2O_2Pt^+$.

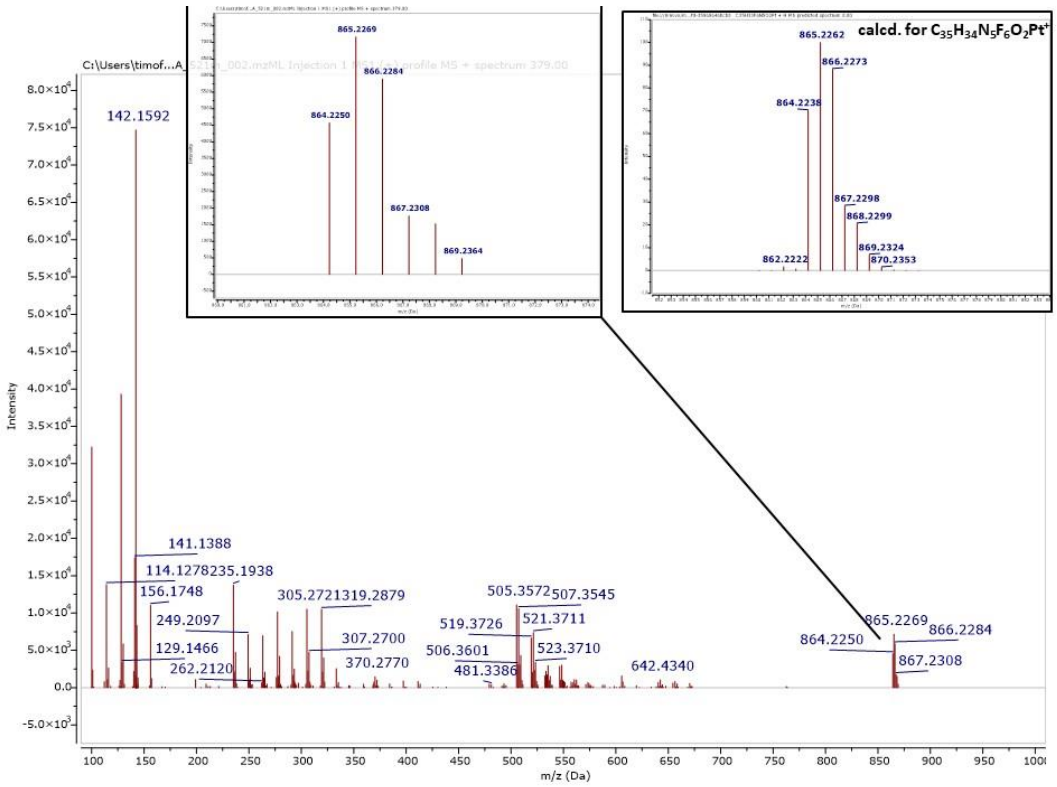

Figure S6.69. HRESI^{+}-MS of **2f** with calculated isotopic distribution for $C_{35}H_{34}N_5F_6O_2Pt^{+}$.

S7. References

1. M. A. Kinzhalov, M. V. Kashina, A. S. Mikherdov, E. A. Mozheeva, A. S. Novikov, A. S. Smirnov, D. M. Ivanov, M. A. Kryukova, A. Y. Ivanov, S. N. Smirnov, V. Y. Kukushkin and K. V. Luzyanin, Dramatically Enhanced Solubility of Halide-Containing Organometallic Species in Diiodomethane: The Role of Solvent···Complex Halogen Bonding, *Angew. Chem. Int. Ed.*, 2018, **57**, 12785–12789.
2. M. A. Kinzhalov, S. A. Katkova, E. P. Doronina, A. S. Novikov, I. I. Eliseev, V. A. Ilichev, A. A. Kukinov, G. L. Starova and N. A. Bokach, Red photo- and electroluminescent half-lantern cyclometalated dinuclear platinum(II) complex, *Z. Kristallogr. - Cryst. Mater.*, 2018, **233**, 795–802.
3. E. V. Sokolova, M. A. Kinzhalov, A. S. Smirnov, A. M. Cheranyova, D. M. Ivanov, V. Y. Kukushkin and N. A. Bokach, Polymorph-Dependent Phosphorescence of Cyclometalated Platinum(II) Complexes and Its Relation to Non-covalent Interactions, *ACS Omega*, 2022, **7**, 34454-34462.
4. S. A. Katkova, E. V. Sokolova and M. A. Kinzhalov, Bisisocyanide cyclometallated platinum(II) complexes: synthesis, structure, photophysical properties and mechanochromic behavior, *Russ. J. Gen. Chem.*, 2023, **93**, 46-56.
5. K. Suzuki, A. Kobayashi, S. Kaneko, K. Takehira, T. Yoshihara, H. Ishida, Y. Shiina, S. Oishi and S. Tobita, Reevaluation of Absolute Luminescence Quantum Yields of Standard Solutions Using a Spectrometer with an Integrating Sphere and a Back-Thinned CCD Detector, *Phys. Chem. Chem. Phys.*, 2009, **11**, 9850.
6. G. M. Sheldrick, SHELXT - Integrated space-group and crystal-structure determination, *Acta Crystallographica a-Foundation and Advances*, 2015, **71**, 3-8.
7. O. V. Dolomanov, L. J. Bourhis, R. J. Gildea, J. A. K. Howard and H. Puschmann, OLEX2: a complete structure solution, refinement and analysis program, *Journal of Applied Crystallography*, 2009, **42**, 339-341.
8. M. Frisch, G. Scalmani, T. Vreven and G. Zheng, Analytic second derivatives for semiempirical models based on MNDO, *Molecular Physics*, 2009, **107**, 881-887.
9. A. D. Becke, DENSITY-FUNCTIONAL THERMOCHEMISTRY .3. THE ROLE OF EXACT EXCHANGE, *J. Chem. Phys.*, 1993, **98**, 5648-5652.
10. D. Andrae, U. Haussermann, M. Dolg, H. Stoll and H. Preuss, ENERGY-ADJUSTED ABINITIO PSEUDOPOTENTIALS FOR THE 2ND AND 3RD ROW TRANSITION-ELEMENTS, *Theor. Chim. Acta*, 1990, **77**, 123-141.
11. R. Peverati and D. G. Truhlar, Screened-exchange density functionals with broad accuracy for chemistry and solid-state physics, *Phys. Chem. Chem. Phys.*, 2012, **14**, 16187-16191.
12. J. Tomasi, B. Mennucci and R. Cammi, Quantum mechanical continuum solvation models, *Chem. Rev.*, 2005, **105**, 2999-3093.
13. F. L. Hirshfeld, Bonded-atom fragments for describing molecular charge densities, *Theoretica chimica acta*, 1977, **44**, 129-138.
14. T. Lu and F. W. Chen, Multiwfn: A multifunctional wavefunction analyzer, *J. Comput. Chem.*, 2012, **33**, 580–592.
15. N. M. O'Boyle, A. L. Tenderholt and K. M. Langner, cclib: A library for package-independent computational chemistry algorithms, *J. Comput. Chem.*, 2008, **29**, 839-845.
16. R. L. Martin, Natural transition orbitals, *J. Chem. Phys.*, 2003, **118**, 4775-4777.

17. M. Ito, H. Noguchi, K. Ikeda and K. Uosaki, Substrate dependent structure of adsorbed aryl isocyanides studied by sum frequency generation (SFG) spectroscopy, *Physical Chemistry Chemical Physics*, 2010, **12**, 3156-3163.

18. A. I. Solomatina, D. V. Krupenya, V. V. Gurzhiy, I. Zlatkin, A. P. Pushkarev, M. N. Bochkarev, N. A. Besley, E. Bichoutskaia and S. P. Tunik, Cyclometallated platinum(ii) complexes containing NHC ligands: synthesis, characterization, photophysics and their application as emitters in OLEDs, *Dalton Trans.*, 2015, **44**, 7152-7162.

19. Z. M. Hudson, C. Sun, M. G. Helander, Y.-L. Chang, Z.-H. Lu and S. Wang, Highly Efficient Blue Phosphorescence from Triarylboron-Functionalized Platinum(II) Complexes of N-Heterocyclic Carbenes, *J. Am. Chem. Soc.*, 2012, **134**, 13930-13933.

20. Y. Unger, D. Meyer, O. Molt, C. Schildknecht, I. Münster, G. Wagenblast and T. Strassner, Green–Blue Emitters: NHC-Based Cyclometalated [Pt(C^C*)(acac)] Complexes, *Angew. Chem., Int. Ed.*, 2010, **49**, 10214-10216.

21. A. Tronnier, U. Heinemeyer, S. Metz, G. Wagenblast, I. Muenster and T. Strassner, Heteroleptic platinum(ii) NHC complexes with a C^C* cyclometalated ligand – synthesis, structure and photophysics, *J. Mater. Chem. C*, 2015, **3**, 1680-1693.

22. K. Li, G. Cheng, C. Ma, X. Guan, W.-M. Kwok, Y. Chen, W. Lu and C.-M. Che, Light-emitting platinum(ii) complexes supported by tetradentate dianionic bis(N-heterocyclic carbene) ligands: towards robust blue electrophosphors, *Chem. Sci.*, 2013, **4**, 2630-2644.

23. S. Fuertes, A. J. Chueca, L. Arnal, A. Martín, U. Giovanella, C. Botta and V. Sicilia, Heteroleptic Cycloplatinated N-Heterocyclic Carbene Complexes: A New Approach to Highly Efficient Blue-Light Emitters, *Inorg. Chem.*, 2017, **56**, 4829-4839.

24. T. Fleetham, Z. Wang and J. Li, Efficient deep blue electrophosphorescent devices based on platinum(II) bis(n-methyl-imidazolyl)benzene chloride, *Org. Electron.*, 2012, **13**, 1430-1435.

25. T. Fleetham, J. Ecton, Z. Wang, N. Bakken and J. Li, Single-Doped White Organic Light-Emitting Device with an External Quantum Efficiency Over 20%, *Adv. Mater.*, 2013, **25**, 2573-2576.

26. X.-C. Hang, T. Fleetham, E. Turner, J. Brooks and J. Li, Highly Efficient Blue-Emitting Cyclometalated Platinum(II) Complexes by Judicious Molecular Design, *Angew. Chem. Int. Ed.*, 2013, **52**, 6753-6756.

27. G. Li, S. Liu, Y. Sun, W. Lou, Y.-F. Yang and Y. She, N-Heterocyclic carbene-based tetradentate platinum(ii) complexes for phosphorescent OLEDs with high brightness, *J. Mater. Chem. C*, 2022, **10**, 210-218.